ÇUKUROVA UNIVERSITY
INSTITUTE OF NATURAL AND APPLIED SCIENCES

MSc THESIS

Muhammed Murat AKSOY

PASSIVE FLOW CONTROL DOWNSTREAM A CIRCULAR CYLINDER USING PERFORATED CIRCULAR CYLINDER IN DEEP WATER

DEPARTMENT OF MECHANICAL ENGINEERING

ADANA, 2013

ÇUKUROVA UNIVERSITY
INSTITUTE OF NATURAL AND APPLIED SCIENCES

PASSIVE FLOW CONTROL DOWNSTREAM A CIRCULAR CYLINDER USING PERFORATED CIRCULAR CYLINDER IN DEEP WATER

Muhammed Murat AKSOY

MSc THESIS

DEPARTMENT OF MECHANICAL ENGINEERING

We certify that the thesis titled above was reviewed and approved for the award of degree of the Master of Science by the board of jury on 12/08/2013

…….....	……..…….	…….
Prof. Dr. Hüseyin AKILLI	Prof. Dr. Beşir ŞAHİN	Assoc. Prof. Dr. Mehmet BİLGİLİ
SUPERVISOR	MEMBER	MEMBER

This MSc Thesis is written at the Department of Institute of Natural And Applied Sciences of Çukurova University.
Registration Number:

Prof. Dr. Mustafa GÖK
Director
Institute of Natural and Applied Sciences

This thesis was supported by the Scientific and Technological Research Council of Turkey under contract no: 109R001.

ABSTRACT

MSc THESIS

PASSIVE FLOW CONTROL DOWNSTREAM A CIRCULAR CYLINDER USING PERFORATED CIRCULAR CYLINDER IN DEEP WATER

Muhammed Murat AKSOY

ÇUKUROVA UNIVERSITY
INSTITUTE OF NATURAL AND APPLIED SCIENCES
DEPARTMENT OF MECHANICAL ENGINEERING

Supervisor : Prof. Dr. Hüseyin AKILLI
Year: 2013, Page: 141
Jury : Prof. Dr. Hüseyin AKILLI
: Prof. Dr. Beşir ŞAHİN
: Assoc. Prof. Dr. Mehmet BİLGİLİ

The aim of the present study was to control the vortex shedding downstream of a circular cylinder (inner cylinder) by the existence of outer perforated cylinder concentrically located around the inner cylinder in deep water. The flow characteristics downstream of concentrically placed coupled (shrouded) cylinders were investigated quantitatively by the Particle Image Velocimetry (PIV) technique. Diameter of the outer perforated cylinder was kept constant as D_o=100 mm while diameter of the inner cylinder was varied within the range of $25 \leq D_i \leq 90$ mm. The depth-averaged free-stream velocity was also kept constant as U=100 mm/s which corresponded to the Reynolds number of Re_{Do}=10,000 based on the outer cylinder diameter. Experiments were conducted for seven porosities (β=0.25, 0.30, 0.40, 0.50, 0.60, 0.70 and 0.80) and nine diameter ratios (D_i/D_o=0.25, 0.30, 0.40, 0.50, 0.60, 0.70, 0.80 and 0.90) in order to show the effect of these parameters on the flow control. Maximum values of both Reynolds shear stress and turbulence kinetic energy significantly decreased with the existence of outer perforated cylinder and also, the location of peak magnitudes of turbulence statistics occurred at locations further downstream compared to the bare cylinder cases. The most effective control was revealed for the porosity range of $0.50 \leq \beta \leq 0.60$ for all diameter ratios. It was concluded that the perforated cylinder could be used as a passive control element as indicated by the results presented in this study.

Key Words: Cylinder, Passive control, PIV, Turbulence Kinetic Energy, Deep water

ÖZ

YÜKSEK LİSANS TEZİ

DERİN SUDA DAİRESEL SİLİNDİRİN ARKASINDAKİ AKIŞIN DELİKLİ SİLİNDİR KULLANILARAK PASİF KONTROLÜ

Muhammed Murat AKSOY

ÇUKUROVA ÜNİVERSİTESİ
FEN BİLİMLERİ ENSTİTÜSÜ
MAKİNA MÜHENDİSLİĞİ ANABİLİM DALI

Danışman : Prof. Dr. Hüseyin AKILLI
Yıl: 2013, Sayfa: 141
Jüri : Prof. Dr. Hüseyin AKILLI
: Prof. Dr. Beşir ŞAHİN
: Doç. Dr. Mehmet BİLGİLİ

Mevcut çalışmanın amacı, derin suda dairesel kesitli bir silindirin (iç silindir), iç silindire eş merkezli olarak yerleştirilen delikli dış silindir vasıtasıyla aşağı akım yönünde olan girdap kopmasının kontrol edilmesidir. Eş merkezli olarak yerleştirilen silindir çiftlerinin akış karakteristikleri nicel olarak Parçacık Görüntülemeli Hız ölçme tekniği ile incelenmiştir. İç silindirin çapı $25 \leq D_i \leq 90$ mm arasında değişirken, dış silindirin çapı 100 mm olarak sabit tutulmuştur. Derinlik ortalamalı serbest akım hızı da dış silindir çapına bağlı Reynolds sayısı 10,000'e karşılık gelen U=100 mm/s'de sabit tutulmuştur. Deneyler, parametrelerin akış kontrolüne etkisini göstermek için yedi geçirgenlik oranı (β=0.25, 0.30, 0.40, 0.50, 0.60, 0.70 ve 0.80) ve dokuz çap oranı (D_i/D_o=0.25, 0.30, 0.40, 0.50, 0.60, 0.70, 0.80 ve 0.90) için yapılmıştır. Hem Reynolds kayma gerilmesi hem de türbülans kinetik enerjinin maksimum değerleri dış silindirin mevcudiyetiyle önemli derecede azalmıştır, ayrıca türbülans istatistiklerinin en üst değerlerinin yeri, yalın silindire göre aşağı akımın daha ileri noktalarında meydana gelmiştir. Bu çalışmada, en etkili akış kontrolü tüm çap oranları için $0.50 \leq \beta \leq 0.60$ geçirgenlik oranlarında gerçekleşmiştir. Çalışmanın sonuçlarına göre, delikli bir silindirin pasif kontrol yöntemi olarak kullanılabileceği sonucuna ulaşılmıştır.

Anahtar Kelimeler: Silindir, Pasif kontrol, PIV, Türbülans Kinetik Enerji, Derin su

ACKNOWLEDGEMENTS

This list endless if I have to thank all the people that made possible this work. My first thanks goes to my advisor Prof. Dr. Hüseyin AKILLI for his support, guidance and encouragement. He has been a great source of motivation, both personal and technical. His generous advices, encouragements and constant faith have made my time with him is a very challenging and rewarding experience.

I sincerely thank Prof. Dr. Beşir ŞAHİN for his continuous and effective advices to improve myself.

I would like to thank Prof. Dr. Orhan BÜYÜKALACA who is Rector of Osmaniye Korkut Ata University for his continuous and effective advices to improve myself.

My heartfelt thanks go to Engin PINAR, Göktürk M. ÖZKAN and Tahir DURHASAN. They always have been with me throughout the study. Without their moral and support it might be so difficult to finish this investigation.

I would like to thank all the academic staff of Energy Systems Engineering Department at Osmaniye Korkut Ata University.

In addition, I would like to thank Nehir TOKGÖZ, Erhan FIRAT and Bengi GÖZMEN for their continuous friendship, geniality and moral support.

Although the words are not sufficient to imply their importance, lastly and most importantly I would like to thank my family members who are my father Murat AKSOY, my mother Emine AKSOY, my brother Ömer Faruk AKSOY and my sister Merve AKSOY.

CONTENTS **PAGE**

LIST OF FIGURES **PAGE**

LIST OF ABBREVIATONS

D_i	: Inner cylinder diameter
D_o	: Outer perforated cylinder diameter
d	: Hole diameter of outer perforated cylinder
D_i/D_o	: Diameter ratio
β	: Porosity
H_W	: Water depth
H_L	: Laser height
U_∞	: Depth-averaged flow velocity
Re	: Reynolds number depending on the outer perforated diameter
TKE	: Time-averaged turbulence kinetic energy
$< u'v' >$	: Time-averaged Reynolds shear stress correlations
$<\omega>$	: Time-averaged vorticity
x	: Coordinate in streamwise direction
y	: Coordinate in spanwise direction
z	: Coordinate in crossflow direction

1. INTRODUCTION

Substantial research efforts have been established in studying flow characteristics over a bluff body immersed in fluids. Interaction of fluid and bluff bodies with each other may cause separation, shear layer instability and vortex shedding. Vortex shedding form which is occurred separation of flow from either sides of the body induces fluctuating pressure forces on the surfaces of the body. Thus, flow separation on a bluff body tends to vortex shedding which is reason of Vortex Induced Vibration (VIV) and that causes fatigue, vibrations, noise problems, and shortens the life of bluff bodies. For this reason experimental and numerical flow control investigations have been investigated to alleviate or annihilate VIV for practical applications.

1.1. Flow Around a Cylinder

Flow around a circular cylinder has been an attractive topic for more than a century due to its engineering significance and in part due to its tempting simplicity in setting up arrangements in experimental or numerical studies. Offshore risers, bridge piers, periscopes, chimneys, towers, masts, cables, wires, antenna, stacks and cooling towers are some of practical applications of flow around a cylinder (Said et al., 2008).

Roshko (1954) was, firstly, defined velocity fluctuation, spectra, and frequency of flow regimes for different Reynolds numbers. Flow dynamics, thus, around a cylinder depends only on the Reynolds number ($Re= \rho U_\infty D /\mu$ where ρ is the fluid density, U_∞ is the free-stream velocity far from the cylinder, D is the diameter of the cylinder and μ is the dynamic viscosity). There are different flow regimes from creeping flows ($Re<<1$) to fully turbulent flows ($Re\approx10^7$) and they can be classified as follows:

For $Re < 6$, the flow is steady and two-dimensional with only one separation point at the rear stagnation point.

For the range 6 < Re < 47, the flow is still steady and two-dimensional, in addition flow separates from the trailing edge of the cylinder and a vortex pair emerges with the wake region of the cylinder, whose recirculation length directly proportional with the Re. Vortex shedding slightly arises when the Reynolds number gets closer to the critical value of 47 due to the increasing instability, despite all of the imposed conditions are being held steady and these results in a well-known von Karman vortex street.

Gerrard (1964) proposed the vortex shedding mechanism as seen Figure 1.1. When a vortex starts growing (say the upper side vortex) being fed with vorticity from the respective shear layer, it draws the shear layer on the opposite side across the wake (lower side). This drawn shear layer (forming lower vortex) carries fluid with oppositely signed vorticity along with it and thus annihilates and cuts the vorticity supply to the upper vortex resulting in the shedding of the upper vortex. In the next turn, this lower vortex when grown sufficiently, would pull the upper shear layer across the wake (carrying fluid with oppositely signed vorticity) and due to vorticity annihilation, lower vortex would be shed downstream. This process repeats itself leading to alternate shedding of vortices from either side forming a vortex street downstream of the body (Kumar et al., 2008).

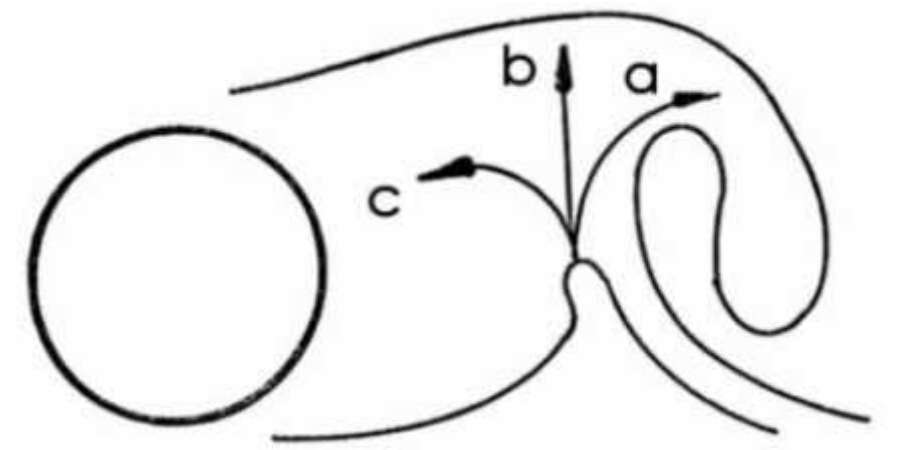

Figure 1.1. Mechanism of vortex formation by Gerrard (1964). a, b – fluid entrainment c – reverse flow

Unsteady and periodically oscillating forces are taken place after trailing edge of the cylinder for 47<Re<200. Periodic oscillations cause to change the surface

pressure distribution significantly around the cylinder as the cylinder was exposed to a sudden impulse. These vortices generate alternating high and low pressure regions on the leeward side or windward of the body in such a way that the cylinder experiences a periodic net force. This oscillation may amplify the vortex shedding, because now the cylinder itself is moving in the flow, forcing the vortex street to occur with large amplitude. The frequency of the vortices is given by dimensionless Strouhal number St (Strouhal number, $S_t = fD/U_\infty$, where f is the frequency, D is the cylinder diameter, U_∞ is the free-stream velocity) and the vortices produced in this manner are termed Strouhal vortices.

Finally for higher values of Re, i.e. Re>200, the flow becomes three-dimensional and turbulent.

1.2. Karman Vortices and Kelvin – Helmholtz Vortices

Laminar and transitional wakes of cylinders are stated that two types streamwise vortices which are Karman and Kelvin – Helmholtz vortices. “Transition waves” appears in the shear layer separating from the surface of the cylinder at a sufficiently high value of Reynolds number. These detectable waves are in the region of the wake extending from the separation point on the body to the first appearance of the large-scale Karman vortex. As a result, a vortex is shed from the cylinder when the local pressure changes periodically. Therefore, the cylinder is subjected to a fluctuating drag and lift in addition to the mean drag and lift. The drag, lift and vortex shedding frequency are normally expressed in non-dimensional forms as the drag coefficient C_D, the lift coefficient C_L, and the Strouhal number St, respectively. These three non-dimensional parameters depend on the nature of both the approaching flow characteristics and the cylinder location. When the cylinder is located near a plane boundary, the bed proximity and the velocity gradient in the boundary layer, as well as the turbulent characteristics of the boundary layer, also have some influence on these parameters.

When the value of Reynolds number is sufficiently high, then these transition waves take the form of train of Kelvin-Helmholtz vortices shown in Figure 1.2.

Kelvin-Helmholtz vortices in the shear layer are an essential feature of the transition from a laminar to turbulent state. In the bluff body community, these small-scale vortices are often referred to as Bloor-Gerrard vortices. The onset of “transition waves” is expected to be strong function of the disturbance level of the free stream, in view of the fact that they arise from convective-type instability, as described by Ho and Huerre (1984). Bloor (1964) detected the small-scale vortices for the range of Reynolds number Re>1300, however, Unal and Rockwell (1988) first noted these vortices at Re_d=1900. Wu et al. (2007) discussed the possible influence of background disturbance levels and observed these waves over the range of Reynolds numbers $1000 \leq Re \leq 3000$. As a consequence of this transition process, the first Karman vortex formed from the cylinder at Re_D=5000 is essentially turbulent (Figure 1.2).

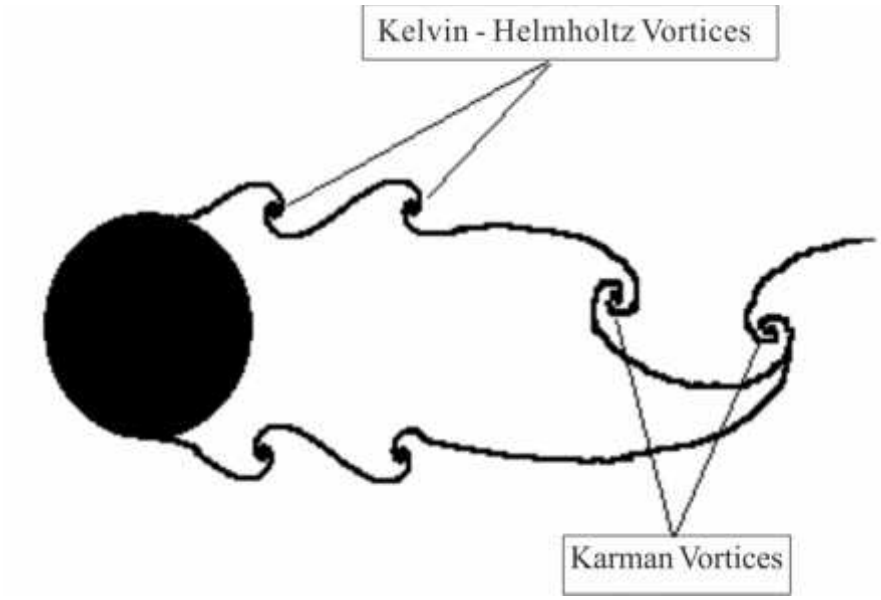

Figure 1.2. Karman and Kelvin – Helmholtz (secondary) vortices from circular cylinder

Govardhan and Williamson (2000) presented in terms of the true reduced velocity, U_rSt/f^*, where St is Strouhal number and f* is ratio of cylinder response frequency to natural frequency measured in still water, to explain the fluctuations and frequency response of the cylinder. When the structure is free to move in the streamwise direction, resonance will occur when the shedding frequency matches

half the response frequency, $U_rSt/f^* = 0.5$, as the drag forces F_D fluctuate at a frequency twice that of the lift forces F_L and vortex shedding.

The amplitude response of a cylinder oscillating in the streamwise direction is characterized by two branches, the first of which occurs for $U_rSt/f^* \approx 0.35\text{-}0.45$ which is called Kelvin Helmholtz vortices. Von Karman Street (which two vortices shed alternately from either side of the cylinder) is observed for $U_rSt/f^* \geq 0.4$ (Cagney and Balabani, 2013). Karman and Kelvin Helmholtz vortices observed in the wake of stationary cylinder as shown Figure 1.3. by Cagney and Balabani (2013).

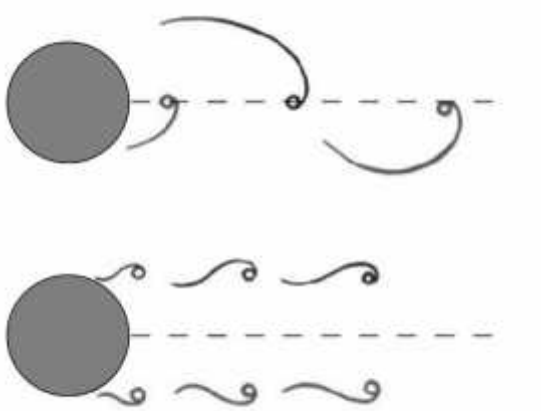

Figure 1.3. Von Karman Street (upper one) and Kelvin – Helmholtz vortices (lower one) in the wake of circular cylinder (Cagney and Balabani, 2013)

1.3. Flow Control

If a bluff body exposed to a flow having sufficiently high Re Numbers, the flow separates from a wider section of the body resulting in periodic vortex shedding. This condition results in a significant pressure drop on the rear surface of the body. Vortex shedding from bluff bodies causes serious structural vibrations, acoustic noise and resonance; enhanced mixing (which is also advantageous for better heat transfer) and increases in the mean lift and drag fluctuations. Hence, effective control of the vortex shedding is very important in many engineering applications.

Roshko first measured the period of Karman vortex shedding downstream of a bluff body in 1955 and after his invention researchers started to investigate the vortex

shedding and near-wake flows. Two factors are centrally important in the vortex formation and shedding (a) the shear layers should roll up to form vortices with a sufficient strength (b) the shear layers should interact closely with each other. If any one of these factors (or both of them) is disabled or disrupted, then, it would prevent proper roll up of shear layers and thus, the vortex shedding phenomenon which would ultimately suppress the VIV (Kumar et al., 2008). Furthermore, investigators focused on suppression of the vortex shedding since it is a serious problem for many areas of science.

In this manner, many passive and active control methods were carried out to control vortex shedding downstream of a two-dimensional bluff body, such as a circular cylinder and a two-dimensional blunt-based bluff body. Examples include base bleed, splitter plates, stream-lining the structural geometry, oscillation, suction and blowing, acoustic excitation, and electromagnetic control. For these control techniques, a classification may be done by dividing the control methods into two categories, namely passive and active flow control.

1.3.1. Passive Control

Passive control aims perturbation of the flow structure with placing external parts into the downstream of flow or modifications on the bluff body. Passive control techniques include geometric shaping to manipulate the pressure gradient, the use of fixed mechanical vortex generators for separation control.

Passive control techniques are widely used for flow control applications. They have same advantages of being easier to implement, less expensive in cost, and more stable. The methods have proved successful particularly in offshore explorations and marine hydraulics.

Zdravkovich (1981) proposed control techniques that can be classified into three categories:

(i) The control of shear layer by surface protrusion (tripping wire, fin, helical strakes, helical wires, studs, etc.), which affects flow separation lines (James and Truong, 1972); this can be further subdivided into omnidirectional and unidirectional. The omnidirectional techniques are those not affected by the direction

of flow velocity; for example, helical strakes, and helical wires. The unidirectional are those effective only for a given direction of flow velocity; for example, straight fins. The full shrouds are omnidirectional, while incomplete shrouds become unidirectional.

(ii) The control of the entrainment layers by shrouds (perforated gauze, axial rods, etc.) that supply irrotational fluid to the entrainment layers (Knell, 1969)

(iii) The instability control of wakes by near-wake stabilizers (splitter plate, guiding plates, base-bleed, slits cut along the models, etc.) that reduce the interaction of two opposite shear layers (Roshko, 1954, Bearman, 1965, Wood, 1967, Aplet, West and Szewczyck, 1973).

Blevins (1990) summarized some of passive control techniques in his study. He achieved to control by stream lining the structural geometry or introducing passive control devices on the cylinder (Figure 1.4).

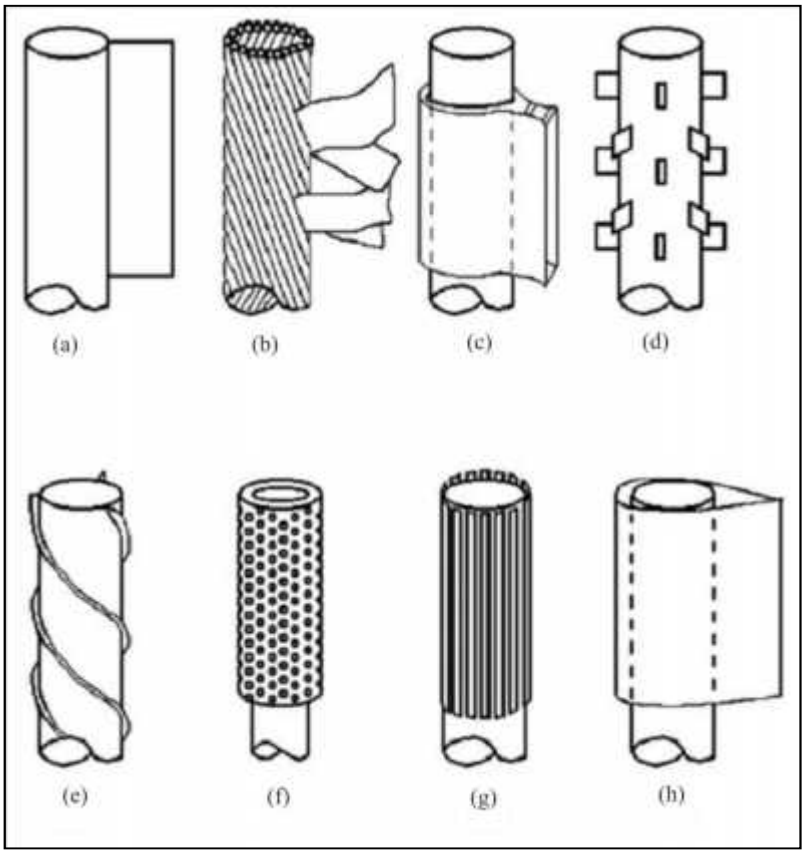

Figure 1.4. Passive control devices for suppressing VIV; (a)-splitter plate, (b)-ribboned cable, (c)-guide vanes, (d)-spoiler plate, (e)-helical strake, (f)-shroud, (h)-streamlined fairing (Blevins,1990)

1.3.1.1. Splitter Plate

Splitter plate is a well-known external part to control vortex shedding. The use of splitter plates to control bluff bodies vortex shedding provides an important change in flow structure downstream of the cylinder. A short splitter plate is placed along the wake center plane. Attached plates perform great changes on the shedding frequency depending on the length. At high Reynolds number, the vortex shedding frequency doesn't decrease monotonically as the length of the splitter plate increases; the shedding frequency decreases for l<D and increases for D<l<2dD, and then it decreases as the length of the plate further increases.

The vortex shedding downstream of a circular cylinder completely disappears when the length of the splitter plate is larger than a critical length, and this critical length is found to be proportional to the Reynolds number.

The net drag is significantly reduced by the splitter plate, and there exists an optimum length of the plate for minimum drag at a given Reynolds number.

This optimum length of the plate is nearly the same as the size of the time-averaged deformed separation bubble due to the plate.

Schematic representation of attached splitter plate to the circular cylinder is shown in Figure 1.5.

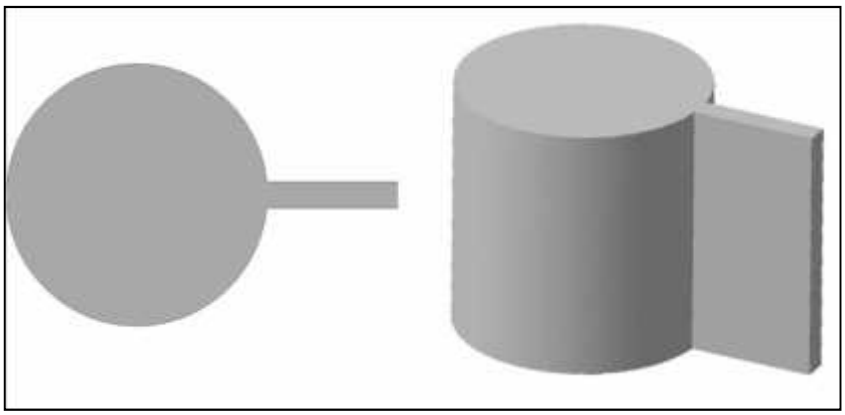

Figure 1.5. Schematic representation of attached splitter plate; top view (left) and isometric view (right)

1.3.1.2. Small Cylinder

Vortex shedding past a circular cylinder is controlled over a limited range by the proper placement of a smaller control cylinder close to the main cylinder. There exists a domain close to the main cylinder where the placement of a control cylinder can completely suppress the vortex shedding for flows at a Reynolds number of 80 or less. The actual extent of this domain depends on the Reynolds number of the flow and the ratio of the diameter of the both two cylinders. Even though the flow remains unsteady for Reynolds numbers larger than 80, the presence of the control cylinder has a significant effect on the flow. It has also been reported that in certain cases suppression of vortex shedding is accompanied by a significant reduction in the mean drag coefficient.

1.3.1.3. O-Ring

O-rings (or it can be called helical strake) are installed as surface protrusions for controlling the flow around a cylinder. The test cylinders are supported at both sides using identical load-cells: one for measuring force and the other a dummy for balancing. Figure 1.6 represents the models of helical strake.

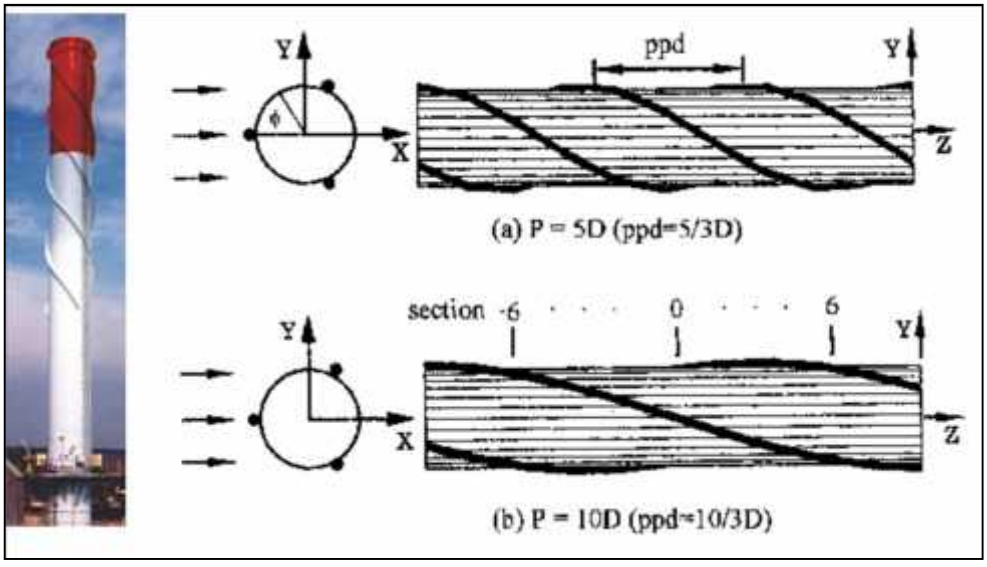

Figure 1.6. Surface protrusions schematic of diagrams of models

1.3.1.3. Base Bleed

Another well-known method for the suppression of vortex shedding from bluff bodies consists in bleeding fluid from the blunt base. The aim is to suppress vortex shedding completely at some supercritical Reynolds number by the base bleed. The application of base bleed through the passive ventilation from the limited regions of base could significantly reduce pressure drag for bluff bodies.

1.3.2. Active Control

Active control methods, applying some sorts of energy into the flow, have been developed in order to solve vortex shedding problems. The aim of active control is to exploit the instability of the wake, which is the cause of the vortex formation, to indirectly modify the mean wake velocity profile and drag.

There are two primary advantages to the active flow control methods that aren't achievable by the passive flow control techniques. First active flow control technique leverages and controls a natural stability of the flow to attain a large effect using small localized energy input. Control is most effective when the control input is introduced locally at a high receptivity region. Secondly, active control can be used to control complex, dynamical processes like turbulence production in turbulent boundary layers to reduce skin friction and hence viscous drag where the reduction is proportional to the surface area covered by the actuators. On the other hand, to put energy from outside is the disadvantage of the active control techniques. There are various active control techniques such as; feedback control, electro-magnetic control, rotating circular cylinder, wake heating, suction and blowing.

1.3.2.1. Feedback Control

Feedback control method has been studied by many researchers in the last two decades. This control method has been applied to various problems in thermal and

fluid engineering. Very recently; the effect of the feedback control on the fluid force on the cylinder was examined experimentally by Fujisawa et al. (2003, 2004).

A hot-film probe, a phase shifter, amplifiers and a dynamic shaker are used to apply feedback control method. In order to produce strong signal of vortex shedding, the hot-film probe is placed in one of the shear flows of the wake. The signals from the feedback probe are phase-shifted and amplified to drive the shaker which is connected to the cylinder to generate perturbations in the wake. A monitor hot-film probe is also placed in the wake to assess the control effect on vortex shedding. Signals from both the feedback and the monitor probes are converted into frequency spectra by a computer.

So as to measure the controlled flow field parameter, a sensor is also placed downstream of the actuator in the feedback control loop.

1.3.2.2. Electro-Magnetic Control

The main advantage of electromagnetic control strategy for electrically conducting fluids is that the Lorentz force acts as a volume force inside the fluid, and it may be tuned to act only in specific region of the flow. Many techniques using electric and magnetic fields have been developed in weakly conducting fluids since 1960s so as to achieve turbulent boundary layer control, transition delay and drag reduction.

The cylinder body is covered with electrodes and the permanent magnets side by side in the order of positive electrode, N-pole magnet, negative electrode, S-pole magnet, and a sequence which is repeated once more ending with a positive electrode in the axial direction of the circular cylinder. So, the Lorentz force occurs (acts) in the circumferential direction of the cylinder. If it is desired Lorentz force’s direction can be changed by altering the poles of the each electrode.

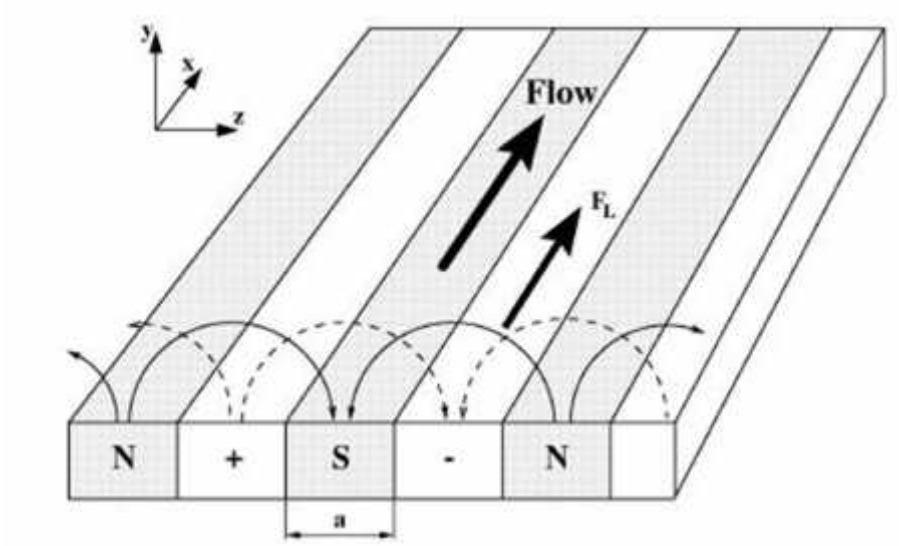

Figure 1.7. Lorentz force generated by crossed magnetic fields

Weier et. al.(1998), visualized the flow field at Re=760, using a 2 cm diameter circular cylinder and numerically simulated at Re=200 under the Lorentz Force directed with the mean flow in the range from 5° to 175° from the stagnation point along the cylinder circumference (Figure 1.7). Figure 1.8 shows a sketch of the cylinder used for the experiments.

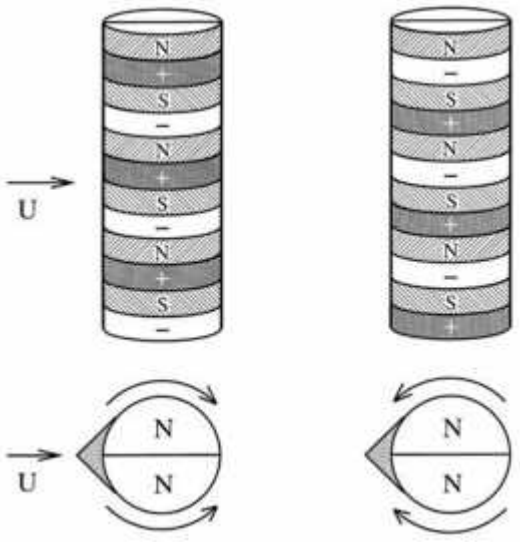

Figure 1.8. Sketch of the cylinder equipped for experiments of Weier et. al.

1.3.2.3. Rotating Circular Cylinder

The flow is controlled by a rotating circular cylinder which is placed in the flow field. Schematic representation of rotating circular cylinder is shown in Figure 1.9. At this control method, the forcing frequency and natural shedding frequency are observed: when the forcing frequency is lower than the natural shedding frequency an initial clockwise vortex is formed on the lower half of the cylinder when the cylinder is rotated in the counter-clockwise direction and a counter-clockwise vortex is formed on the upper half when the clockwise rotation starts. This leads to a non-synchronized vortex formation mode which cannot lead to the suppression of Karman vortex shedding.

When the forcing frequency is higher than the natural shedding frequency an initial reactive clockwise vortex is formed on the upper half of the cylinder when the cylinder is rotated in the counter clockwise direction and a counter clockwise vortex is formed on the lower half when the clockwise rotation starts which leads to a synchronized vortex mode (this is one of the reasons why the optimal values for the forcing frequency obtained in the previous section cannot be lower than the vortex shedding frequency).

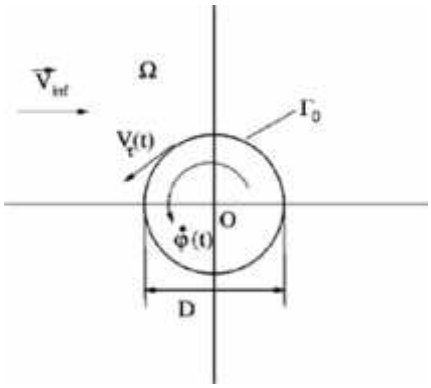

Figure 1.9. Rotating circular cylinder flow configuration

The behavior of the drag coefficient C_D is determined by the fact that flow separation is a major source of pressure drag and the moving-wall effects will postpone this separation. Separation is completely eliminated on the side of the cylinder where the wall and the free-stream move in the same direction and on the other side of the cylinder separation is developed only incompletely.

1.3.2.4. Rotary Oscillation of the Small Cylinders Located Downstream of the Main Cylinder

The flow is aimed to control by using small amplitude transverse cylinder oscillations with displacement of a few percent of the cylinder diameter in this technique. Near the main cylinder, two control cylinders are placed and these control cylinders rotate with an obvious rate.

Utilizing rotating control cylinders depends on a variety of parameters. Some of them are the relative sizes of the main and control cylinders, their relative arrangements, and the rotation rate of control cylinder.

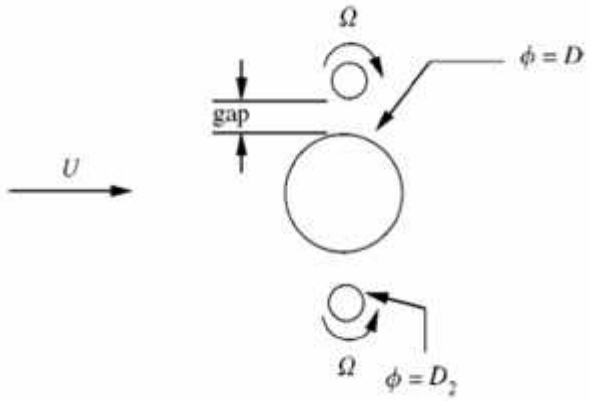

Figure 1.10. Description of the relative location of the main and control cylinders

1.3.2.5. Wake Heating

The control of vortex shedding downstream of a horizontal cylinder or a flat ribbon can be easily realized using heat input to the cylinder. In air flow, increase of the heat input to the cylinder or ribbon leads to a suppression of the vortex shedding while in a liquid flowing around a heated cylinder or ribbon the effect is the opposite. However in liquids the range of heating conditions where the buoyancy effects can be ignored is more limited.

Behaviors' of liquids and gases are opposite. And this suggests that this control is due to both changes of dynamic viscosity and density with temperature and does not only dependent on density changes as claimed by Yu and Monkewitz (1990). This opposite behavior found in air and in water suggests that the effect of the

change of viscosity is predominant. The changes of the density and the viscosity due to the heating of the near wake lead to slight changes in velocity profiles and consequently instability conditions and amplitude of the shedding vortices.

1.3.2.6. Suction and Blowing

One of the methods of active control is suction and blowing. When wake flows controlled by suction and blowing, the flow's global stability state can be interpreted by considering the modification of the near wake profiles, and its implications on the flow's stability properties. There are two main effects of suction applied to cylinder base: the suction increases the magnitude of negative velocities, which acts in favour of instability increase in terms of local temporal growth rate increase. The second effect of suction is that it decreases the length of the recirculation zones and thus decreases the streamwise extent of absolute instability.

On the other hand, the effects of blowing are opposite to suction's effects: linear temporal growth rates in the near wake are expected to be decreased, due to decreased back flow, and the extent of absolute instability is expected to increase. Therefore, in both cases, one has to rely on phenomenological observations, to determine which action prevails for a given combination of the problem parameters.

2. PRELIMANARY WORK

2.1. Flow Control Techniques

Several control techniques are involved in the literature survey. Some of important scientists such as Bearman (1984, 2011), Sarpkaya(2004) and Williamson (2004) overemphasized importance of vortex shedding suppression downstream of a 2-D bluff body such as circular cylinder. Choi et al. (2008) summarized both active and passive control techniques in his review. He, also, discussed the Reynolds-number dependence, the lowest possible drag by control, and control efficiency. Another familiar review by Kumar et al. (2008) mentioned only passive control methods. The review indicates that patented passive control techniques are used for practical applications such as marine deep water environments.

2.1.1. Passive Flow Control Techniques

2.1.1.1. Splitter Plate

Roshko (1954) was notably one of the first to report periodic vortex formation suppression using a circular cylinder connected with a splitter plate for a Reynolds number of 1.45×10^4. He also showed that, by positioning this splitter plate at different fixed distances in the fully developed cylinder-wake, the Strouhal number St diminishes as the distance between the cylinder and the plate increases up to a limit position (G ≈2.7D). He also observed that a splitter plate of chord 5D, attached to the cylinder, results in suppression of shedding. A plate of chord 1D does not inhibit formation of vortices but changes the shedding frequency slightly.

Roshko (1955) observed flow changes at $Re_D=1.45\times10^4$ when splitter plates were inserted behind a cylinder. When the plate was attached on the cylinder base and the length of the splitter plate (l) was larger than 5D, the vortex shedding disappeared, and thus drag was significantly reduced. On the other hand, he also observed flow changes as the plate of l=d moved downstream. When the splitter

plate was located downstream less than 4d, the Strouhal number S_t decreased and the base pressure increased as the splitter plate moved downstream. However, when the splitter plate was located farther downstream, the flow field did not show much difference from the natural vortex shedding.

Bearman (1965) investigated the flow downstream of a two-dimensional model with a blunt trailing edge and fitted with splitter plates at Reynolds numbers between 140000 and 256000. He measured the base pressure and shedding frequency and showed that the existence of a splitter plate increases the base pressure significantly (thereby reducing the pressure drag), even for very short plate length. These studies suggest that the effect of the splitter plate and base bleed is to delay the upper and lower separated shear layers interacting with each other and hence they increase the formation length (position at which the vortices are fully formed or, in a time-average sense, the length of the mean recirculation region). As a result, vortex shedding disappears for a connected splitter plate length L_{sp} equal to 2D.

Gerrard (1966) studied a mechanism of vortex generation downstream of a cylinder. He conducted experiments at $Re_D=2\times10^4$ to study the vortex size, frequency, and effect of the splitter plate attached on the cylinder, effects of free-stream turbulence. From that study, he showed that the Strouhal number S_t decreased when the length of the splitter plate was smaller than d, but it increased for $D<L<2D$. He also showed that the swirling formation zone is under a strong elongation in the presence of a SP and that two modes of swirling formation could appear according to the length of the separating element and its distance from the model.

Unal and Rockwell (1987) divided the wake region into two separate regions: the pre-vortex formation region and the post-vortex formation region. They found that the pressure on the splitter plate was suddenly changed when the plate moved from the pre-vortex formation regime to the post-vortex formation regime.

Vortex shedding from bluff bodies with splitter plates was experimentally investigated by Nakamura, 1996. It was shown that vortex shedding from bluff bodies with extended splitter plates is characterized by the impinging shear layer instability, where the Strouhal number S_t in terms of splitter plate length increases in stepwise direction with increasing splitter plate length.

Recently, Kwon and Choi (1995) investigated the effect of the splitter plate on the laminar vortex shedding downstream of a circular cylinder at Reynolds numbers of 80-160. They showed that for $Re_D \geq 120$ the shedding frequency changed similarly as just described, whereas for $Re_D \leq 100$ the shedding frequency monotonically decreased as the plate length increased. They attributed the increased shedding frequency at L >D in the case of $Re_D \geq 120$ to a generation of the secondary vortex at the tip of the splitter plate. This secondary vortex near the tip of the splitter plate may also be a strong source of the flow-induced noise.

Cimbala and Garg (1991) investigated the effect of the attached splitter plate on the flow characteristics downstream of a fixed cylinder and a freely rotating cylinder, respectively. For the case of a freely rotating cylinder, the flow field with the plate of L>2D was similar to that of the fixed cylinder with an attached plate. However, when L<2D, the flow field was similar to that without the splitter plate. They also showed for the case of a fixed cylinder that the Strouhal number S_t increased for D<L<2D and it decreased as the length of the plate further increased.

An experimental investigation was carried out by Mansingh and Oosthuizen, (1990) to study the effect of a splitter plate on the two-dimensional wake of a bluff body with fixed separation points. This experimental study has shown that the characteristics of the wake downstream of a bluff body with fixed separation points can be considerably altered by placing a splitter plate on the wake centerline downstream of the bluff body. The effect of splitter plates on the wake flow characteristics of a rectangular cylinder with a splitter plate shows a relatively small change in the Reynolds number.

Miau et al. (1993) carried out measurements of instantaneous pressure fluctuations on a trapezoidal cross-sectional cylinder. Their results indicate that the low frequency variations embedded in the vortex-shedding process can be successfully suppressed by insertion of a splitter plate whose length is twice the maximum width of the trapezoidal cylinder.

The angular motion of a freely rotatable cylinder with splitter plate has been studied numerically by Xu et al. (1993). It is found that, for subcritical the Reynolds numbers, the splitter plate aligns itself in the flow direction. On increasing the

Reynolds number, a symmetry breaking bifurcation appears and the splitter plate migrates to a stable off-axis position.

Unal and Rockwell (1988) carried out a similar study with a plate that is detached from the cylinder. They found that by placing the plate appropriately, compared to a cylinder with no control, it is possible to obtain more than double the vortex formation length. For low the Re the vortex shedding is completely eliminated while for the higher Re the large scale shedding is suppressed but the shear layer instability remains.

Ozono (1999) studied the effect of a plate of length 1D kept at various locations, including those away from the wake centerline, downstream of the cylinder for $6.7\times10^3 < Re_D < 2.5\times10^4$. Beyond a certain critical gap between the plate and the cylinder, for a certain range, the Strouhal number S_t exceeds the natural one. This is because of a flow mode in which the shear layer separated from the cylinder is forced to interact with the splitter plate.

The flow around a circular cylinder with a few interference elements shifted along the wake was investigated (Ozono, 1999). It was concluded that the vortex shedding can be suppressed critically even when the splitter plates are asymmetrically arranged downstream of the cylinder.

Lin and Wu (1994) conducted a numerical study for the $Re_D = 100$ flow to see the effect of a splitter plate. They found that a splitter plate of length 2D attached to the cylinder is sufficient to completely suppress vortex shedding. It was also found that a splitter plate whose upstream edge is located at more than 2.5D from the cylinder is ineffective of suppressing vortex shedding.

Roshko (1993) controlled the flow around a circular cylinder by attaching a splitter plate downstream of the cylinder and investigated the suppression of vortex shedding. When the gap between the cylinder and splitter plate was large, the effect of the splitter plate became strong. The parameter that had the greatest effect on the vortex shedding was the gap width rather than the length of splitter plate.

Zhou et al. (2005) conducted a numerical study on suppression of fluid forces on a square cylinder in cross-flow controlled by a flat plate. They found that the existence of the control plate changes the flow features in front of the square cylinder

totally. The drag acting on the square cylinder and the total drag acting on the 2 bodies (the square cylinder together with the control plate) are normally reduced by the control plate. The maximum reduction of the drag acting on the square cylinder and the optimum position of the control plate are given for a particular control plate height. They also revealed that the amplitude of the fluctuating lift on the square cylinder is well suppressed if the control plate is used. The fluctuating lift can be completely suppressed if the control plate with a certain height is placed at an appropriate position.

Akıllı et al. (2005) investigated the effect of splitter plate on the suppression of vortex shedding in shallow water using the Particle Image Velocimetry (PIV) technique. Splitter plates with a length of 50 mm, which is equal to the diameter of the cylinder (D), were used during the experiments. Gap distance between the base of the cylinder and the leading edge of the splitter plate ranged from 0 to 2D. Velocity vector field and corresponding vorticity contours and streamline topology and Reynolds stress concentrations were used to explain the characteristics of the flow. The splitter plates having different thicknesses presented the same influence on the flow characteristics. The splitter plate has a substantial effect on suppression of the vortex shedding for the gap ratio between 0 and 1.75D. In this gap ratios, shear layers extend up to the trailing edge of the splitter plate preventing the entrainment of the free- stream flow into the base region. For G/D=1.75, the normalized Reynolds stress has a peak value of 0.0158 which is approximately 8.5 times smaller than the concentrations occurring for a bare cylinder. After passing the splitter plate, the flow starts to oscillate with smaller frequency compared to the natural frequency of the bare cylinder. When the splitter plate was located at 2D location, no effect of the splitter plate was observed.

Akıllı et al. (2008) investigated experimentally passive control of vortex shedding downstream of a circular cylinder by splitter plates of various lengths attached on the cylinder base in shallow water flow (Re=6300). At this study the length of the splitter plate was varied from L/D=0.2 to L/D=2.4 in order to see the effect of the splitter plate length on the flow characteristics. Instantaneous and time-averaged flow data clearly indicate that the length of the splitter plate has a

substantial effect on the flow characteristics. They found the flow characteristics in the wake region of the circular cylinder sharply change up to the splitter plate length of L/D=1.0 and above this plate length, small changes occur in the flow characteristics.

Turki (2008) numerically investigated the passive control of flow by introducing a splitter plate downstream of a square cylinder inside a horizontal channel at the Reynolds number within the range of $110 \leq Re \leq 200$ and for a fixed blockage ratio of $\beta = h/H = 1/4$ and a fixed position of the square cylinder. In examining the instantaneous flow fields, he found that the critical length of the splitter plate L_c, characterizing the disappearance of vortex shedding, can be correlated by a linear relationship: $L_c = 0.0373\ Re–3.4373$. He also analyzed the effect of the splitter plate length and its location in the wake region on the Strouhal numbers S_t, and the drag C_d and lift C_l coefficients. He came on the conclusion that, by varying the splitter plate length, the Strouhal number shows two different behaviors for the Reynolds number investigated. And finally he observed that in the variation of the S_t and the C_d with the splitter plate location G and for Re = 150 and 200, a sudden increase in those quantities was noticed at the optimal location of G=3.27.

Shukla et al. (2009) studied the problem of a hinged-splitter plate in the wake of a circular cylinder where the splitter plate can rotate about the hinge at the base of the cylinder due to the unsteady fluid forces acting on it, and hence the communication between the two sides of the wake is not totally disrupted as in the rigid splitter plate case. They investigated that this problem in the limit where the stiffness and internal damping associated with the hinge are negligible, and the mass ratio of the splitter plate is small. It is concluded that the splitter plate oscillations increase with Reynolds numbers at low values of Re, and are found to reach a saturation amplitude level at higher Re, such as Re > 40000.

Assi et al. (2009) achieved suppression of cross-flow and in-line VIV of a circular cylinder, with resulting drag coefficients C_d less than that for a fixed plain cylinder using two-dimensional control plates. He demonstrated how vortex-induced vibration can be practically eliminated by using free-to-rotate, two-dimensional

control plates and further conclusion is that these devices achieve VIV suppression with drag reduction. He found the largest drag reduction to have a drag coefficient equal to about 60% of that for a plain, fixed cylinder over the Reynolds number range of the experiments, up to 30 000.

Assi et al. (2010) studied on a pair of circular cylinders to investigate the effectiveness of pivoting parallel plates as wake-induced vibration suppressors. Measurements of amplitude of vibration and average drag are presented for a circular cylinder, free to respond in the cross-flow direction, with mass ratio of 2 and a damping level of 0.7% of critical damping. Reduced velocities were up to nearly 30, with associated Reynolds numbers up to $2.3x10^4$ and the results presented are for a center-to-center separation of cylinders of 4 diameters. They showed how vortex-induced vibration and wake-induced vibration of the downstream cylinder of a tandem pair can be practically eliminated by using free to rotate parallel plates. They also presented the results for a single splitter plate and helical strakes for comparison.

Gozmen et al. (2013) investigated the effects of splitter plates having different heights and lengths located in the downstream of the circular cylinder. The length of the splitter plate (L) was varied within the range of $0.5 \leq L/D \leq 2$ and ratio of plate height (h_p) to water height (h_w) is between 0.25 to 1.0. They obtained that flow structures changed significantly with height and length ratios of splitter plates in shallow water. The wake region downstream of the cylinder was elongated along the streamwise direction with increasing plate length and depth. The case of $h_p/h_w=0.75$ for L/D=2 was the most effective case on the control of vortex shedding. The transverse Reynolds normal stress was more effective on the attenuation of turbulent kinetic energy than the streamwise Reynolds normal stress. The peak value of transverse Reynolds normal stress was reduced to 90% of that of the bare cylinder at most.

Bao and Tao (2013) numerically investigated the wake control of a circular cylinder by dual plates symmetrically attached at the rear surface of the cylinder within the low Re number regime. The two flat plates were placed in parallel form and the angle was varied in the range $\theta_f=0 - 90^o$. The results showed that dual plates increased drag reduction and caused stronger wake suppression at relatively shorter

plate lengths. The attachment angle had a crucial effect on the control efficiency. For the range of $40^o \leq \theta_f \leq 50^o$, the free shear layers reattached on the outside surface of the control plates. So, this regime between $40^o \leq \theta_f \leq 50^o$ was the most effective range associated with the maximum drag reduction.

2.1.1.2. Base Bleed

In essence, Chen and Jirka, (1995) demonstrated that it is possible to completely attenuate the mechanism of absolute (global) instability leading to large-scale vortex formation in the shallow wake.

This result is in accord with the investigation of a wake of very large spanwise extent past a porous plate, investigated by Inoue (1985).

These findings build upon the earlier investigation of Castro (1971), who demonstrated attenuation of the near-wake vortex formation via base bleed from porous plates of large spanwise extent.

Base bleed has also been shown to substantially alter the formation process of vortices from a streamlined body with a blunt trailing edge, as demonstrated by Wood (1964, 1967) and Bearman (1967).

Another approach, which is equivalent to the aforementioned concept of base bleed, is self-bleed through a slit cut along the entire span of the cylinder, as described by Igarashi (1978), who demonstrated that the region of vortex formation was displaced significantly downstream, relative to the case of a plain cylinder.

Wong (1985) pursued a more advanced approach involving self-injection at two locations near the base of the cylinder, whereby the injection flow was through an annulus opened at the forward stagnation point. This technique was applied to an elastically mounted cylinder, and it was demonstrated that vibrations could be suppressed completely when the effective injection rate was very small. In all of these investigations involving base bleed, with some exceptions, relatively little information is available on the quantitative flow structure associated with the concept of base bleed.

More recently, in a somewhat broader sense, Amitay et al. (2004) studied wake interference through synthetic surface jets in an effort to alter the aerodynamic performance of two dimensional circular cylinders.

Patnaik and Wei (2002) injected angular momentum into the base region of square cylinders at a low Reynolds number to suppress the wake instability, while Lu et al. (1999) reported drag reduction and wake stabilization benefits from base bleeding to the spheres. The effects of base bleed (or base injection) in the generic two-dimensional square cylinder configuration have not been studied previously in detail and also only a limited amount of information on the performance of this type of wake interference has been reported for the studied aerofoil type geometries. Additionally the potential value of the above setup or other variants of similar type within the context of an active or passive control flow device warrants further investigations into the details of these complex unsteady separated flows.

Baek and Karniakidis (2009) numerically investigated the hydrodynamic effect of a slit in circular cylinders with the goal of finding a geometric modification that minimizes vortex-induced vibrations (VIV) without any energy consumption. A slit parallel to the incoming flow is introduced and found to be very effective in suppressing VIV by either weakening or detuning vortex shedding. Through a series of simulations, they found the optimal size of the slit to suppress VIV at Reynolds number of 500; this size is smaller at a higher Re = 1000. They confirmed the effectiveness of the slit in suppressing VIV over a wide range of values of the reduced velocity. They also reported that the jet flow through a slit changes the stability in the wake of cylinder by inducing two small pockets of absolute instability at the back of the cylinder followed by bands of convectively and absolutely unstable regions.

2.1.1.3. Wavy Cylinder

In recent years, increasing attention has been focused on the three-dimensional phenomena in the nominally two-dimensional flow behind a smooth cylinder. As a natural extension of these studies, there has been heightened interest in the flow

around cylinders with a wavy geometry. Certain wavy cylinder geometries have been found to bring about considerable drag reduction and suppression of vortex-induced-vibration (VIV) (Bearman and Owen 1998; Owen et al. . 2001), making them suitable for passive flow control. This characteristic has further prompted several studies on flow around wavy cylinders by measuring the drag force, surface pressure and flow velocity profiles.

Bearman and Tombazis (1993) and Tombazis and Bearman (1997) investigated the three-dimensional features of the wake downstream of a blunt-based model with a wavy trailing edge at a Reynolds number of 40 000. For a two-dimensional body at high Reynolds numbers, it was noted that vortex dislocations appeared in the wake apparently randomly in time and spanwise position. However, they observed that the introduction of a spanwise waviness at the trailing edge fixed the positions of these vortex dislocations along the span of the body. They found that by increasing the wave steepness, defined as the ratio of peak-to-peak wave height divided by the wavelength, the base pressure was increased which resulted in a drag reduction. The maximum drag reduction of 34% at a Reynolds number of 40 000 occurred for a wave steepness of 0.14 (the non-dimensional wavelength, defined as the wavelength divided by the base height, was equal to 3.5). Based on these facts, they concluded that encouraging the formation of dislocations in the wake reduces the drag.

Bearman and Owen (1998) experimentally investigated the influence of spanwise waviness of the separation lines on the flow around common bluff forms. By performing the experiments in wind tunnel, they concluded that the drag of thin plates and rectangular cross-section bodies can be substantially reduced by the introduction of spanwise waves into the flow separation lines. They also indicated that drag reductions of up to at least 30% are achieved and for wave steepnesses in excess of between 0.06 and 0.09, vortex shedding is completely suppressed.

Keser et al. (2001) used a 3-D discrete vortex method to simulate the separated flow around a circular cylinder with sinusoidal waviness along its span. However, all the above studies were based on various assumed forms for the flow field from the nodal to the saddle point of attachment.

In their experimental study, Ahmed and Bays-Muchmore (1992) measured the surface-pressure distributions of a set of wavy cylinders with different axial wavelengths based on the mean cylinder diameter, D. The Re in their experiment was 20 000 and the mean static pressure data was determined using linear interpolation. Their results showed that the separated flow structures near the geometric nodes were distinctly asymmetric for a large fraction of time, and the sectional drag coefficients C_d at the geometric nodes are greater than at the geometric saddle.

In addition, Ahmed et al. (1993) visualized the wake of a sinusoidal cylinder and measured the total pressure, mean velocity profiles and Reynolds stress. They described the topology of the boundary layer separation lines and the subsequent 3D development of turbulent structure of the wake. Formation of trailing streamwise vortices downstream of the nodal points of separation resulted in a locally narrower wake, a more rapid wake velocity recovery and suppression of turbulence development within the separated boundary layer.

Lam et al. (2003) used a LDV system to measure the velocity profiles of the wake downstream of a sinusoidal cylinder in the range of Re=3,000–9,000. They concluded that the long vortex formation length of wavy cylinder should bring about drag reduction and suppression of Vortex induced vibration.

Nguyen (2004) investigated flow characteristics of the near-wake downstream of two sinusoidal cylinders (model 1 with $\lambda/Dm=1$ and model 2 with $\lambda/Dm=2$) by measuring the drag coefficients C_d, mean velocity and turbulence intensity profiles over Reynolds numbers ranging from 5,000 to 20,000. The sinusoidal cylinder with axial wavelength $\lambda/Dm=2$ was found to reduce the drag coefficient C_d by about 22% at Re=10,000, compared with the corresponding smooth cylinder.

A large eddy simulation of cross-flow around a sinusoidal wavy cylinder at Re = 3000 is performed by Zou and Lin (2008) by introducing the load cell measurement for the validation test. In the study, they presented the mean flow field and the near wake flow structures and compared with those for a circular cylinder at the same Reynolds number. They found that the mean drag coefficient C_d for the wavy cylinder is smaller than that for a corresponding circular cylinder due to the formation of a longer wake vortex generated by the wavy cylinder. The fluctuating

lift coefficient of the wavy cylinder is also greatly reduced. This kind of wavy surface leads to the formation of 3-D free shear layers which are more stable than purely 2-D free shear layers. From that study, they also showed that such free shear layers only roll up into mature vortices at further downstream position and significantly modify the near wake structures and the pressure distributions around the wavy cylinder.

2.1.1.4. Surface Protrusions

Zdravkovich (1981) studied various methods of suppressing vortices shed from a cylinder. He mentioned that the main factor governing the efficacy of a vortex suppression method is its ability to modify the vortex formation length. However, he did not study the effect of the vortex suppression methods on the large-scale coherent structure. One effective method for controlling the flow around a body is to install protrusions on the body's surface. These protrusions modify the wake structure by changing separation lines and/or direction of surface f1ow.

Bandyopadhyay (1986) compiled an excellent review of drag reduction technique and surface modification methods in his study on the mean f1ow over longitudinal grooves and outer-layer devices. In addition, many researchers have studied the effects of surface modifications on turbulent boundary layers.

Nebres and Batill (1992) measured time-averaged wake velocity profiles behind two different models (yawed stranded cables and cylinders wrapped with four small helical wires) using a single hot-wire probe, and analyzed the f1ow characteristics around bluff bodies with helical surface protrusions.

Naudascher and Rockwell (1994) used surface modifications to alter the loading and structural vibration of a circular cylinder. They modified the surfaces of cylinders in numerous ways, for example by applying straight and helical wires, staggered wires, and collars and rings.

Lee and Kim (1997) investigated the f1ow characteristics of the wake downstream of a circular cylinder (D=40 mm) helically wrapped with three small wires (d = 0.075D, d is the wire diameter) with pitches of 5D and 10D. They found

that the surface protrusions elongated the vortex formation region, and decreased the vortex shedding frequency and wake width.

Most previous studies have investigated the flow structure over riblet surfaces placed on a flat plate. Walsh 1983 investigated drag reduction of longitudinal ribs of rectangular, triangular, and transversely curved shapes. He reported that the drag reduction was associated with a decrease of momentum thickness and turbulent velocity fluctuations and depended mainly on the riblet configuration such as the height h, spacing s, and shape. He suggested that a riblet with sharp peaks and large valley curvature is one of the optimum riblet shapes for drag reduction.

Owen et al. (2000) carried out an experimental investigation to measure the drag and vortex-induced vibration amplitudes of a circular cylinder, a circular cross-sectional body with a sinuous axis and a circular cylinder with hemispherical bumps attached. They studied a wide range of Reynolds number up to a maximum value of 10^5 and observed suppression of vortex shedding and drag reductions up to 47% for the body with a sinuous axis. They also recorded drag reductions of about 25% and suppression of vortex shedding for the cylinder with bumps.

Lee and Lee, 2001 investigated the flow structure over a semicircular riblet surface. They measured the near-wall turbulent structures over semicircular(U-type) grooves of s=3mm using a laser based particle image velocimetry (PIV) measurement technique and found how the semicircular riblet reduces the drag acting on the surface. As an extension of this study to a bluff body, we tested the U- and V-grooved cylinders having the same groove spacing of s=3 mm in the present study.

Bearman and Brankovic (2003) investigated the vortex-induced vibration of a plain circular cylinder and cylinders fitted with strakes and bumps. They carried out the experiments in water with mass ratios in a range from about 1.5 to 5.5 and combined mass and damping values between about 2×10^{-3} and 7×10^{-3} by taking the Reynolds number within the range of 10^3 to 10^4. They indicated that although the wakes of fixed cylinders with strakes or bumps show little or no evidence of regular vortex shedding it was found to establish itself across a range of reduced velocity when the mass and damping parameters are sufficiently small. However, the amplitudes of vibration were found to be less than those for a plain cylinder. They

also observed that the modes of shedding found for an oscillating plain cylinder are present for a responding cylinder fitted with vortex suppression devices.

Nakamura and Igarashi (2007) attached cylindrical rings along the span of a cylinder at an interval of several diameters to reduce the drag and fluctuating forces caused by fluid flow. They performed the experiments at Reynolds numbers based on the cylinder diameter d ranging between Re_d = 3000 and 38,000 for taking the aspect ratio of the cylinder, L/d, as approximately 20. Their experimental results revealed that the drag force F_D on the ring-attached cylinder was lower than for the 2D cylinder, even though the projected area was higher. They found the optimum ring configuration for drag reduction to be D/d = 1.3, W/d = 1.0, and P/d = 6 at Re_d ~ 30 000, where D is the ring diameter, W is the spanwise width of the ring, and P is the spanwise pitch of the ring. This configuration reduced the drag force by 15%.

Turhal and Cuhadaroglu (2010) performed experiments to investigate some aerodynamic parameters of the flow around perforated-surface square, horizontal, and diagonal cylinders. The surface pressures of the perforated surface square cylinders were measured for the cases of injections through the top, rear, top-rear, and all surfaces separately at Re values of 10,000, 16,000, and 24,000. The C_D and St were determined based on pressure coefficient C_p measurements and vortex shedding frequency measurements, respectively. Their experimental results showed that the injection through the various surfaces of a square cylinder has some effects on the aerodynamic characteristics of the square cylinder, depending on the position of the perforated surface. They concluded that C_D of a horizontal square cylinder can be reduced by injection through all the surfaces, and for a diagonal square cylinder; it also can be reduced by injection through the rear surfaces. They also revealed that the vortex shedding frequency of the flow around a horizontal square cylinder can also be decreased by high-momentum injection through the rear surface.

2.1.1.5. Control Cylinders

Kuo et al. (2007) numerically studied the passive wake control downstream of a circular cylinder in uniform flow for Re_D ranging from 80 to 300. They used two

small control cylinders, with diameter ratio d/D = 1/8, placed at x/D = 0.5 and y/D = ±6 and Reynolds numbers is varied from 80 to 300. Their mechanism, which can significantly reduce the fluctuating lift force F_L and the form drag force F_D on the main cylinder, is explored without completely suppressing the vortex street for Re_D = 80–300. They reported that, by this control, the vortex street downstream of the main cylinder is still maintained but the fluctuating lift force F_L and the form drag force F_D on the main cylinder decreases monotonously with increasing the Reynolds number.

Passive flow control using two-dimensional hydrofoils to reduce vortex-induced vibrations (VIV) and drag force F_D on a cylinder of circular cross-section was studied by Galvao et al. (2008). They test the hypothesis that by using foils to bend the streamlines around the cylinder, and hence forcing the flow to approach potential flow-like patterns VIV and drag will be reduced. They showed that properly positioned foils can significantly alter the flow around a circular cylinder to eliminate VIV and reduce drag.

Kuo and Chen (2009) revealed the wake flow structures downstream of a circular cylinder manipulated by two small control cylinders and elucidate the primary mechanism that leads to a reduction of the lift and the pressure drag on the main cylinder. They found that when the control cylinders lie within $0.8 \leq X_C/D \leq 3.0$, the fluctuating lift on the main cylinder shows a 70–80% reduction without completely suppressing the vortex street.

2.1.2. Active Flow Control Techniques

2.1.2.1. Perturbation

Griffin (1992) has given many experimental results to demonstrate the relationship between the cross-flow vibration amplitude and the mass-damping product.

Brika (1993) performed an experimental study of the vortex-induced oscillations of a long flexible circular cylinder. The stationary amplitude they obtained exhibited a hysteresis loop somewhat different from earlier studies.

Techet (1998) measured the forces at both ends of the forced harmonic motion and free vibrations of uniform and tapered cylinders at the Reynolds number (defined via the cylinder diameter) value, Re =3800. Their results showed that free-vibration tests of a uniform cylinder with low equivalent structural damping yield the amplitude response curve as a function of the nominal reduced velocity in agreement with previous results (Khalak and Williamson, 1996)

Dutsch et al. (1998) investigated numerically the laminar flow induced by the harmonic in-line oscillation of a circular cylinder.

With the use of a spectral element spatial discretization, Blackburn (1996) explored the vortex-induced vibration problem by solving the two-dimensional Navier–Stokes equations in an accelerating frame of reference attached to the cylinder at the Reynolds number value Re =250.

Newman (1996) performed a direct numerical simulation (DNS) study of the flow past a freely vibrating cable using body-fitted coordinates at the Reynolds number Re= 100 and 200.

Baz and Kim (1993) made attempts to control the vibration of a cylinder in a cross-flow. In their studies, surface-bonded piezo-ceramic patches were activated by a closed-loop control system to exert a force on the cylinder under resonance, that is, the vortex shedding frequency coincided with the natural frequency of the cylinder. The control increased the flow structure system damping and subsequently reduced the vortex-induced vibration.

Cheng et al. (2003) developed a ‘smart cylinder’ with piezoceramic actuators embedded underneath the structural surface of a rigid square cylinder. The excitation of these actuators created a surface perturbation, which drastically altered the fluid–structure interaction given an appropriate excitation signal.

Griffin and Votaw (1972) concluded that, when the cylinder vibrates transversely to the oncoming flow, the vortex frequency adjusts itself to the forcing frequency. An increase in the relative amplitude, A/D, where A is the vibration

amplitude and D is the cylinder diameter, induces an increase in the drag and a reduction in the longitudinal distance of the vortices until they disappear completely at some threshold amplitude.

Smith and Stansby (1988) considered the locking-on of vortex shedding due to cross-stream vibration of the circular cylinder in uniform and shear flows. They showed that, in both flows, the vortex shedding frequency locked onto the cylinder frequency and onto sub-multiples of the cylinder frequency.

Based on the study of a phenomenological model of FIV, Yuan and Cheng (2007) experimentally investigated the high-frequency perturbation effects on the performance of suppressing flow-induced vibration (FIV). They found the possibility to suppress both structural vibration and wake vortex by introducing a perturbation input at a high-frequency range well-exceeding resonant frequency of structure.

Konstantinidis and Balabani (2007) experimentally studied on the symmetric mode in the wake of a circular cylinder induced by periodic perturbations imposed on the in-flow velocity. They examined the wake field by PIV and LDV for the Reynolds number about 1200 and for a range of perturbation frequencies between three and four times the natural shedding frequency of the unperturbed wake. In this range, they found that a strong competition between symmetric and anti-symmetric vortex shedding occurs for the perturbation amplitudes employed. Their results show that symmetric formation of twin vortices occurs close to the cylinder synchronized with the oscillatory component of the flow. The symmetric mode rapidly breaks down and gives rise to an anti-symmetric arrangement of vortex structures further downstream. The downstream wake may or may not be phase-locked to the imposed oscillation. The number of cycles for which the symmetric vortices persist in the near wake is a probabilistic function of the perturbation frequency and amplitude. From that study, they also showed that symmetric shedding is associated with positive energy transfer from the fluid to the cylinder due to the fluctuating drag.

2.1.2.2. Oscillating

Studies on flow past an oscillating cylinder can be divided into the following two categories depending on the motion of the cylinder. In the first category, the cylinder oscillates translationally at an angle of 0º or 90º with respect to the free stream. They are in-line and transverse oscillation, respectively. Many experimentalists [Bishop and Hassan (1964), Koopmann (1967), Taneda (1972) Griffin and Ramberg (1974), Bearman and Currie (1979), Bearman (1984), Ongoren and Rockwell (1988a, b), Williamson and Roshko (1988)] had shown that the vortex shedding phenomenon can be dramatically altered for the cylinder undergoing in-line and transverse oscillation in a fluid stream. For in-line oscillations, vortex lock-on occurs when the oscillation frequencies are approximately twice the Strouhal frequency (the frequency of the vortex shedding from a stationary cylinder). For transverse oscillations, lock-on usually occurs near the Strouhal frequency (Griffin and Hall 1991; Meneghini and Bearman 1995). In the second category, the cylinder performs a rotational oscillation about its axis in mean flow. It is well known that lock-on or resonance occurs when the body and wake oscillations have the same frequency that is near one of the characteristic frequencies of the structures. Vortex lock-on can also be realized with rotational oscillations of a circular cylinder.

Viscous flow around a rotationally oscillating cylinder was investigated experimentally by Okajima et al. (1975) for Reynolds numbers (Re_D) of 40-160 and 3050-6100. Their results showed that, when the oscillation frequency of the cylinder is at or near the frequency of vortex shedding from a stationary cylinder, the vortex shedding synchronizes with the cylinder motion.

Okajima et al. (1975), Taneda (1978) and Filler et al. (1991) studied the effect of rotary oscillations of a circular cylinder at relatively low Reynolds numbers. They demonstrated the possible modification of vortex shedding and found that the extent of cylinder peripheral speeds which affected the vortex shedding was smaller than 3% of the free-stream velocity.

More recently, the frequency response of the shear layers separating from a circular cylinder undergoing small amplitude rotational oscillation has been

investigated experimentally by Filler et al. (1991) in water at a Reynolds number range of 250-1200. By referencing the lock-on analyzer to the cylinder oscillations, the amplitude and phase of the response to different frequency oscillations were measured directly. They found that rotational oscillations corresponding to cylinder peripheral speeds of between 0.5 and 3% of the free-stream velocity, U_∞, can be used to influence the primary (Karman) mode of vortex generation. For Re greater than 500, such oscillations can also excite the shear-layer vortices associated with the instability of separating shear layers.

Ingham (1983) and Badr et al. (1989) numerically investigated the rotating cylinder flow in the laminar steady regime (Re_D <47) for relatively small rotational speeds. They found that, although vortex shedding does not occur in the wake, the rotation delays and even inhibits the boundary-layer separation. The flow in the laminar vortex shedding regime (47≤ Re_D <200) has also been investigated in the literature.

Tokumaru and Dimotakis (1993) experimentally investigated flow past a circular cylinder with both net steady rotation and forced oscillations at $Re_D \approx 10^3$ by suggesting the so-called virtual vortex method. They found that a higher cylinder aspect ratio yields a higher maximum lift coefficient in the case of steady rotation and the addition of forced rotary oscillations to the steady rotation increases or decreases the lift coefficient.

Gioria et al. (2009) investigated the flow around a circular cylinder submitted to forced transverse oscillations. Their goal is to investigate how the transition to turbulence is initiated in the wake for cases with different Reynolds numbers (Re) and displacement amplitudes (A). The procedure consists of performing a Floquet type analysis of time-periodic base flows, computed using the spectral/*hp* element method. With the results of the Floquet calculations, considerations regarding the stability of the system are drawn, and they obtained form of the instability at its onset. The critical Reynolds number is observed to change with the amplitude of oscillation. They also observed instabilities for the oscillating cylinder are distinctively stronger in the braid shear layers. Other unstable modes similar to mode

B are found. Quasi periodic modes are observed in the 2S wake, and sub harmonic mode occurrences are reported in P + S wakes.

The flow characteristics of the near-wake downstream of a rotationally oscillating circular cylinder are investigated experimentally with varying the frequency ratio F_R by Lee et al. (2007). The velocity fields in the near-wake for each system were measured using a dynamic PIV technique. They found the rotational oscillatory motion of a circular cylinder to be an effective and promising method for controlling the near-wake flow structure. In addition, their results show that temporally resolved quantitative and qualitative flow information is useful in understanding the cyclic variation of vortex structure and in analyzing the effect of open-loop active flow control on the near-wake flow structure.

Zhang et al. (2010) numerically studied on the nonlinear optimal control approach based on the adjoint flow field for the cylinder wake control. They obtained the optimal control *N(t)* varying with the transient flow field and found that under the action of *N(t)*, the oscillations of drag and lift are suppressed, the total drag coefficient C_D decreases dramatically where the pressure drag C_P decrease is a dominant effect, and the lift keeps at zero level.

2.1.2.3. Suction and Blowing

Another possibility is flow manipulation through the application of suction or blowing. Early experiments on a porous cylinder made of sintered bronze were carried out by Pankhurst and Thwaites (1950). They made experiments with continuous suction, but also combined suction with a flap in the form of a short splitter plate placed at various angles. At an angle of 180°; i.e., along the downstream symmetry line, and for sufficient suction, the separation is entirely prevented and a remarkably close approximation to the potential flow solution is achieved, as attested by the pressure distribution and by mean flow velocity profiles of the wake. They concluded from their experiments that the values of $Cq\sqrt{\mathrm{Re}}_D$ larger than ≈30 were needed to avoid separation (a critical value of the bleed coefficient

$Cq = U_0 / U_\infty = 0.214$, where U_0 is the bleed velocity) (Antonia and Rajagopalan, 1990). They also reported values of the drag coefficient C_D, but did not do any time-resolved measurements to determine the vortex shedding frequency.

Boundary layer measurements on the same porous cylinder were performed by Hurley and Thwaites (1951) and in general good agreement was found with the laminar boundary layer theory.

Continuous blowing through the whole surface has also been studied experimentally by Mathelin et al. (2001).

Glezer and Amitay (2002) show that synthetic jets on a selected positions over the cylinder can give a delay of separation for different Reynolds numbers (i.e., both for a turbulent and a laminar boundary layer). They argued that this delay was caused by increased mixing within the boundary layer. In addition, the interaction between the jet and the cross flow has a profound effect both on the separated shear layer and on the wake; the magnitude of the Reynolds stresses is reduced indicating that the delay in separation is not merely the result of a transition to turbulence in the boundary layer.

Feng et al. (2010) studied to control the flow around a circular cylinder by a synthetic jet positioned at the rear stagnation point using a novel synthetic jet. The suction duty cycle factor k, defined as the ratio between the time duration of the suction cycle and the blowing cycle, is used as the parameter to characterize the novel synthetic jet signal They indicated that, when increasing the suction duty cycle factor, the momentum coefficient is also enhanced, and a stronger and larger scale synthetic jet vortex pair is generated and it can reach further downstream. This characteristic has a significant influence on the wake vortex shedding of the circular cylinder

Similar study is experimentally investigated with a two-dimensional particle image velocimeter (PIV) system in quiescent flow by Wang et al. (2010). The novel signal wave pattern realized by changing the suction duty cycle factor k for a two dimensional synthetic jet and the development and evolution of the vortex pair trajectories, jet velocity, jet width, flow flux and momentum flux were obtained for different k values. They found that the distributions of the mean and turbulent flow

fields for synthetic jets generated at different k values have similar features to those exhibited for the conventional synthetic jet. Moreover, the vortex pairs generated in the present way have larger convection velocity, stronger entrainment and higher momentum at larger K, which would be of benefit for flow control applications.

2.1.2.4. Acoustic Excitation

The active control of vortex shedding using the internal acoustic excitation was first introduced by Hsiao and Shyu (1991). They investigated the influence of acoustic excitation on the aerodynamic performance of a cylinder, where the acoustic excitation was introduced internally to the flow over a circular cylinder through a slit with a loud speaker.

Baz and Ro (1991) used an electromagnetic actuator installed inside a cylinder to exert a force on the cylinder. The actuator was driven by a feedback hotwire signal measured in the wake, thus increasing damping to the cylinder and effectively reducing the vortex-induced vibration at the occurrence of resonance, when the vortex shedding frequency, f_s, coincided with the natural frequency, f'_n of the system. One common feature in these investigations is to alter the structural dynamics, subsequently influencing the flow field. Another approach is to use acoustic excitation to control the flow- field.

Ffowcs et al (1989) were able to demonstrate, with active, control of vortex shedding downstream of a cylinder with a diameter of 0.6 cm at a speed of 1 m/s and the Reynolds number of 400.

Roussopoulos (1993) concluded that the feedback control was possible only at a Reynolds number 20% higher than at the critical Reynolds number. He claimed that Ffowcs Williams' active control of vortex shedding of around transitional Reynolds number at about 400 was really an active probe when affected, and prevented a second sensor from detecting a vortex shedding. He attempted to show this interference of probes was actually claimed to be control of vortex shedding as claimed by them. He visualized the flow in a water channel and tried to show that there was no control of vortex shedding.

Tao et al. (1996) provided visualization photos between Reynolds numbers 48.5 and 51. This range is 18-24% above the onset of Reynolds number at the shedding frequency of about 1.05-1.1 Hz. At x/d=10 and 30 locations a complete elimination of vortex shedding is achieved, and flow-streak lines are reduced to almost a straight line in the cylinder wake.

Thereafter and Keles (1996) demonstrated experimental details of the transition to turbulence in the wake of a circular cylinder at Re_D=170. In those findings by Keles (1996) the data in the wake of cylinder first time, provides a clear picture of the feedback transition control. The distribution of the amplitude of velocity fluctuation's control was achieved for transitional at about Re_D =170.

The effect of externally imposed sound on the flow over a single cylinder has been reported by Blevins (1985), who concluded that sound levels greater than 130 dB resulted in a reduction in the small variation of the vortex-shedding frequency.

Hsiao and Shyu (1991) investigated the effect of acoustic excitation introduced internally to a circular cylinder through a slit to improve the aerodynamic performance of the cylinder in a uniform flow. They emitted the acoustic disturbances from a speaker system through the slit to the flow over the cylinder with sound pressure levels as high as 130 dB. The dimension of the slit was 1mm wide and 80mm long, while the cylinder diameter was 60mm with the length 200 mm, so that the aspect ratio of the cylinder was as small as 3.3. The drag was evaluated from wake velocity measurements and was found to be reduced by up to 40% at the optimum condition of the forcing frequency and slit location at a Reynolds number 2×10^4. However, the measurement of pressure distributions did not indicate any drag reduction, which suggests that further research should be conducted to confirm the drag reduction by the acoustic excitation.

Amitay et al. (1997) studied the surface pressure distributions around a circular cylinder under internal excitation by using fluidic actuators and found a drag reduction of 25% at a higher Reynolds number, Re=75500.

Caillaud et al. (2000) attempted to actively alter the damping of a flexible tube bundle in a cross-flow using velocity feedback to derive critical velocities, at which

fluid elastic instabilities occur. An attempt has been made to employ acoustic signals to control the flow field.

Lewit (1992) used a feedback hot-wire signal to activate sound waves inside a circular tube. The sound waves interacted with flow through two rows of holes, arranged at ±90º away from the forward stagnation line of the tube, respectively, so that the sound waves through the two rows of holes were in antiphase, thus suppressing vortex shedding from the tube up to $Re_D=10^4$.

Williams et al. (1992) introduced symmetric and antisymmetric acoustic excitations into a water flow (Re=470) at a frequency of about 2 f_s through two rows of holes located at ±45º, respectively, away from the forward stagnation line of the cylinder. He observed a modified behavior of f_s and the flow structure.

Fujisawa and Takeda (2003) investigated the mean fluid forces on a circular cylinder under acoustic excitation control by measuring the time-averaged pressure distributions over the cylinder. The result indicates that the mean drag is reduced up to 30% at Reynolds number 9000. They also measured the distributions of mean and periodic velocities around the cylinder using a standard PIV system and showed that the near-wake velocity profile was considerably modified by the acoustic excitation control.

Muddada and Patnaik (2009) numerically investigated the flow over a circular cylinder with the aid of a control algorithm using multiple-feedback sensors and actuators. They found that the rate of steady state injection depends on the proportionality coefficient, i.e. higher the rate of injection, the faster it will reach steady state and viceversa. They also demonstrated that energy expenditure can be further optimized through nimble control by enabling periodic switch on and off capability.

Jukes and Choi (2009) experimentally investigated the possibility of controlling the global flow field in the near wake of a circular cylinder at Re = 6500 using high-speed Particle Image Velocimetry. Surface plasma actuators were mounted at strategic locations around the cylinder (both fore and aft of the separation point) and used for flow control by producing a body force close to the wall. They found that the plasma can significantly alter the vortex shedding in the wake of the

cylinder, with effectiveness depending upon the actuator location and forcing frequency. They also observed that most dramatic effects were observed when the plasma was located very close to the natural laminar separation point.

2.1.2.5. Electromagnetic Control

Nosenchuck and Brown (1993) measured a reduction of skin friction of up to 90% by means of chessboard like arranged electrodes/magnets to induce a wall-normal Lorentz force in a flat plate boundary layer. The injection of an electrolyte generated a non-uniform electrical conductivity. Spanwise oscillating Lorentz-force (see Berger et al., 2000) was successfully used to reduce the skin friction in a turbulent boundary layer. A considerable scatter of results was found even on very similar arrangements. This could result from inadequate calculations of the Lorentz force in numeric or difficulties with established measurement techniques.

There have been some researches to apply the magnetic fields to control the vortical structure in the wake. They investigated the effect of magnetic fields on the flow structure past a cylinder. Lahjomri et al. (1993) carried out an experimental study and showed that an aligned magnetic field leaded to the suppression of vortex shedding.

Shatrov et al. (1997) and Mutschke et al. (1997) and Mutschke et al. (1998) and Mutschke et al. (2001) investigated the flow instability in the wake in the presence of magnetic fields from their numerical studies. They carried out the stability analysis using the numerical simulation techniques for the time-dependent two- and three-dimensional flow. Depending on the magnitude of applied magnetic fields in the two-dimensional flow region, the vortex shedding can be suppressed or eliminated and as a result the flow becomes stabilized.

Kim and Lee (2000) introduced the electromagnetic force to control the flow around a circular cylinder. They investigated the effect of the electromagnetic force on the cross-flow of a circular cylinder by placing electrodes and permanent magnets side by side alternately in the axial direction of the cylinder.

Chen and Aubry (2003) developed an efficient active control algorithm for manipulating wake flows past a solid cylinder in an electrically low-conducting fluid (e.g. seawater). Their intent is to avoid both vortex shedding and flow separation from the body with reduction in the mean drag significantly. They introduced a Lorentz force in the azimuthal direction generated by an array of permanent magnets and electrodes located on the solid structure and found that vortex shedding behind the cylinder weakens and eventually disappears completely when the Lorentz force is sufficiently large.

A nonlinear adjoint-based optimal control approach of cylinder wake by electromagnetic force is investigated numerically by Zhang et al. (2010). They constituted a cost functional representing the balance of the regulated quantities with different weights and interaction parameter N (Lorentz force), where the regulated quantities related with flow and force are taken as targets of regulation and the Lorentz force, (as interaction parameter N), is taken as a control input. They observed that under the action of optimal N(t), the flow separation is suppressed fully, so that the oscillations of drag and lift are suppressed and the total drag coefficient C_D decreases dramatically. For the different regulations, the control effects have some differences due to the different values of optimal inputs corresponding to the different adjoint flow fields.

3. MATERIAL and METHOD

3.1. Experimental Arrangement

Increasing technological developments, especially in electric and electronic engineering, provide new measuring techniques. All measurement techniques have some advantages and disadvantages associated with the specific method. It is increasingly important not only to measure the mean values at a point in space, but also to measure and characterize turbulent and instantaneous values in the investigated flow field. Particle Image Velocimetry, PIV, is a non-intrusive technique used to measure an instantaneous two dimensional velocity vector field under investigated area. The velocity is determined by measuring the displacement of particles in a flow field that is illuminated by a laser sheet.

3.1.1. Water Channel System

Experiments were carried out in a low turbulence closed-loop, opened surface water channel test section having the following dimensions: a length of 8000 mm, width of 1000 mm, and depth of 750 mm, and made from 15 mm thick transparent plexiglass sheeting. This facility was built in the Fluid Mechanics Laboratory at Cukurova University and schematically represented in figure 3.1. After the inlet tank, a settling chamber exists with a honeycomb. A honeycomb is used to reduce mean or fluctuating variations in transverse velocity (flow direction), with little effect on streamwise velocity because the pressure drop through a honeycomb is small. The water was then conveyed through a two-to-one contraction, which provides accelerate nearer the centerline and slow down near the walls, to reach the test section. The overall length of the water channel is approximately 15000 mm (Figure 3.1). A pump driven by an electric motor having a variable speed controller was used to create a desired mean flow in the test section.

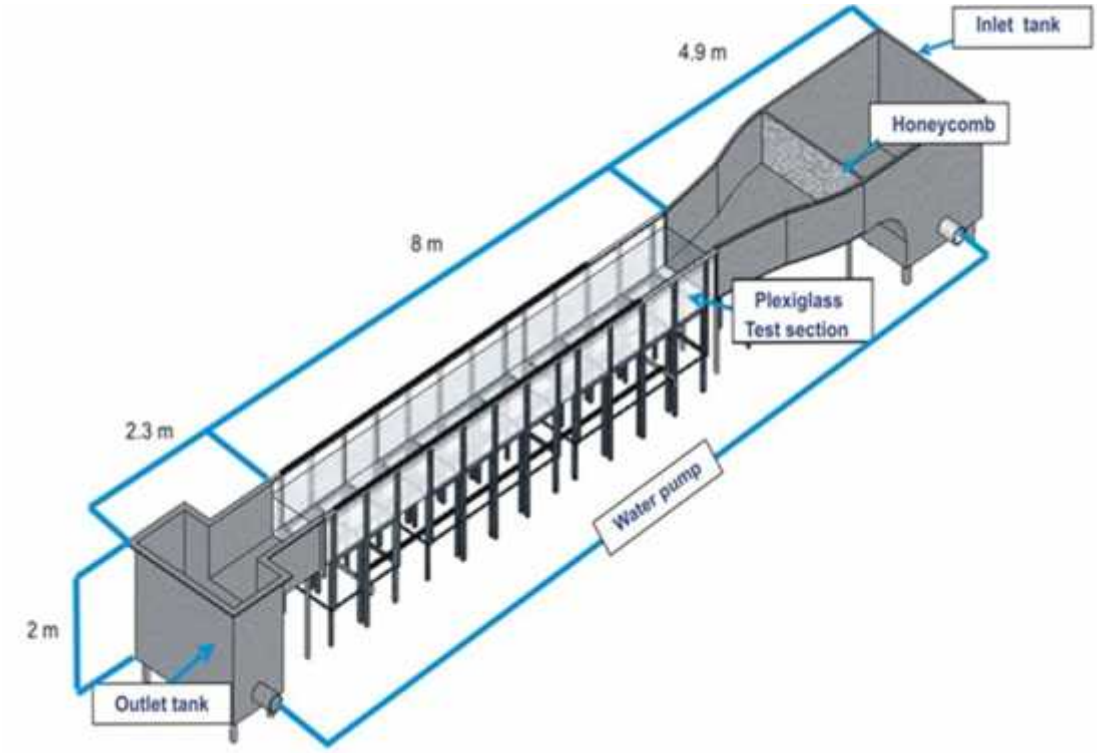

Figure 3.1. Schematic representation of water channel

3.2. Measurement Techniques

3.2.1. Particle Image Velocimetry (PIV) Techniques

The Particle Image Velocimetry (PIV) is a non-intrusive measurement technique used to simultaneously determine the velocities at many points in a flow field. The technique involves seeding the flow field, illuminating the region under investigation and capturing two images of that region in rapid succession. From the displacement of the tracer particles, provided that the time interval between image captures is known, a velocity vector map can be calculated in the flow field.

The theory of PIV was introduced by Adrian (1988) in the late 1980s with the first experimental implementations following shortly afterwards (Kean et al. 1990 and Kean et al. 1991). At the stage, due to hardware limitations, a single photographic frame was multiply exposed and analysed using an auto-correlation technique. However, improved speed of photographic recording soon allowed images to be captured on separate frames for analysis by cross-correlation (Kean et al. 1992).

The introduction of digital camera technology to PIV enabled the direct recording of particle images (Willert et al. 1991), at the expense of reduced resolution, resulting in the development of digital PIV (Westerweel, 1997). As well as these hardware advances, many new algorithms have been developed in the last decade, increasing the accuracy and speed of PIV analysis. One key advantage of the PIV technique over other conventional techniques such as LDV or hotwire anemometry is ability to obtain instantaneous flow-field information is important for probing the structure of turbulent flow fields (Westerweel et al. 1996; Meinhart and Adrian 1995).

3.2.1.1. Principles of PIV

Particle Image Velocimetry (PIV) technique is one of the most reliable method for flow velocity measurement in modern fluid mechanics. Main principle of PIV is based on the definition of speed which is distance over time.

In PIV, the flow property actually measured is the distance traveled by particles in the flow field within a known time interval. These particles are added to the flow and known as seeding. Different types of seeding particle are used depending on the nature of the flow for PIV experiments. The type of seeding particle is chosen to follow the flow, and in order to detect their movement, an area of the flow field is illuminated by a light-sheet. The light-sheet, which is generated by a laser and a system of optical components, is not continuous/permanent, but pulsed to produce a stroboscopic effect, freezing the movement of the seeding particles. The time between the light pulses is the denominator in the equation above. To detect the position of the illuminated seeding particles, a CCD-camera (CCD = Charge Coupled Device) is positioned at right angles to the light-sheet, and particle positions will appear as light specks on a dark background on each camera frame. The pulsing light-sheet and the camera are synchronized so that particle positions at the instant of light pulse number 1 are registered on frame 1 of the camera, and particle positions from pulse number 2 are on frame 2. (Older generations of CCD cameras couldn’t switch frames fast enough, so both the first and the second pulse of the light sheet were recorded on the same camera frame).

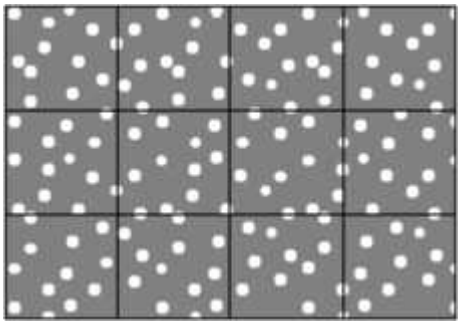

Figure 3.2. Interrogation areas

The camera images are divided into square regions called interrogation areas (Figure 3.2) or interrogation regions, and for each of these interrogation areas the image from the first and the second pulse of the light-sheet are correlated to produce an average particle displacement vector. Doing the same process for all interrogation regions produce a vector map of average particle displacements. Dividing with the known time between the two images captured the displacement vectors are converted into a map of so-called raw velocity vectors. Then validation algorithms can be applied to the raw vector maps, so that outliers, the term for erroneous vectors, can be detected and removed. In the FlowMap PIV system, for reasons of experimental reproducibility, the raw vector map is archived and a new validated vector map is output, and further analysis can produce streamlines, vortices and so on.

From the basic principles the following main topics of PIV emerge:

- Seeding
- Illumination
- Cameras
- Synchronization
- Correlation
- Validation and further analysis

3.2.1.2. PIV Parameters Used in This Study

The experiments were performed and the measured data were processed using Dantec Dynamics PIV system and FLOW MANAGER Software installed on a computer. The measurement field was illuminated by a thin and an intense laser light

sheet by using a pair of double-pulsed Nd:YAG (yttrium aluminum garnet) laser units each having a maximum energy output of 120 mJ at 532 nm wavelength. The two orientations of the laser system use a combination of spherical and cylindrical lenses.

The image capturing was performed by an 8 bit cross-correlation charge-coupled device (CCD) camera having a resolution of 1008×1016 pixels, equipped with a Nikon AF Micro 60 *f* /2.8 *D* lens. In the image processing, 32×32 rectangular interrogation pixels were used and an overlap of 50% was employed. A total of 3844 (62×62) velocity vectors were obtained for an instantaneous velocity field at a rate of 15 frames per second. The plan view of measuring planes covers the downstream of the cylinder with the area of 200 mm x 200 mm for all configurations and the image magnification was 0.0709 mm/pixel. The laser sheet was oriented parallel to the bottom surface of the water channel and the experiments were carried out at the mid-plane of the water height. The time interval between pulses was 1.75 ms for all experiments and the thickness of the laser sheet illuminating the measurement plane was approximately 2 mm. The time interval and the laser sheet thickness were selected such that the maximum amount of particles in the interrogation window was obtained (With the help of a synchronizer, the time between the images to be taken and the laser pulses is synchronized and the velocity vectors of the flow field were measured by comparing the particle movement between two consecutive images). The number of particles in an interrogation area was in between 20 and 25. The uncertainty in velocity relative to depth averaged velocity is about 2% in the present experiments. The water was seeded with approximately 10 μm diameter aluminum coated sphere particles. The instantaneous images were captured, recorded, and stored in order to obtain averaged-velocity vectors and other statistical properties of the flow field. Spurious velocity vectors (less than 3%) were removed using the local median-filter technique and replaced by using a bilinear least squares fit technique between surrounding vectors. The velocity vector field was also smoothed to avoid dramatic changes in the velocity field using the Gaussian smoothing technique. The vorticity value at each grid point was calculated from the circulation around the eight neighboring points.

3.2.2. Experimental Model

In the present study, perforated outer cylinders constructed from a chrome-nickel steel sheet were used to suppression of vortex shedding downstream of circular inner cylinders. Manufacturing steps of perforated cylinders that were used in the experiments as followings: firstly, it was bored circular holes which were 10 mm diameter to the stainless steel sheet that was 1 mm thickness and then, it was achieved circular cylinders which were 100 mm diameter to shroud inner bare cylinders. Perforated cylinders were produced for different porosity (β) values such as β=0.25, 0.30, 0.40, 0.50, 0.60, 0.70 and 0.80. Definition of porosity, β, is ratio of perforated surface area to the whole surface area (Figure 3.3).

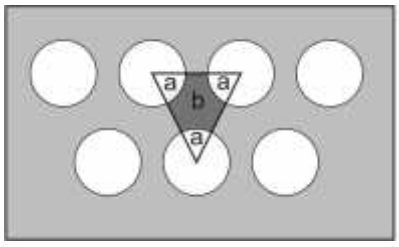

$$\beta = \frac{3a}{3a+b}$$

Figure 3.3. Calculation of porosity, β

In this experiments, nine different inner (bare) cylinders were used (D_i =25mm, 30mm, 40mm, 50mm, 60mm, 70mm, 75mm, 80mm and 90mm) and these bare and perforated cylinders were coupled in a concentric way (shrouded cylinders) for nine diameter ratios (D_i/D_o=0.25, 0.3, 0.4, 0.5, 0.6, 0.7, 0.8 and 0.9). Schematic arrangement of shrouded cylinder is shown in figure 3.4.

All experiments will be carried out above a platform, having a length of 2300 mm, width of 980 mm to obtain fully developed flow condition. The height between top surface of the platform and bottom surface of the channel will be adjusted 220 mm. H_w=400 mm height is modulated between free surface water level and top surface of platform and halve of H_w is arranged for the laser sheet height (Figure 3.5). The free stream velocity, U_∞, will be 100 mm/s which corresponds to a Reynolds number of approximately Re = 10000 based on the outer cylinder diameter. The turbulence intensity is about 0.5% at this Reynolds number thanks to settling

chamber with honeycomb and contraction section. The geometric blockage of the cylinder is 10%.

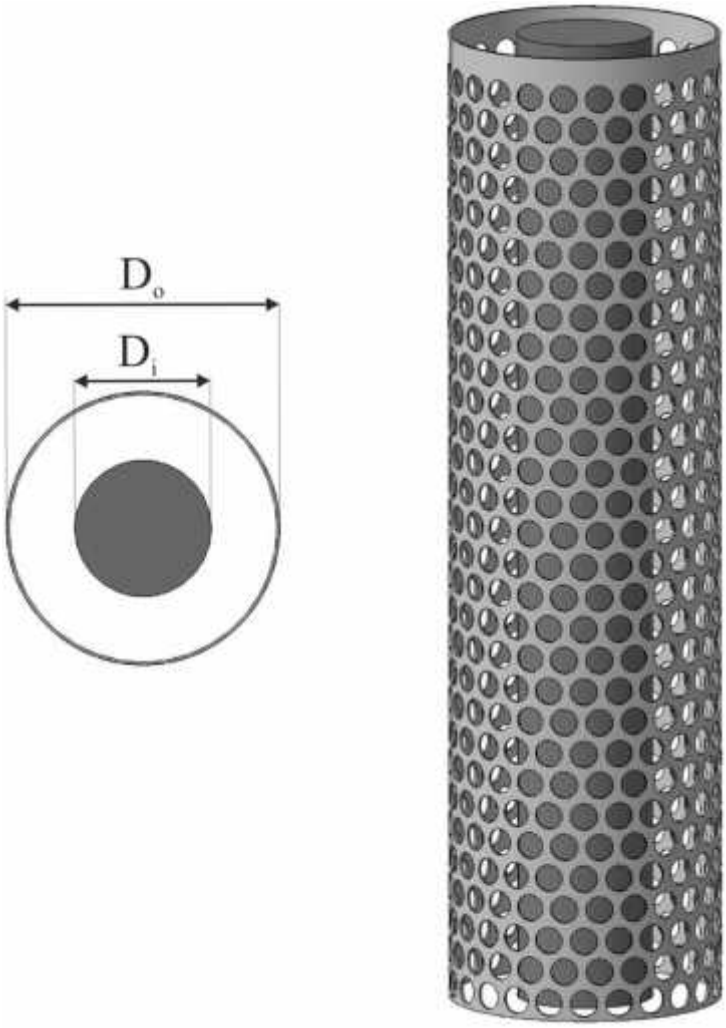

Figure 3.4. Schematically representation of shrouded cylinder

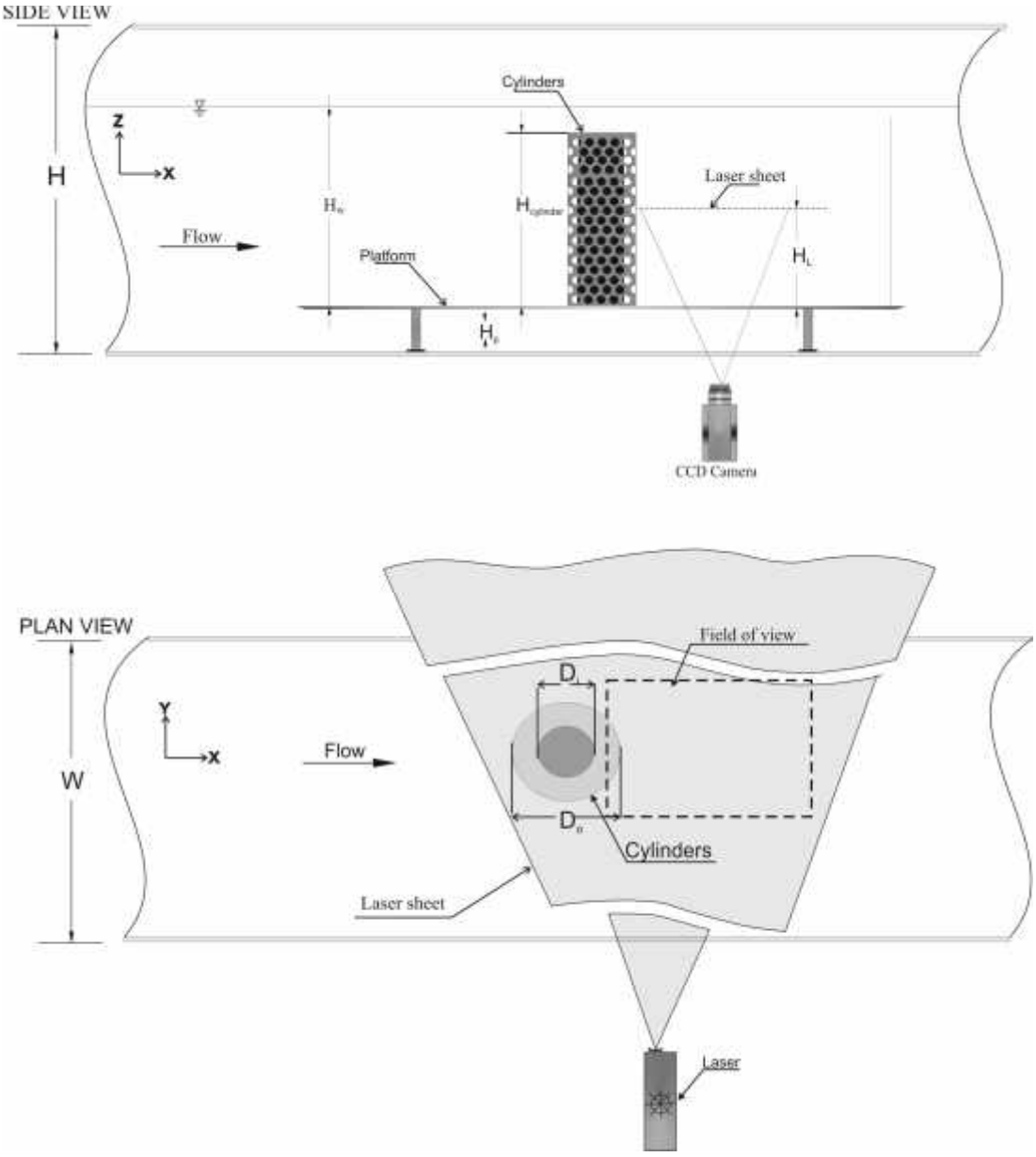

Figure 3.5. Side and plan view of experimental setup

4. RESULTS AND DISCUSSION

The aim of present study is to suppress vortex shedding downstream of a bluff bodies which induces vibrations on the body. Circular cylinders were used as bluff body and the PIV technique is employed to understand the flow structure downstream of the cylinders. Two fields of view were taken into consideration to reveal the detailed flow structure. In this study, nine different bare cylinders (D_{inner}= 25, 30, 40, 50, 60, 70, 75, 80, 90, 100 mm) and eight different perforated cylinders (β=0.25, 0.30, 0.40, 0.50, 0.55, 0.60, 0.70, 0.80 and D_{outer}=100 mm for all perforated cylinders) were used and combination of these inner – outer cylinder (shrouded) cases were conducted (D_i/D_o= 0.25, 0.30, 0.40, 0.50, 0.60, 0.70 0.75, 0.80 and 0.90). Depth – averaged free stream velocity, U_∞, was kept constant at 100 mm/s corresponding to a Reynolds number, Re_o=10000.

Experimental results were presented and analyzed in three main categories which are flow structure around bare cylinders, perforated cylinders, and couple of inner – outer cylinder (shrouded) arrangements.

4.1. Flow around Bare Cylinders in Deep Water

Wake region of bare (inner) circular cylinders were, first of all, investigated for easier comparison with the controlled situations. Time averaged flow characteristics were obtained from 350 instantaneous images. It was concluded from the PIV results that a single field of view is inadequate for determining the flow characteristics of the whole wake region, therefore experiments were performed for two consequent fields of view. Second field of view was obtained by keeping the cylinder positions fixed and shifting the camera and laser 200 mm on direction of the flow (field of view was 200mm x 200mm).

Reynolds shear stress ($<u'v'>$) and turbulent kinetic energy (TKE) have been normalized by dividing them with the square of the depth-averaged free-stream velocity, U_∞^2 for better comparisons. Time averaged vorticity (<ω>) contours are shown in figure 4.1 and minimum and incremental values of <ω> were taken as ±2

and 2, respectively. The solid and dashed lines present positive (counter-clockwise) and negative (clockwise) contours, respectively in the present study. Both positive and negative contours of the time averaged vortices were emanated from the lower and upper shoulders of the cylinder and get close to each other at the end of first field of view (near wake region) for all bare cylinders. This results present a well-known situation which was called von Karman vortex street. Symmetrical shear layers were easily obtained and one field of view was sufficient for vorticity contours. The value of time averaged vorticity magnitude increases with increasing diameter. Figure 4.2 represents the normalized Reynolds shear stress $<u'v'>$ contours where minimum and incremental values were taken as ±0.004 and 0.004, respectively. It is observed that the negative and positive Reynolds shear stress contours are almost symmetrical along the centreline of the cylinders. The magnitude of Reynolds shear stress increases with the increasing cylinder diameter and the wake region grows downstream of the cylinders by generating high magnitude clusters of Reynolds shear stress contours. A lower magnitude positive and negative cluster is formed at rear stagnation point of the cylinders for $60 \leq D_i \leq 100$ mm whereas this flow behaviour is not observed for $25 \leq D_i \leq 50$ mm cases of the bare cylinder.

In two-dimensional PIV, the values of streamwise Reynolds normal stress, $<u'u'>$ and transverse Reynolds normal stress, $<v'v'>$ can be calculated in usual manner (by subtracting the mean values of the velocity components from their instantaneous values and then by averaging the products) from the 350 instantaneous data. Assuming isotropic flow, the third fluctuating velocity component can be estimated by a 2D approximation (Sheng et al. 2000), namely the third component has been supposed to be equal to the half of $(<u'u'>+<v'v'>)$; then TKE, which is directly related to the dynamics of the vortices and usually used as the measurement techniques of the turbulence mixing can be calculated with the following expression (Feng et al. 2010, Schafer et al. 2009)

$$\text{TKE} = \frac{3}{4}\left(<u'u'>+<v'v'>\right) \tag{1}$$

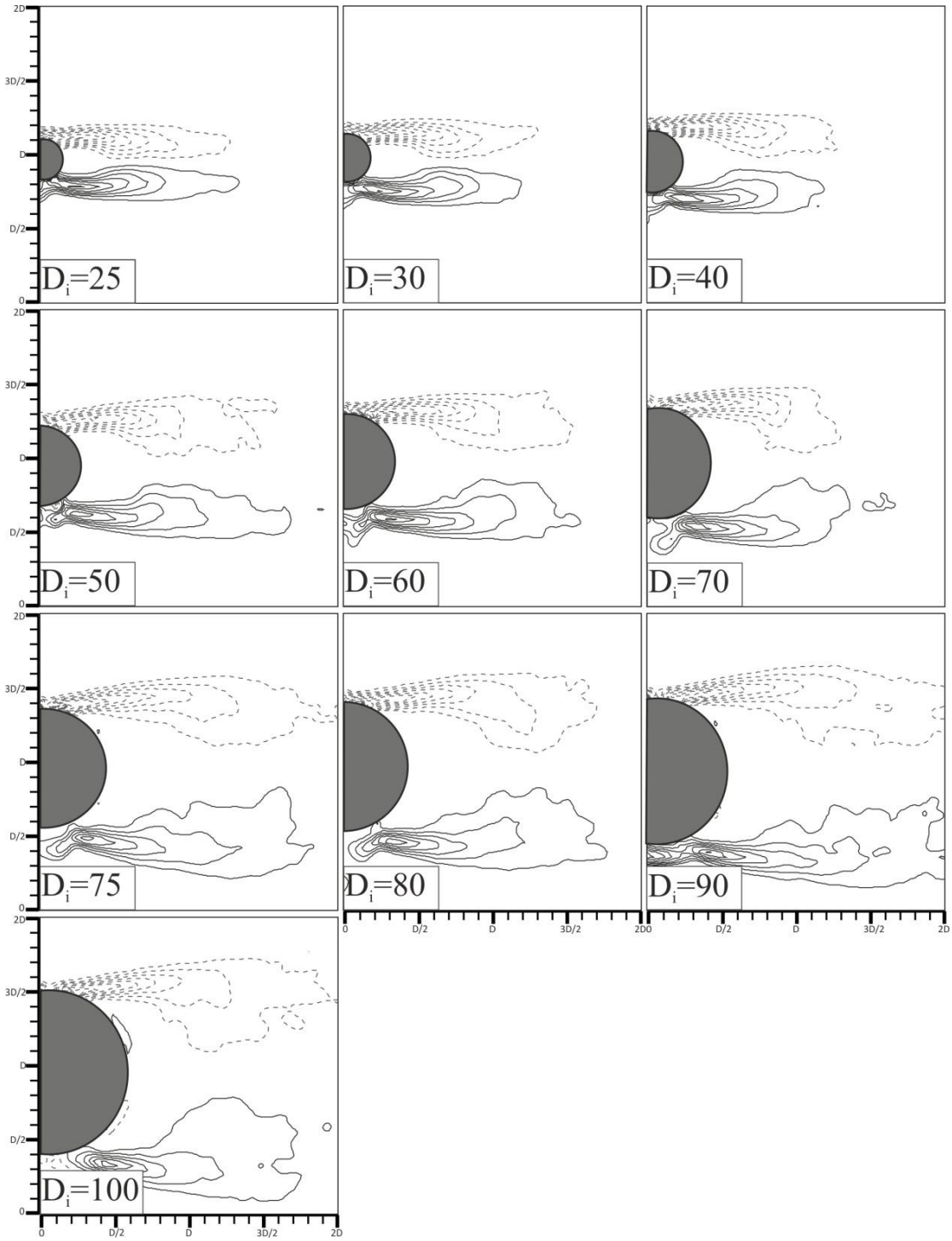

Figure 4.1. Distributions of time averaged vorticity contours (<ω>) downstream of the inner (bare) cylinders for different diameters

According to this definition, TKE contours are evaluated and presented in figure 4.3. The minimum and incremental values of TKE contours were taken as 0.01. It is observed that the flow causes turbulence in the wake region of bare cylinders and with increasing diameter the turbulence intensity also increases and a more distinct structure is formed in the near wake region of the cylinder. It is, also, clearly realized from the figures that increasing diameter causes incrementation of velocity fluctuations strength, and moreover these yield results rising severity of $< u'v' >$ and TKE contours for increasing diameter ranges.

Strouhal number for all bare cylinder diameters were determined between 0.20 and 0.21 by use of the fast Fourier transform (FFT) technique conducted on different points in the flow field. These results were confined with the literature survey.

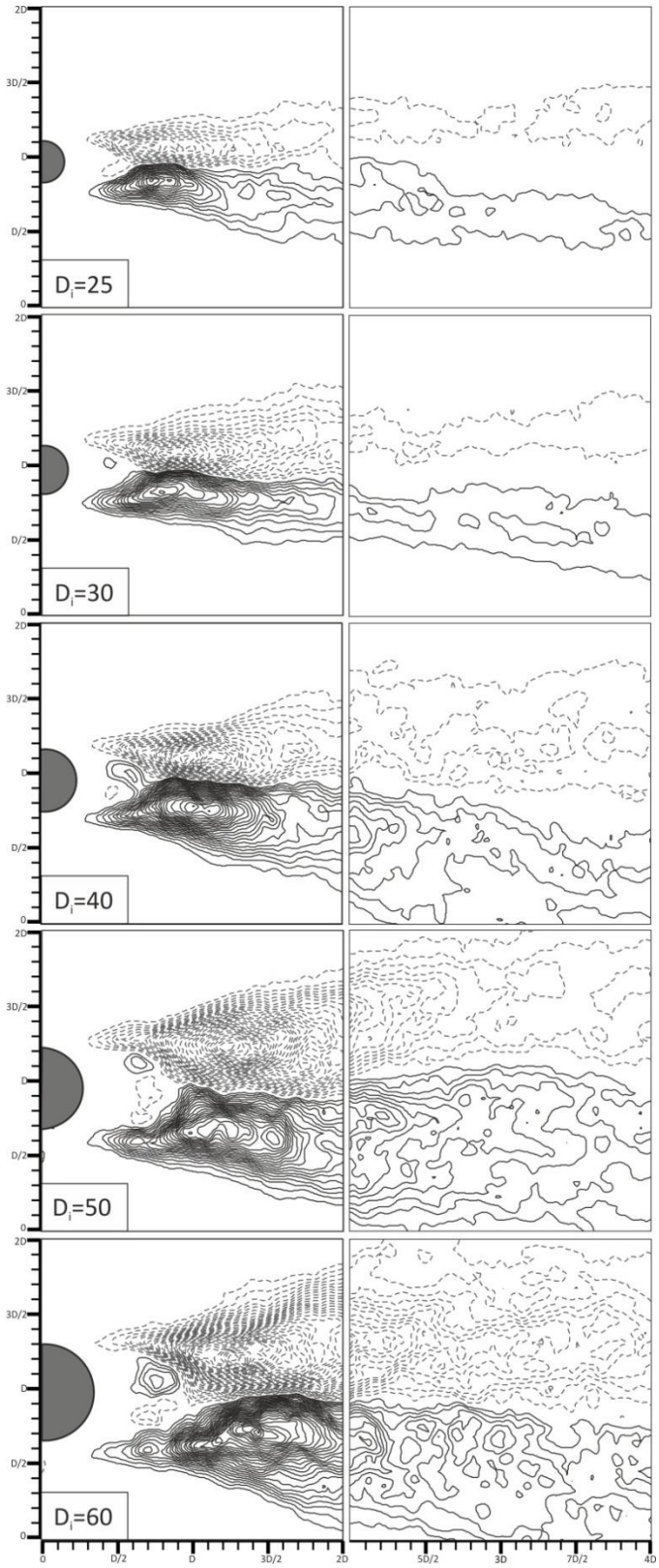
2D
3D/2
D
D/2
0
D_i=25
D_i=30
D_i=40
D_i=50
D_i=60
0
D/2
D
3D/2
2D
5D/2
3D
7D/2
4D

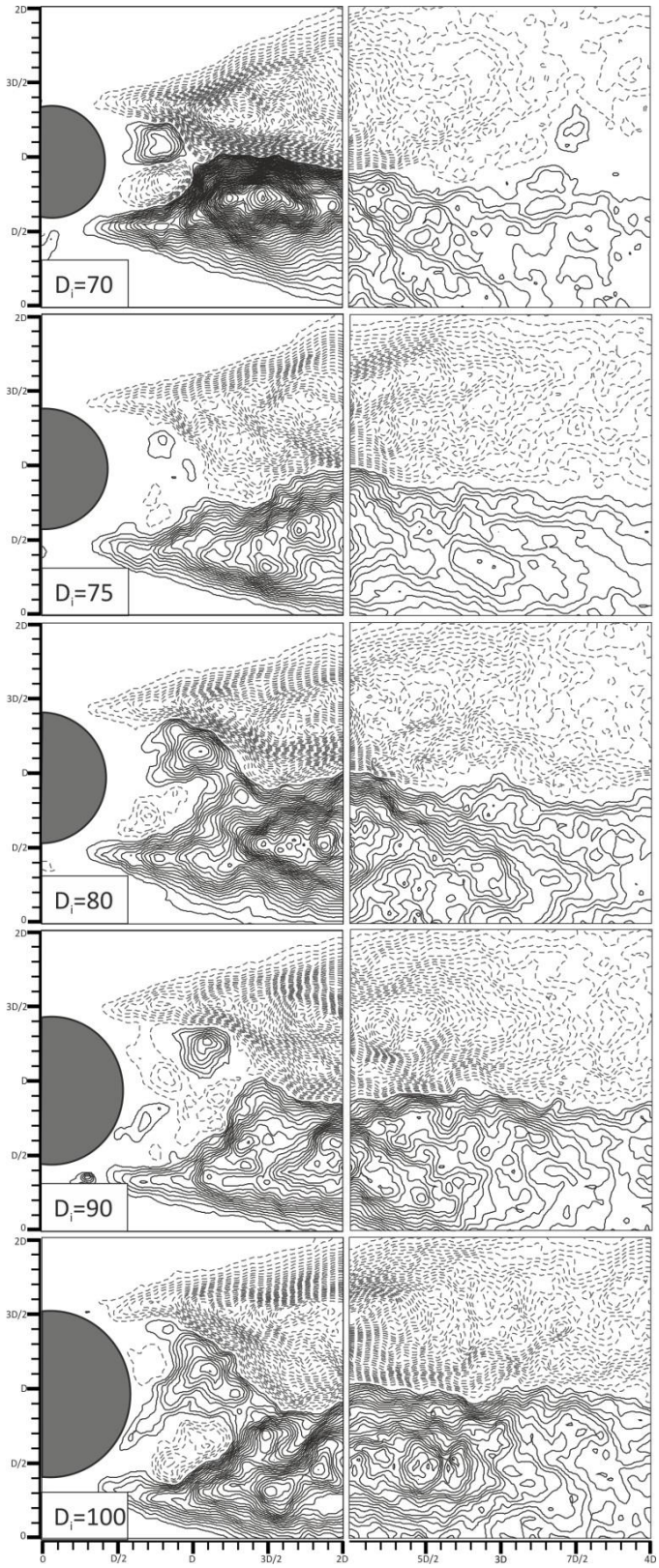

Figure 4.2. Reynolds shear stress distributions downstream of the inner cylinders for different diameter ratios

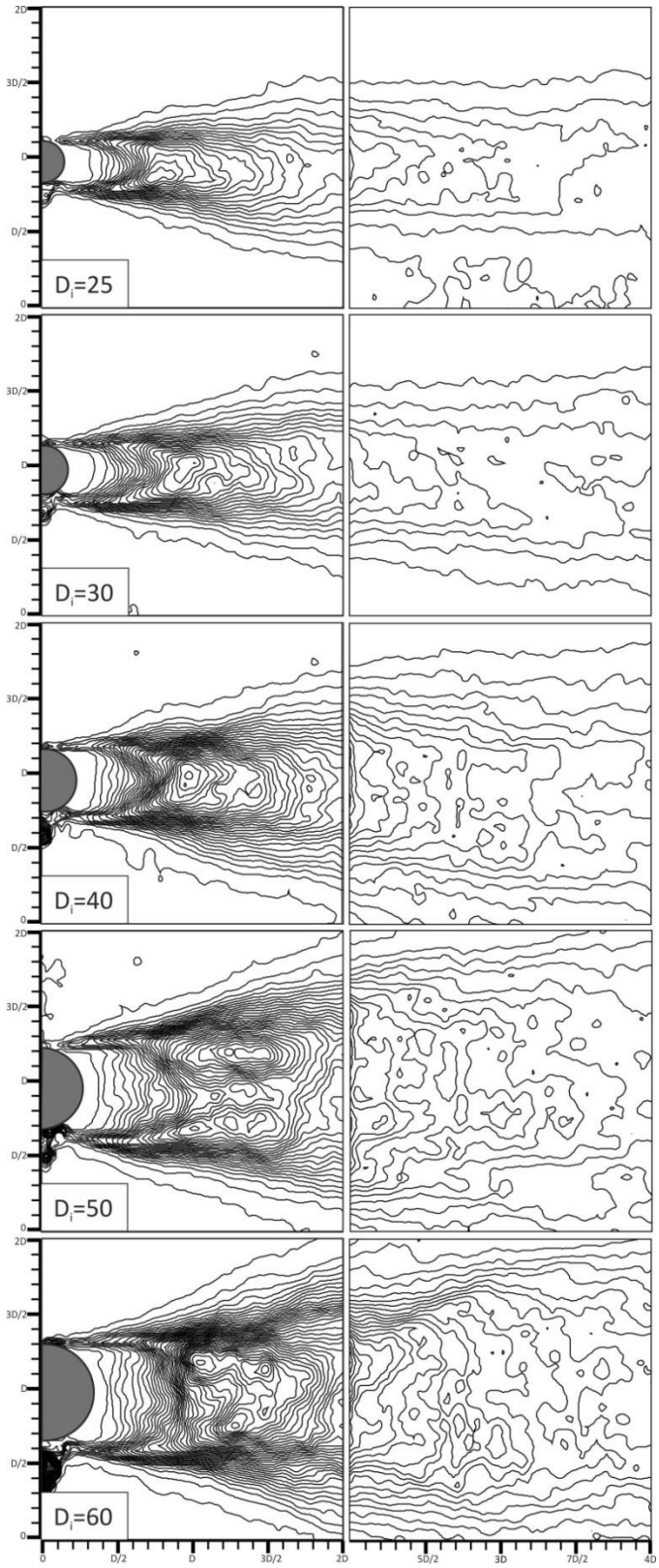
2D
3D/2
D
D/2
0
D_i=25
D_i=30
D_i=40
D_i=50
D_i=60
0
D/2
D
3D/2
2D
5D/2
3D
7D/2
4D

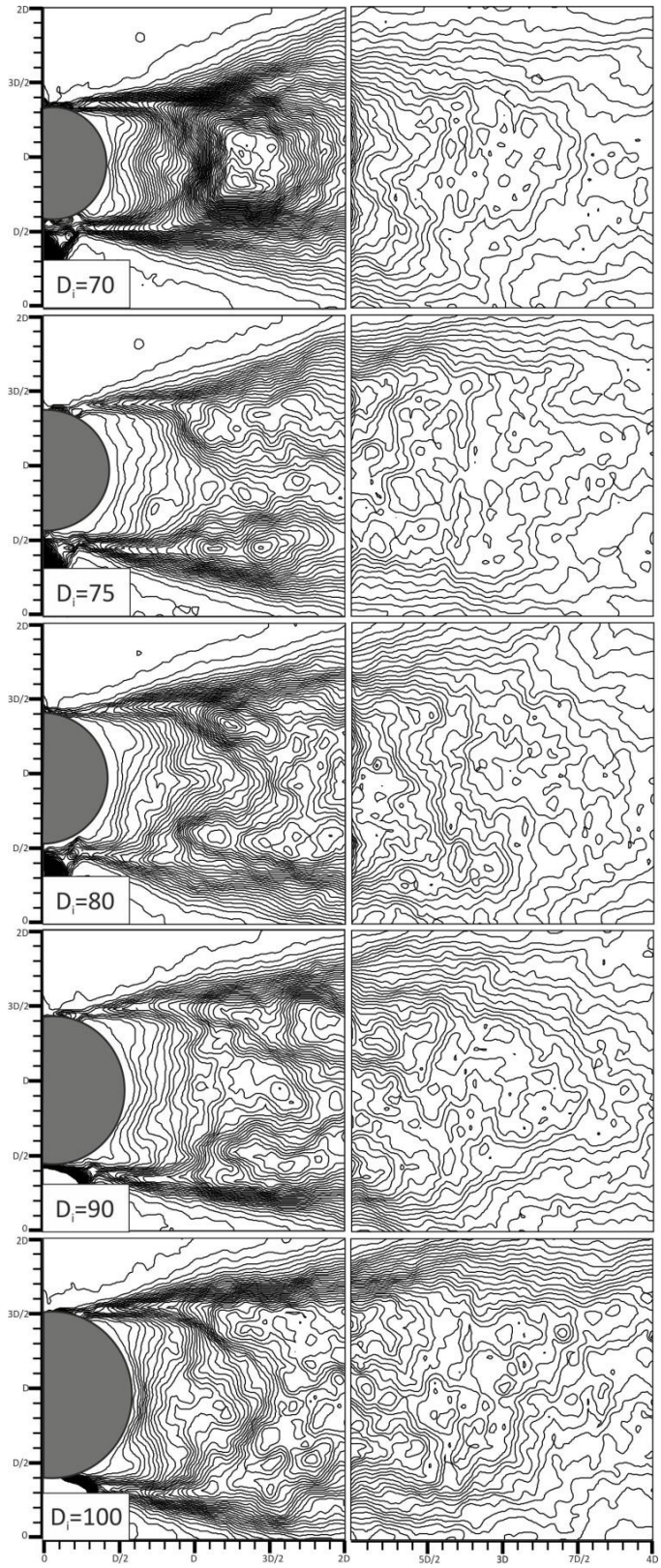

Figure 4.3. Turbulence kinetic energy (TKE) distributions downstream of the inner cylinders for different diameter ratios

4.2. Flow around Perforated Cylinders in Deep Water

Flow structure downstream of perforated cylinders was aimed to understand and introduce the effect of porosity ratio on flow control in this section. Figure 4.4 and 4.5 represents Reynolds shear stress, $<u'v'>$ and turbulence kinetic energy, TKE contours for several outer porous cylinders without an inner bare cylinder in deep water. Experiments were carried out eight different porosity ratios (β=0.25, 0.30, 0.40, 0.50, 0.55, 0.60, 0.70 and 0.80) in which the diameter of all perforated cylinders is 100 mm.

Minimum and incremental values were taken as ±0.005 and 0.005, respectively for Reynolds shear stress, $<u'v'>$ contours. Distributions of counter clock wise (CCW) and clock wise (CW) Reynolds shear stress, $<u'v'>$ contours were occurred symmetrically on both first and second field of view according to base of cylinder. Maximum values of Reynolds shear stress ($<u'v'>$) decrease with increasing porosity ratio since perforations on the cylinder diminish the effect of unsteady flow structure downstream of cylinder. Furthermore, increasing porosity ratio engenders both reductions in bluffness and deteriorates the frequency of periodical flow structure due to Karman Vortex Street. For $0.45 \leq \beta \leq 0.80$ porosity ratios, the maximum Reynolds shear stress, $<u'v'>$ values shift to the second field of view under favour of discharging jet flow from the holes and effect of each jet flow has been seen just behind the cylinder in the near wake region (Figure 4.4). For higher porosity ratios (β=0.70 – 0.80), only effect of shear layer could be observed because of remaining not almost a bluff body upstream direction. In other words, incoming flow structure to the bluff body has nearly equivalent specifications with discharging flow from holes on the bluff body. Proof of this claim: positive (solid lines) and negative (negative lines) $<u'v'>$ contours get closer to each other at approximately 4D in horizontal direction from β=0.50 to β=0.70; meanwhile after β=0.70 ratio, shear layer extends beyond the second field of view and the existence of any approaching shear layers to each other is not observed anymore. Additionally, contours of the jet flow as shown in figure 4.4 attenuate their impact from β=0.25 to 0.80, so it means that effect of jet flow decreases with increasing porosity ratio.

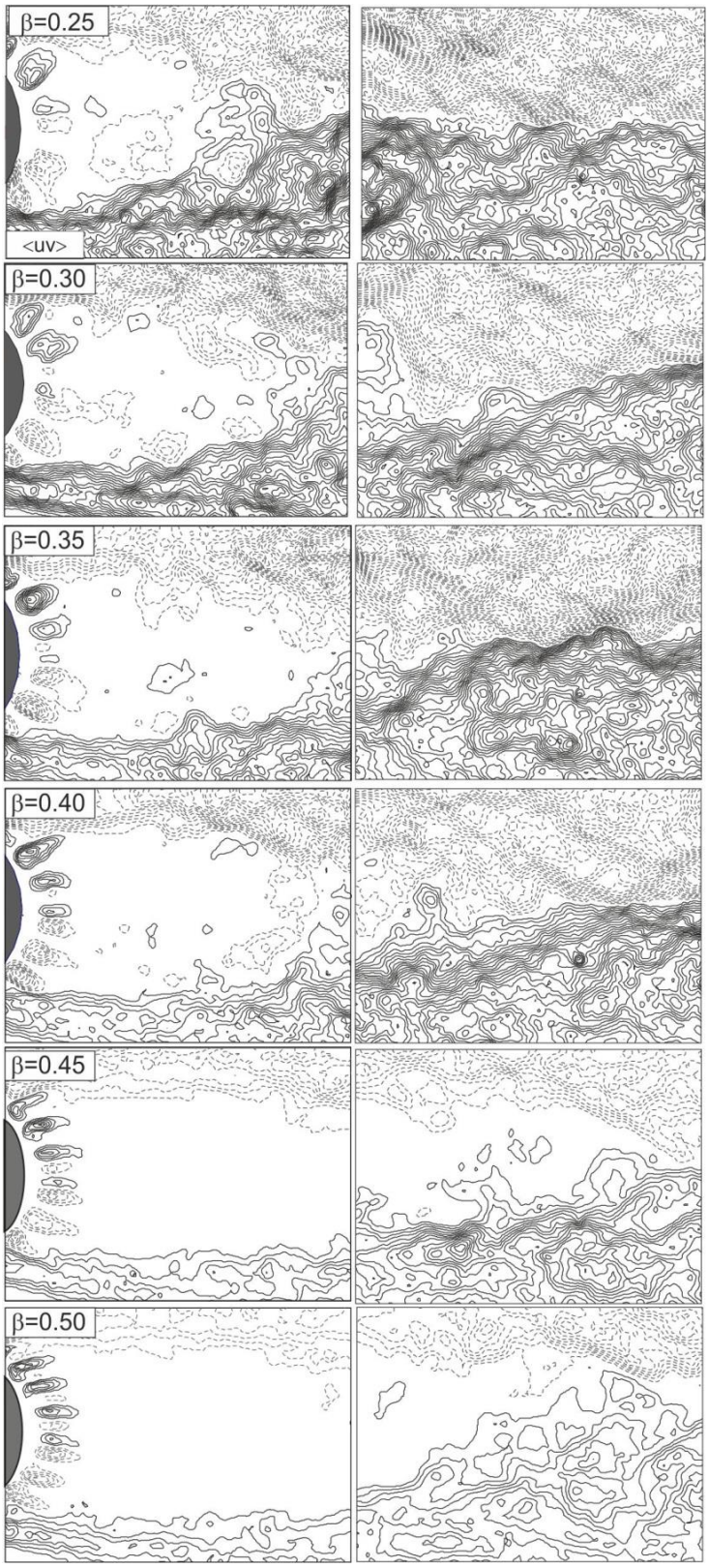
β=0.25
<uv>
β=0.30
β=0.35
β=0.40
β=0.45
β=0.50

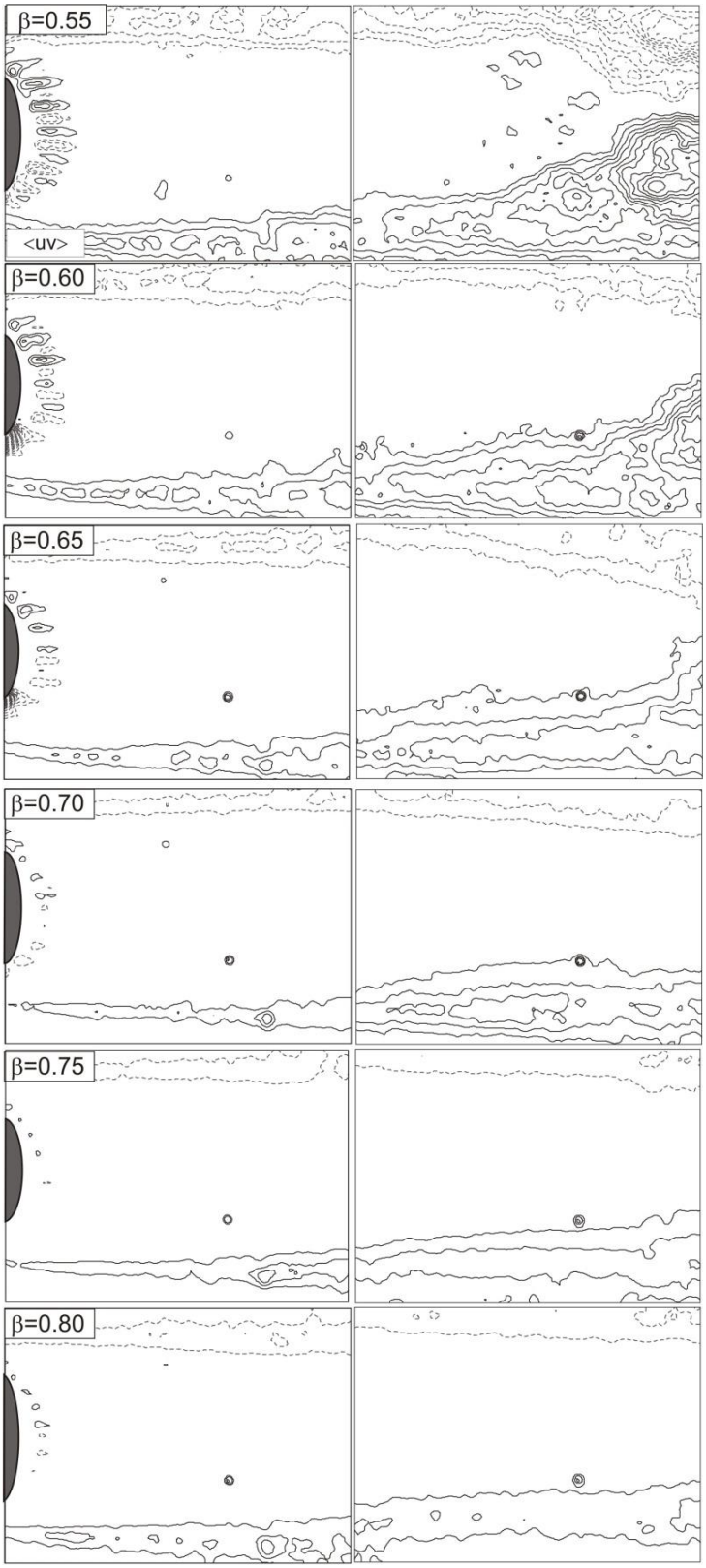

Figure 4.4. Reynolds shear stress distributions downstream of the outer (perforated) cylinders for different porosity ratios

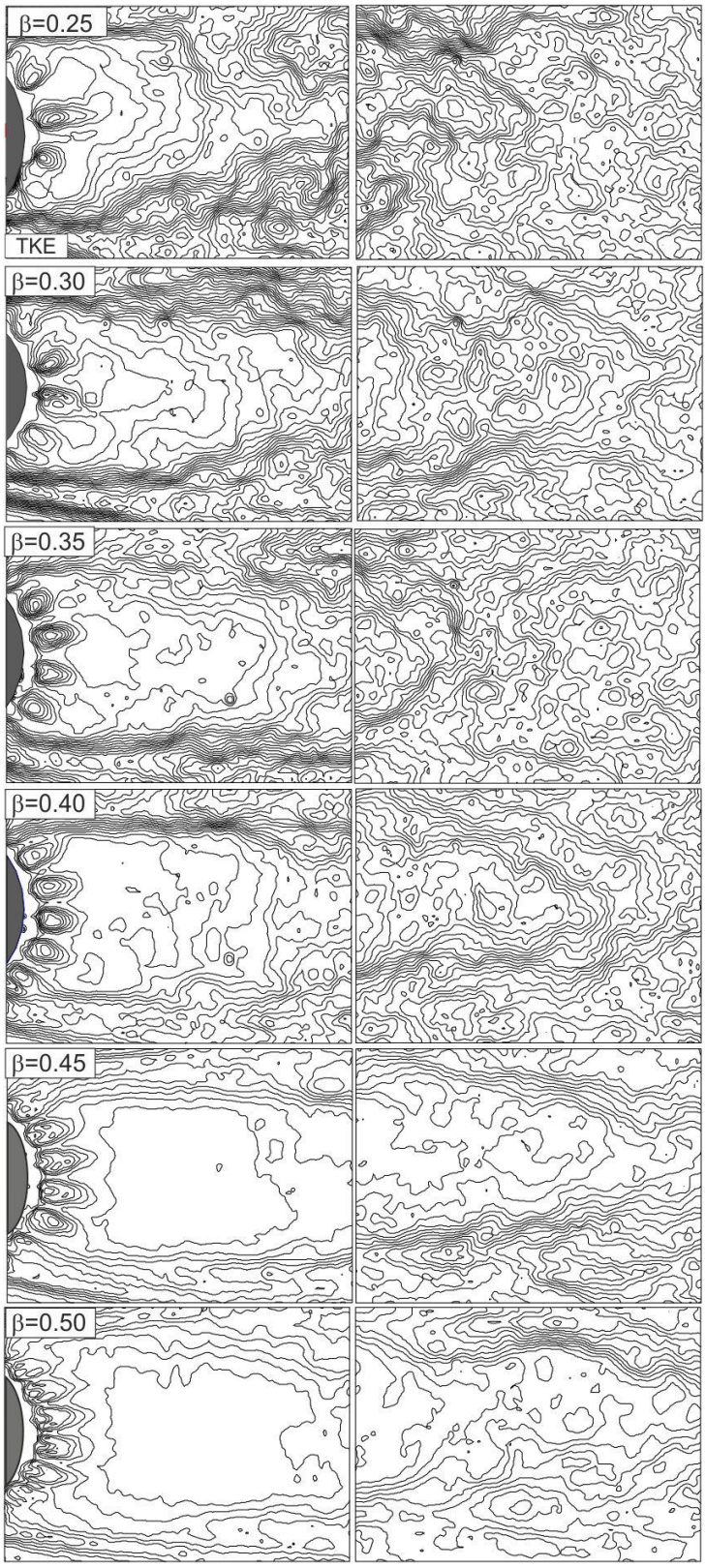
β=0.25
TKE
β=0.30
β=0.35
β=0.40
β=0.45
β=0.50

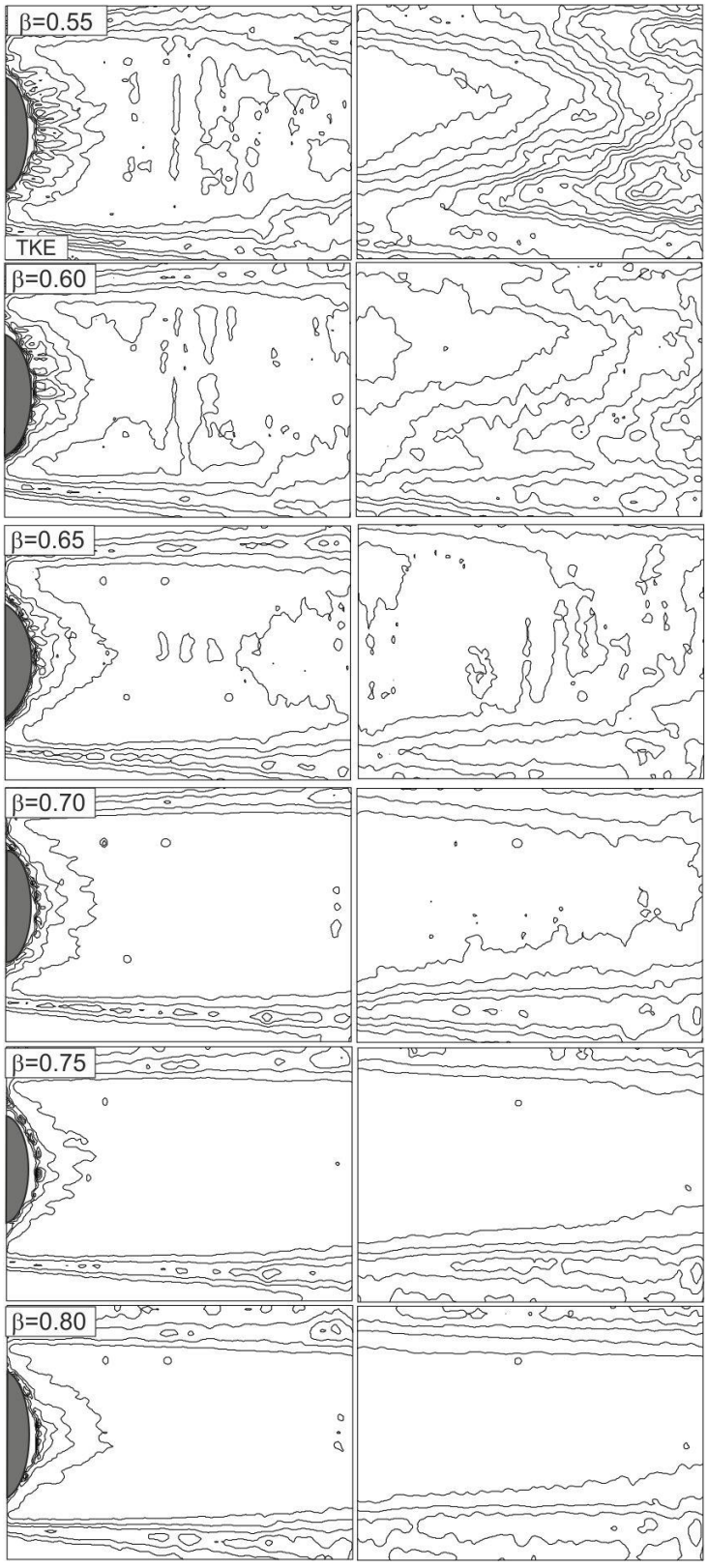

Figure 4.5. Turbulence kinetic energy distributions downstream of the outer cylinders for different porosity ratios

The minimum and incremental values of TKE contours were taken as 0.005 in figure 4.5. Similarly to Reynolds shear stress, $< u'v' >$ contours, maximum values of TKE significantly decrease with increasing porosity ratio and impact of the jet flow is more clearly effective until β=0.50 value and for higher porosity ratios jet flow effect slightly decreases. Turbulence kinetic energy concentration which was focused on shear layers at both sides of the cylinder for high porosity ratios was because of the Kelvin – Helmholtz instabilities as a consequence of prevention of von Karman Vortex Street. Maximum TKE values of perforated cylinders for different porosity ratios are shown in Figure 4.6. Maximum TKE value of 100 mm diameter bare cylinder was determined to be approximately 0.32, however, maximum TKE value suddenly dropped to 0.2 value (62.5 % reduction) for β=0.25. Maximum TKE value decreases to 0.03 with increasing porosity ratio and for $\beta \geq 0.65$; maximum value of TKE almost remains constant. Quantitative values of TKE manifest notable reduction of energy intensity and differences between bare and perforated cylinders.

Both Reynolds shear stress and turbulent kinetic energy data reveal that a cylinder with porous structure could be used as a control element in suppression of large scale vortices formed in the wake region of bluff body. Because increasing porosity ratio indicates positive control effect owing to both reduction of bluffness and jet flows through the holes on the surface of perforated cylinder. Jet flow causes momentum transfer to the wake region downstream of the cylinder and this provides perturbation of fresh (upper and lower sides of the cylinder) and wake flow (aft side of cylinder) regions (Figure 4.4 and 4.5). Flow control can be achieved successfully if bare (inner) cylinders are shrouded concentrically by perforated (outer) cylinders and flow structures of shrouded or coupled cylinders (inner and outer cylinder arrangement) are going to be discussed incoming sections.

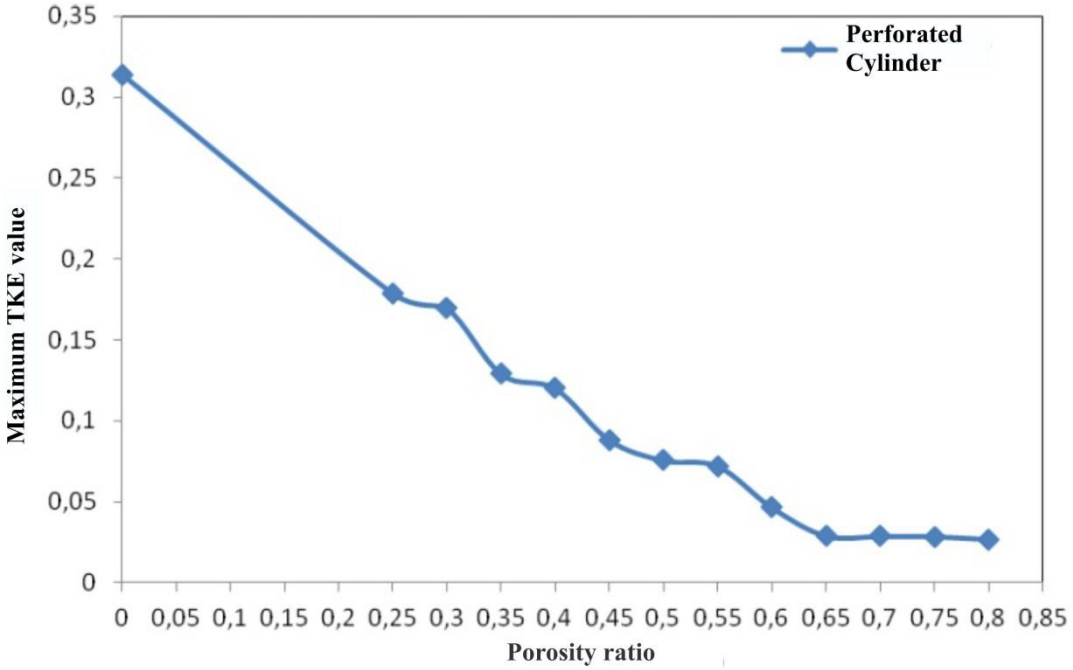

Figure 4.6. Maximum TKE values of perforated cylinders for different porosity ratios

4.3. Flow around Coupled Cylinders in Deep Water

Porosity and diameter ratios of inner – outer cylinder arrangement are investigated as the most important parameters to control unsteady flow structure. Time averaged vorticity, Reynolds shear stress, and turbulence kinetic energy contours are presented in this section to demonstrate the effect of flow control with perforated cylinders (shrouded).

Time averaged vorticity (<ω>) contours downstream of the cylinder couples where bare cylinders were shrouded with perforated cylinders are shown in Figures from 4.7 to 4.15. Each figure shows the effect of porosity within the range of $0.25 \leq \beta \leq 0.80$ on the inner cylinder. Two fields of view are sufficient for all <ω> contours of coupled cylinders as well as for all deep water results of coupled cylinders. However, one field of view was sufficient for bare cylinders in deep water because of flow characteristics get close to free stream properties after first field of view. While the solid lines indicate positive (CCW) vorticity contours, dashed lines show negative (CW) vorticity contours. The minimum and incremental values of time averaged vorticity contours were taken as ±1 and 1, respectively.

Figure 4.7 shows vorticity effects for D_i/D_o=0.25 cylinder couple at different porosities. Almost symmetrical shear layer structure can be observed for all porosity ratios. Shear layers elongates to the second field of view owing to outer cylinder's jet flow effect. Diameter ratio is very low for D_i/D_o=0.25 case, for this reason vorticity contours of bare D_i=25 mm and coupled cylinder arrangements are different from each other. Effect of the outer cylinder is more dominant on the flow structure downstream of coupled cylinder, although control effect is seen. It can be concluded that the shear layers occurring at low porosities from upper and lower sides of the cylinder couple are generated by the outer cylinder. Most effective control situations are revealed for $0.30\leq\beta\leq0.60$ at D_i/D_o=0.25 case. Inner cylinder effect is clearly seen for high porosity ratios of β=0.70 and β=0.80. Two different vorticity pairs (designated by 'A' and 'B' in Figure 4.7) observed for β=0.70 and β=0.80 since increasing porosity causes to reduction of outer cylinder bluffness. The vorticity pair 'A' is occurred due to inner cylinder and 'B' is occurred due to outer cylinder. Accordingly, it can be said that control effect disappeared for β=0.70 and β=0.80 cases compared to other porosity ratios for D_i/D_o=0.25 case. Because shear layers of inner cylinder get close to 0.5D location for β=0.70 and β=0.80 meanwhile interaction of shear layers elongates to the second field of view for $0.25\leq\beta\leq0.60$.

Time averaged vorticity contours for D_i/D_o=0.30, D_i/D_o=0.40 and D_i/D_o=0.50 are shown in Figure 4.8, 4.9 and 4.10, respectively. Flow structure of these coupled cylinders are similar to D_i/D_o=0.25 case but increasing diameter ratio slightly reduces the effect of outer cylinder for flow control; however increase in vorticity magnitude takes place. Outer cylinder is, again, dominant along downstream of the flow for porosity ratios of β=0.25 and β=0.30 cases. For porosities β=0.7 and 0.8, the negative and positive vorticity in near wake region of the cylinder couple get closer to each other similar to diameter ratio of D_i/D_o=0.25. It can be denoted that diameter ratio is an operative parameter on the flow characteristics.

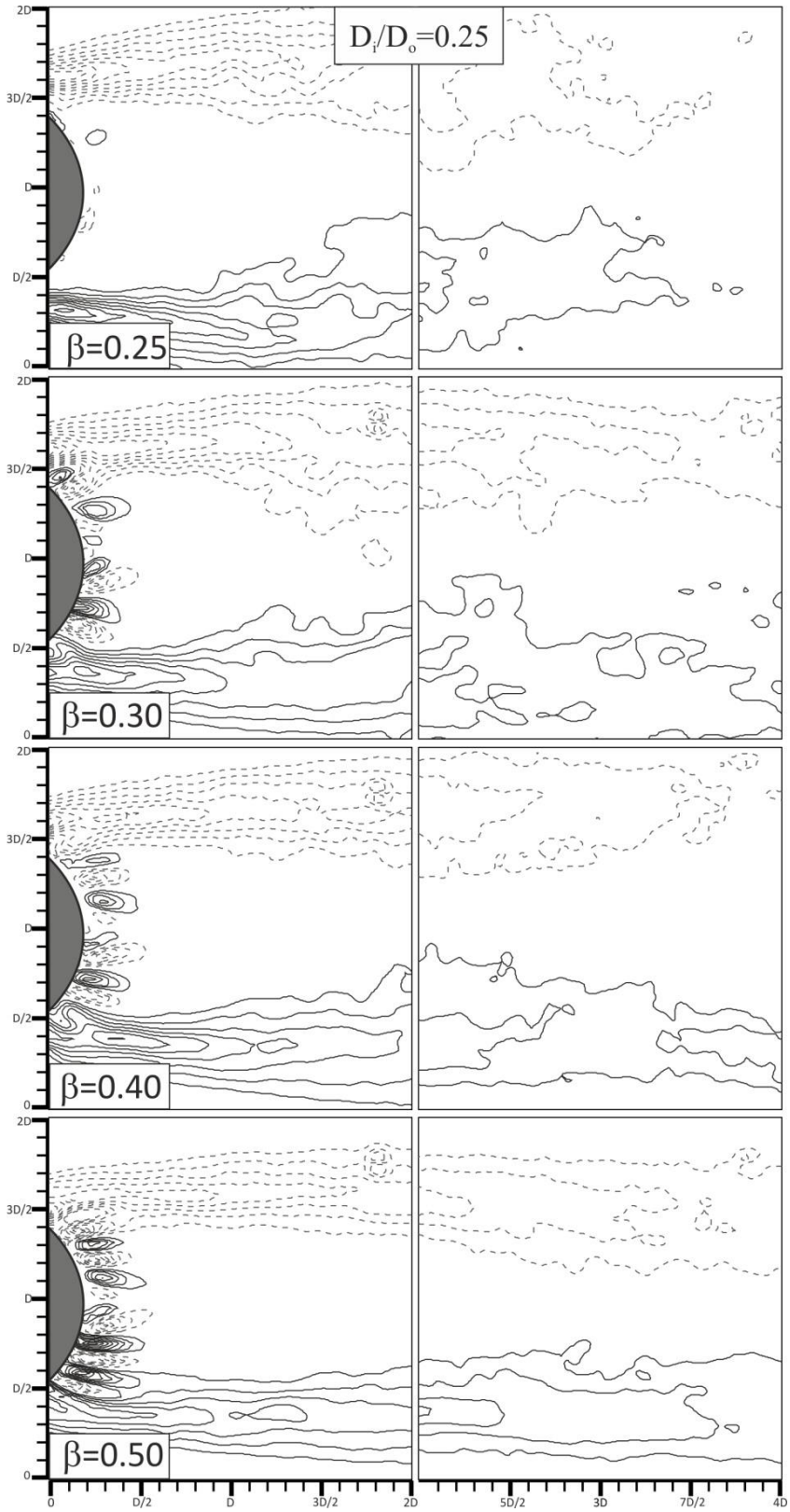
D_i/D_o=0.25
β=0.25
β=0.30
β=0.40
β=0.50
2D
3D/2
D
D/2
0
0
D/2
D
3D/2
2D
5D/2
3D
7D/2
4D

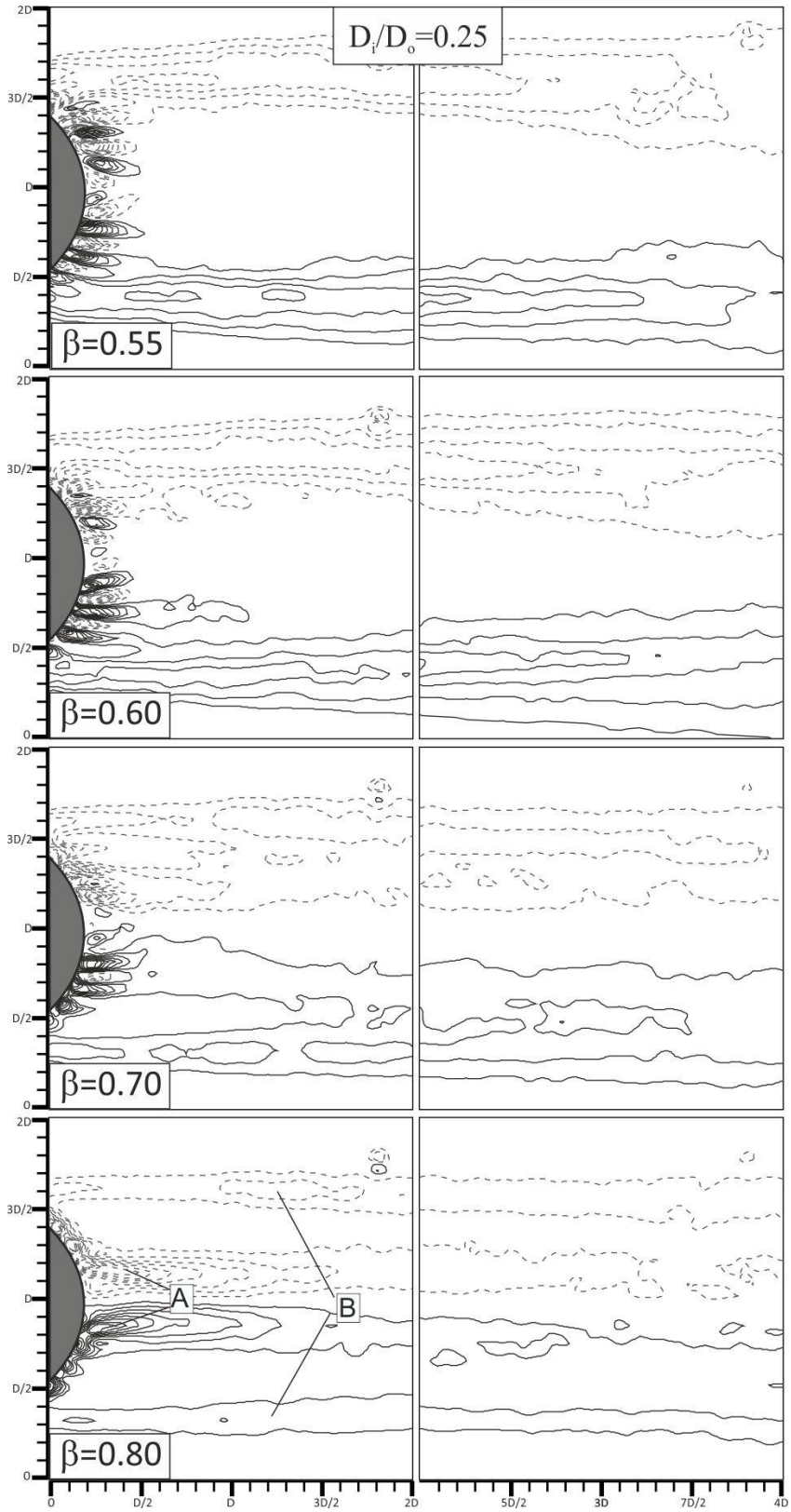

Figure 4.7. Distribution of time averaged vorticity counters at D_i/D_o=0.25 for different porosity

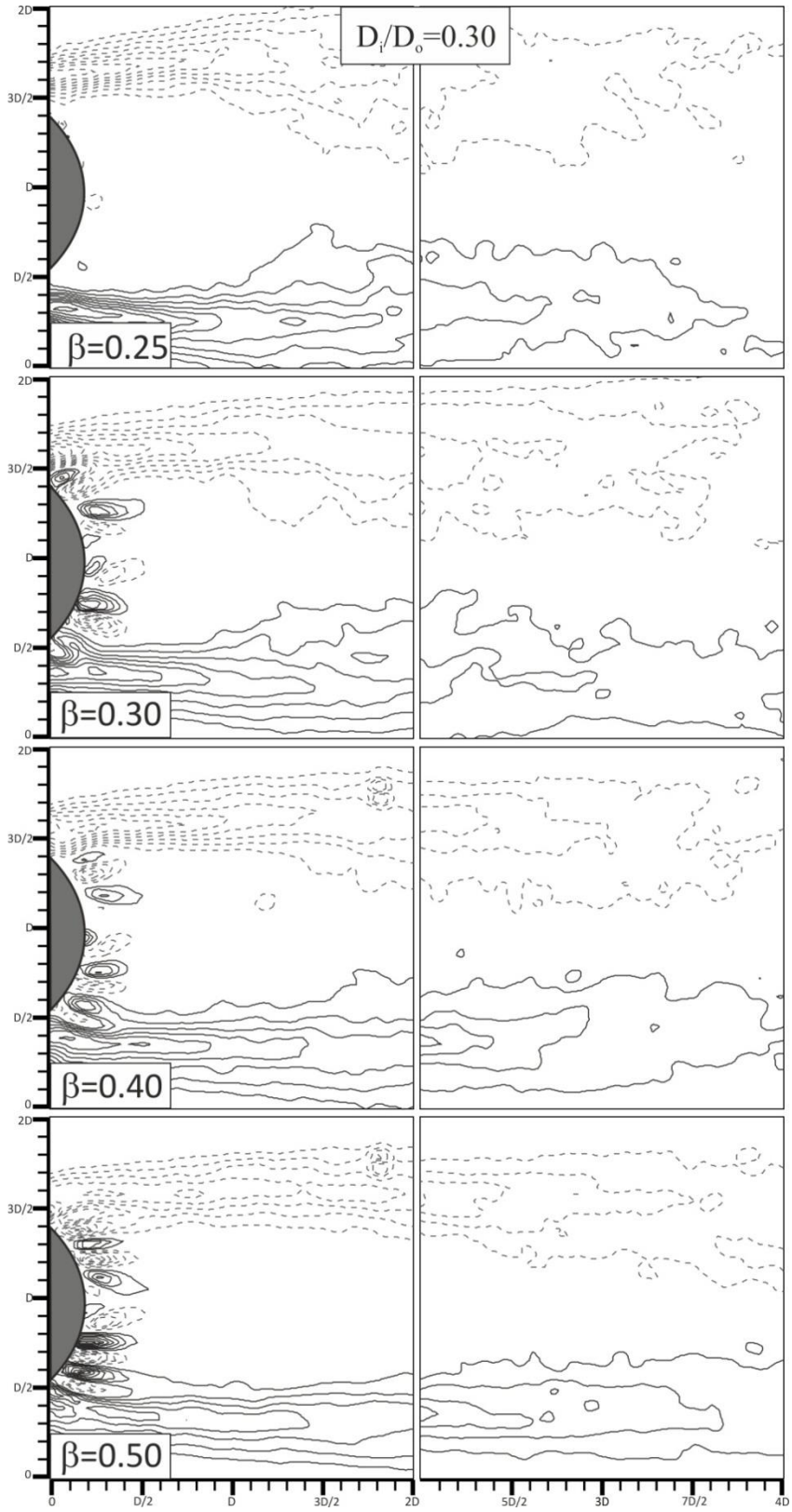
D_i/D_o=0.30
β=0.25
β=0.30
β=0.40
β=0.50
2D
3D/2
D
D/2
0
0
D/2
D
3D/2
2D
5D/2
3D
7D/2
4D

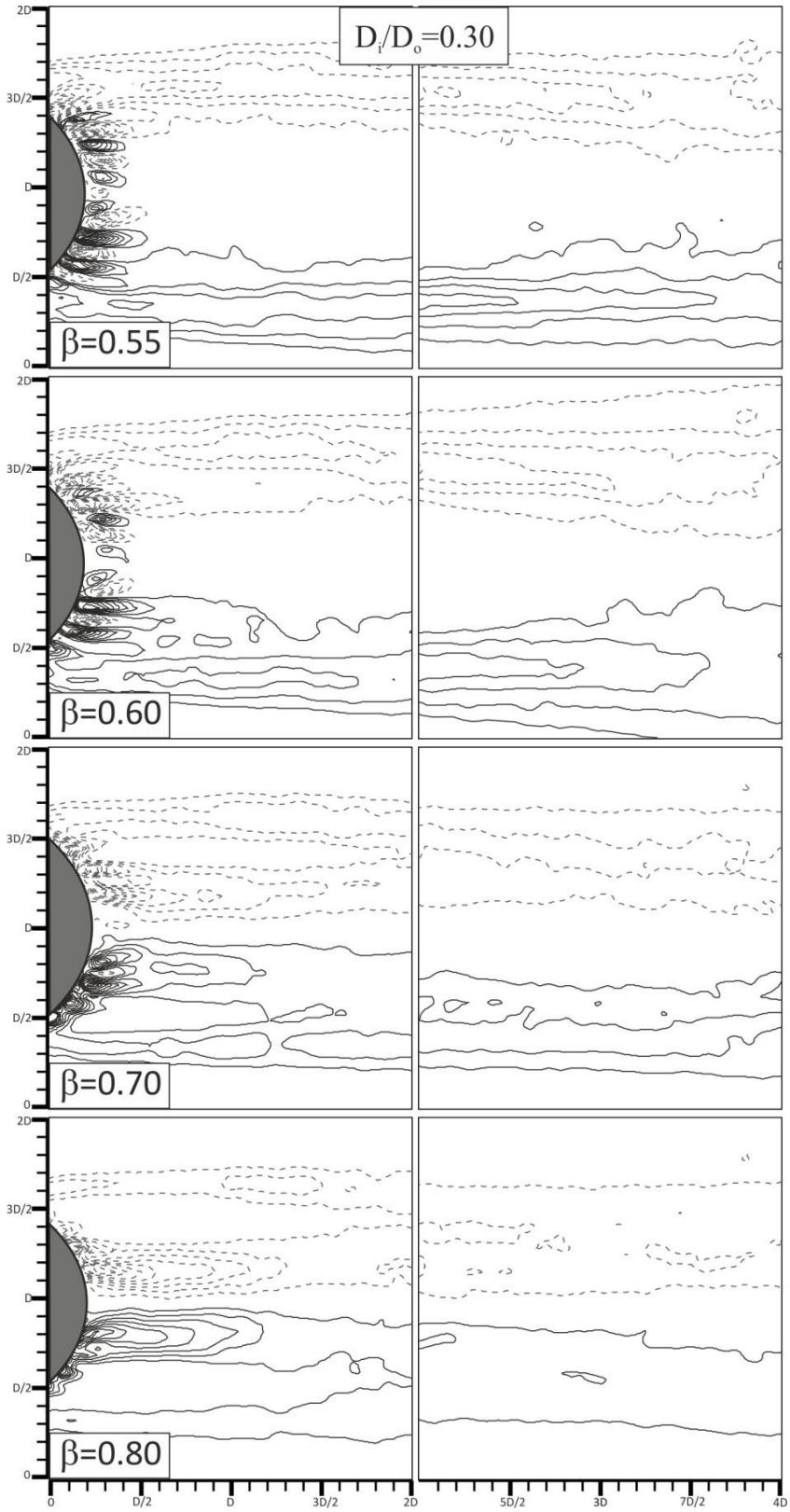

Figure 4.8. Distribution of time averaged vorticity counters at D_i/D_o=0.30 for different porosity

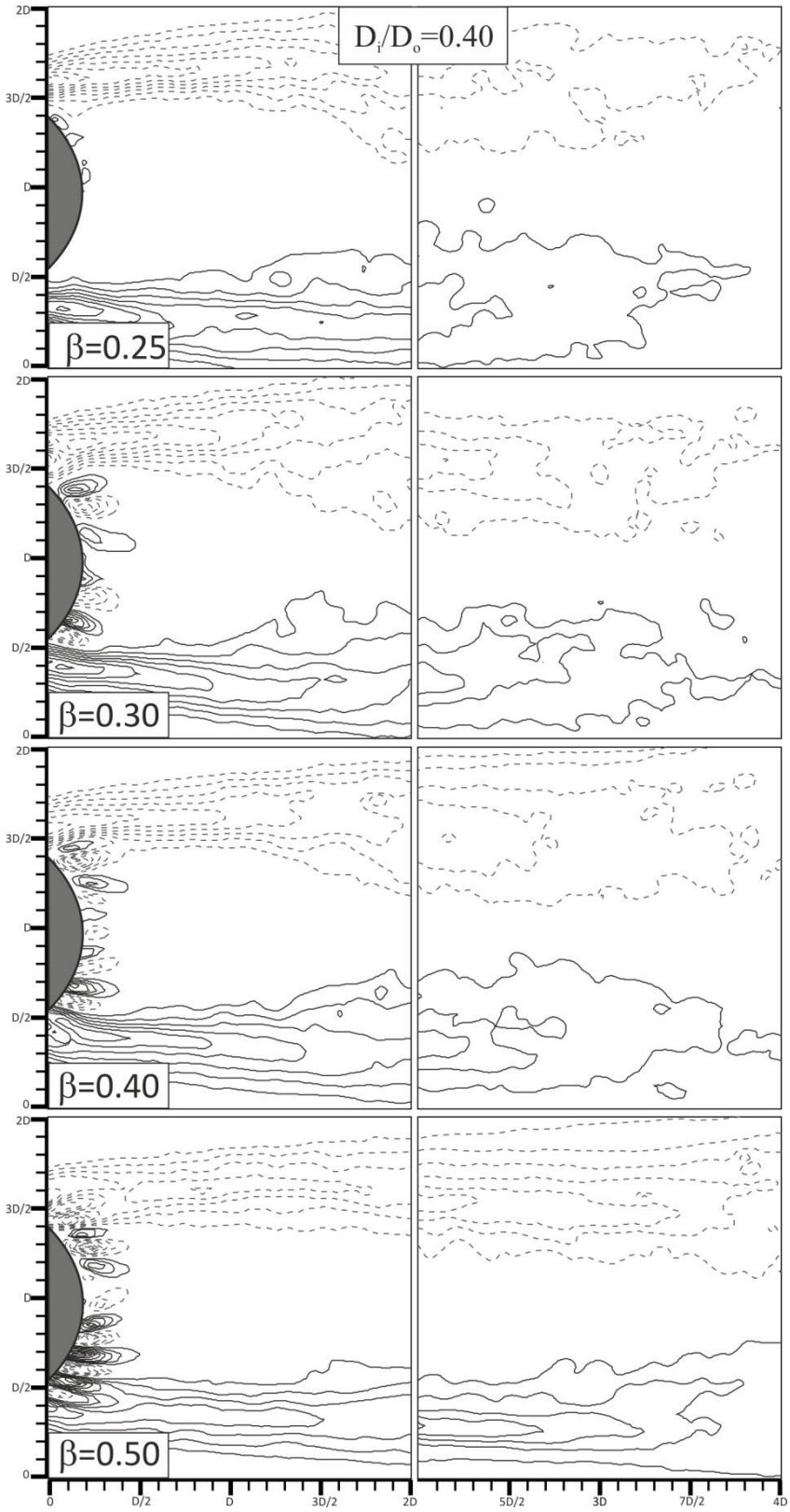
D_i/D_o=0.40
β=0.25
β=0.30
β=0.40
β=0.50
2D
3D/2
D
D/2
0
0
D/2
D
3D/2
2D
5D/2
3D
7D/2
4D

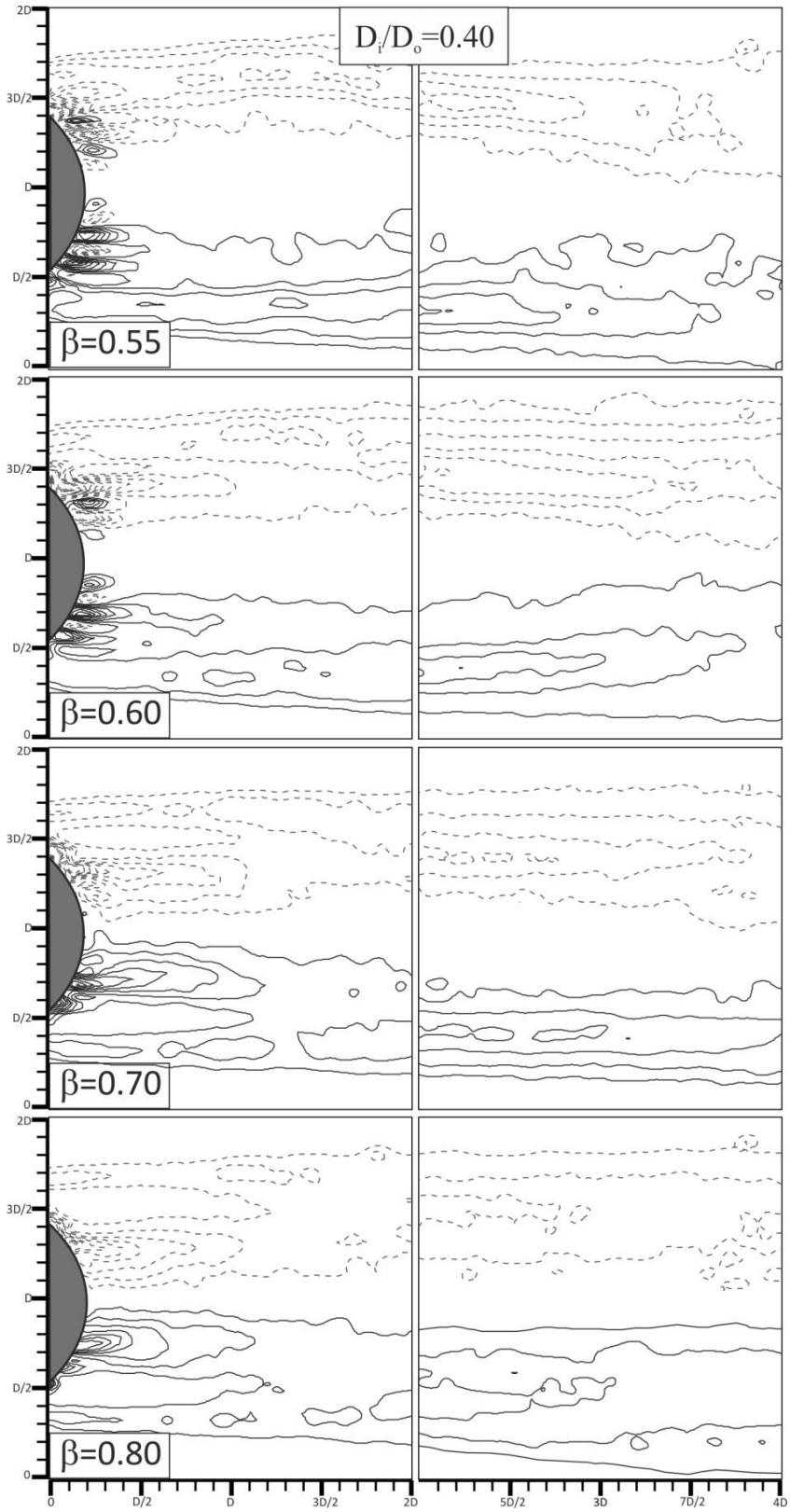

Figure 4.9. Distribution of time averaged vorticity counters at D_i/D_o=0.40 for different porosity

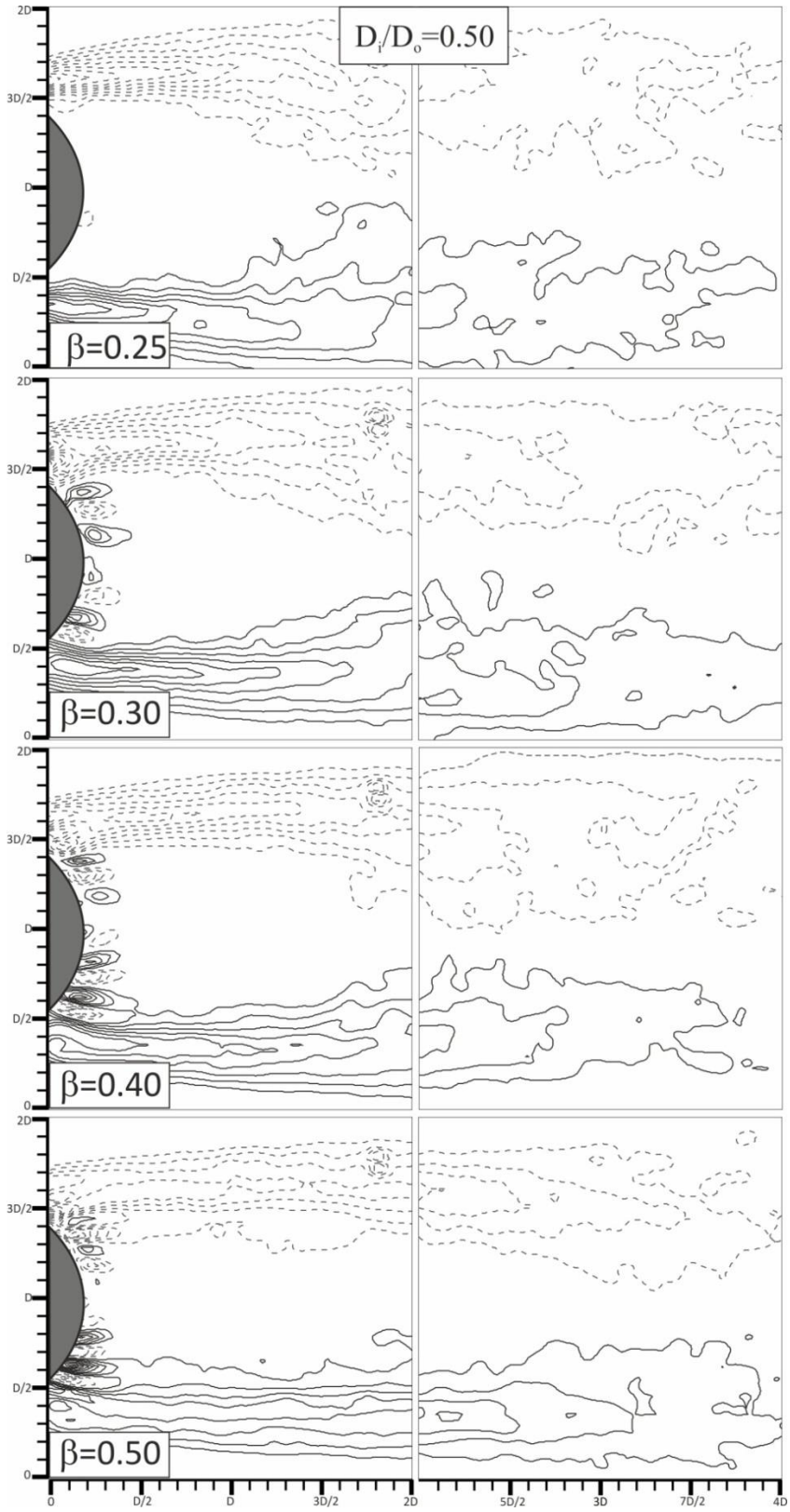
D_i/D_o=0.50
β=0.25
β=0.30
β=0.40
β=0.50
2D
3D/2
D
D/2
0
D/2
D
3D/2
2D
5D/2
3D
7D/2
4D

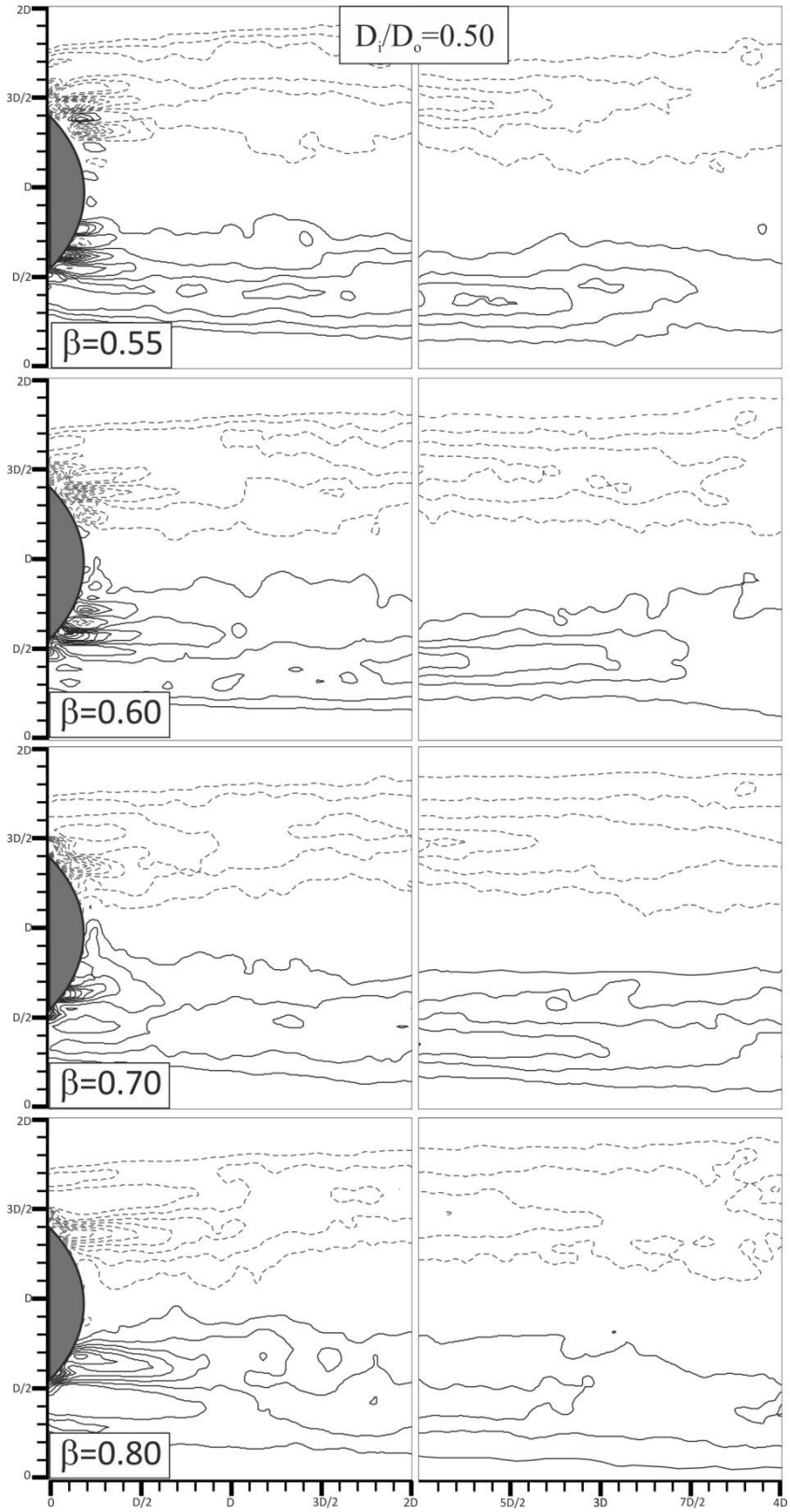

Figure 4.10. Distribution of time averaged vorticity counters at D_i/D_o=0.50 for different porosity

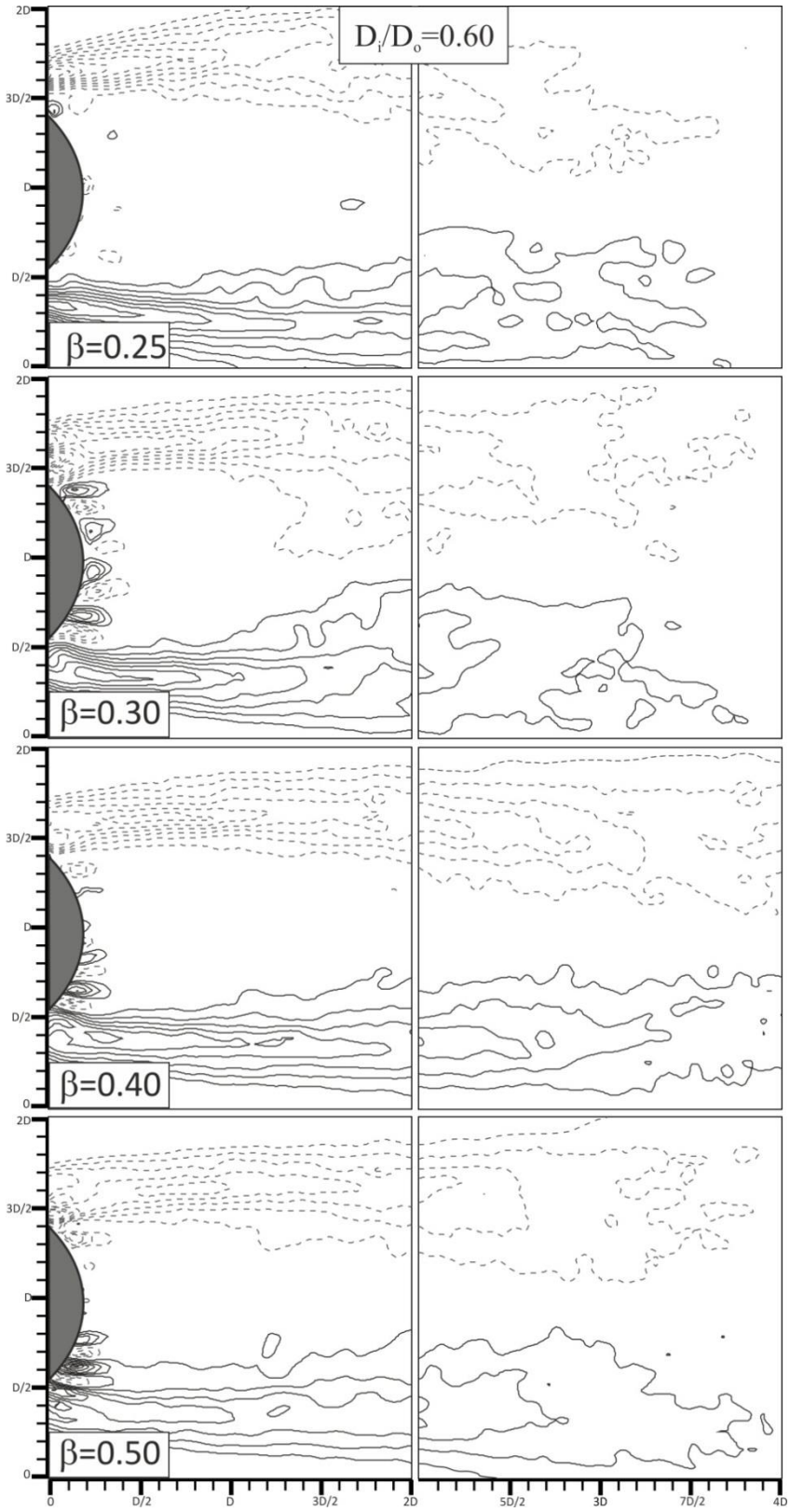
D_i/D_o=0.60
β=0.25
β=0.30
β=0.40
β=0.50
2D
3D/2
D
D/2
0
0
D/2
D
3D/2
2D
5D/2
3D
7D/2
4D

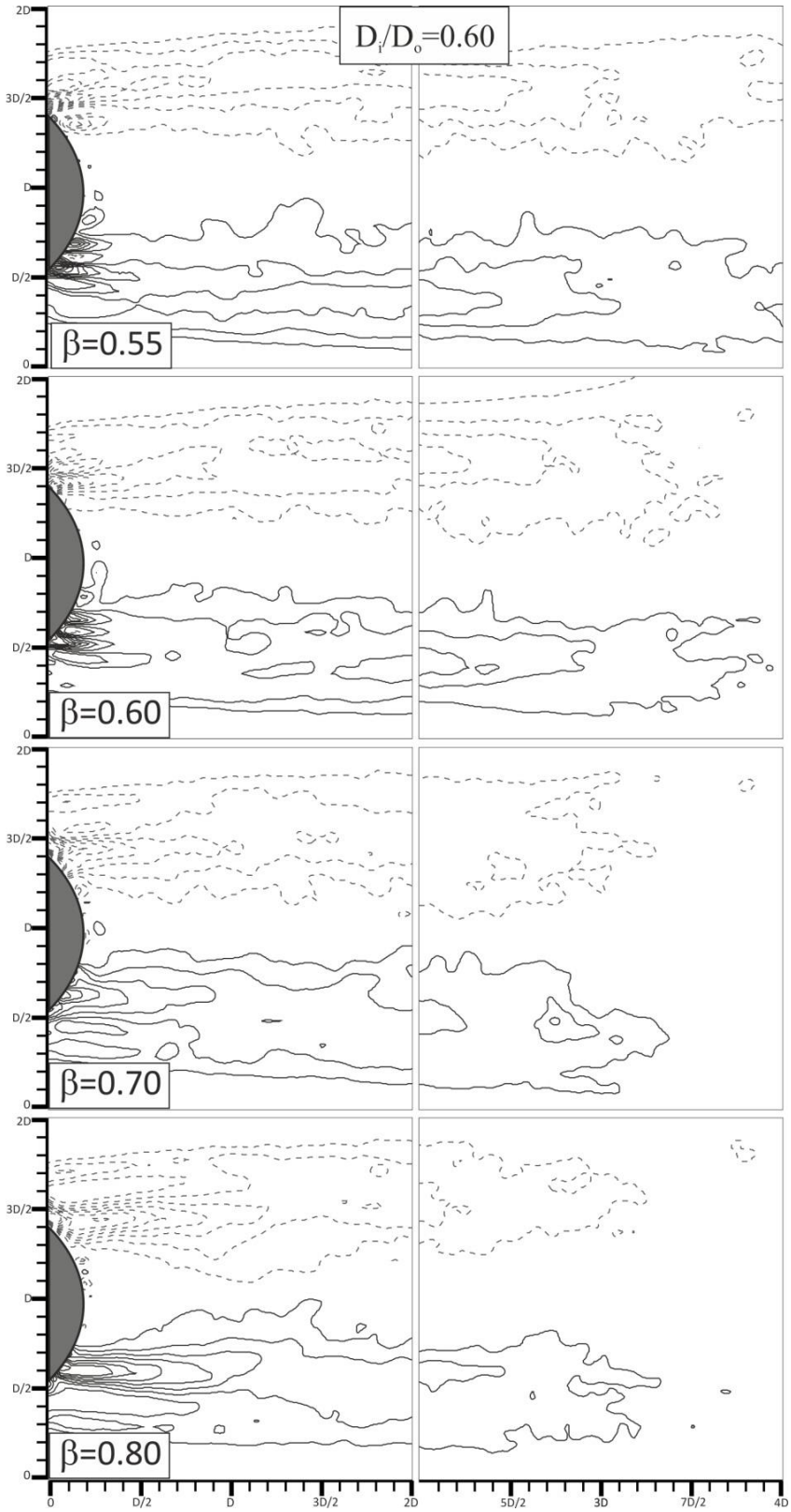

Figure 4.11. Distribution of time averaged vorticity counters at D_i/D_o=0.60 for different porosity

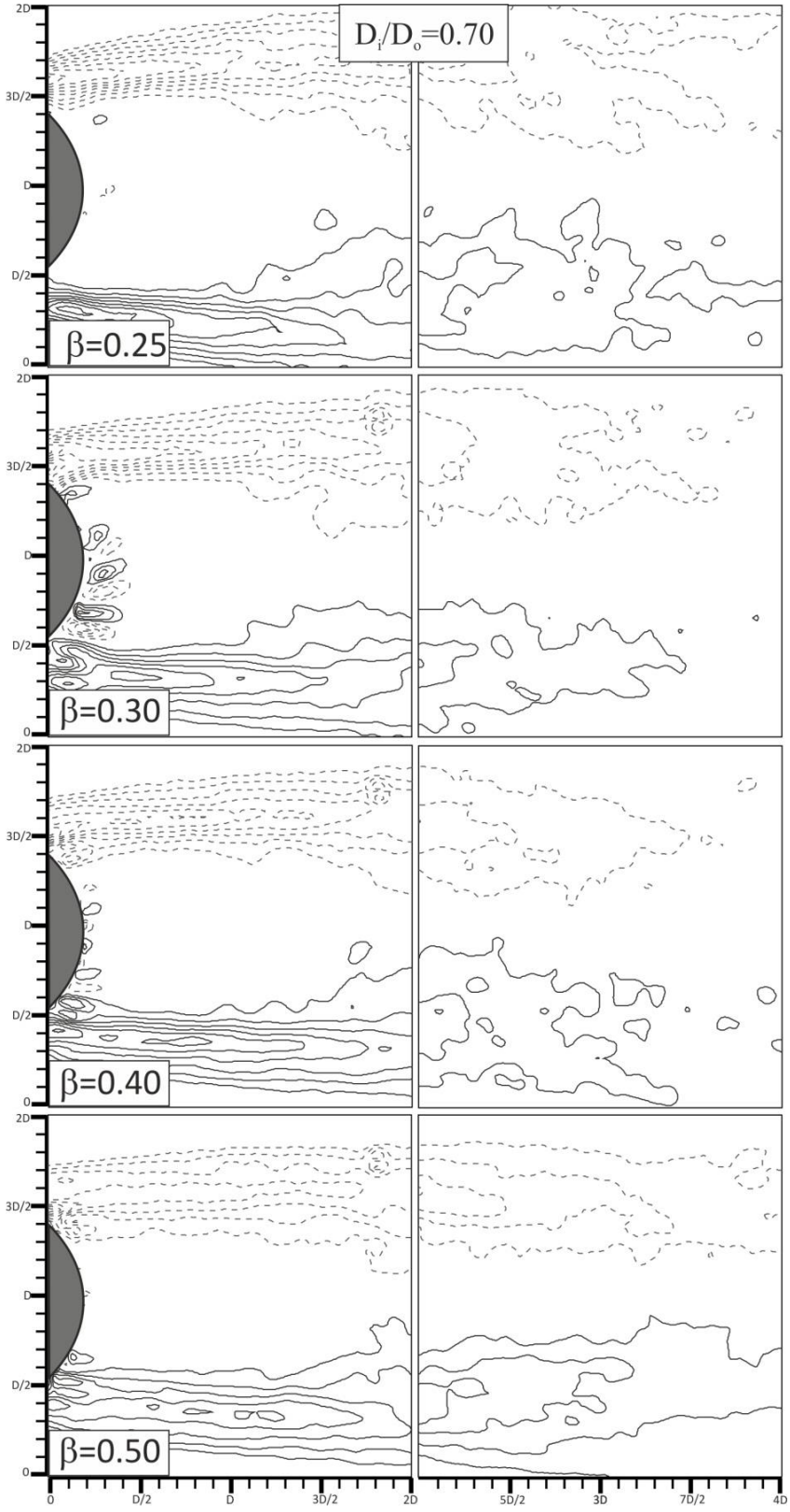
D_i/D_o=0.70
β=0.25
β=0.30
β=0.40
β=0.50
2D
3D/2
D
D/2
0
D/2
D
3D/2
2D
5D/2
3D
7D/2
4D

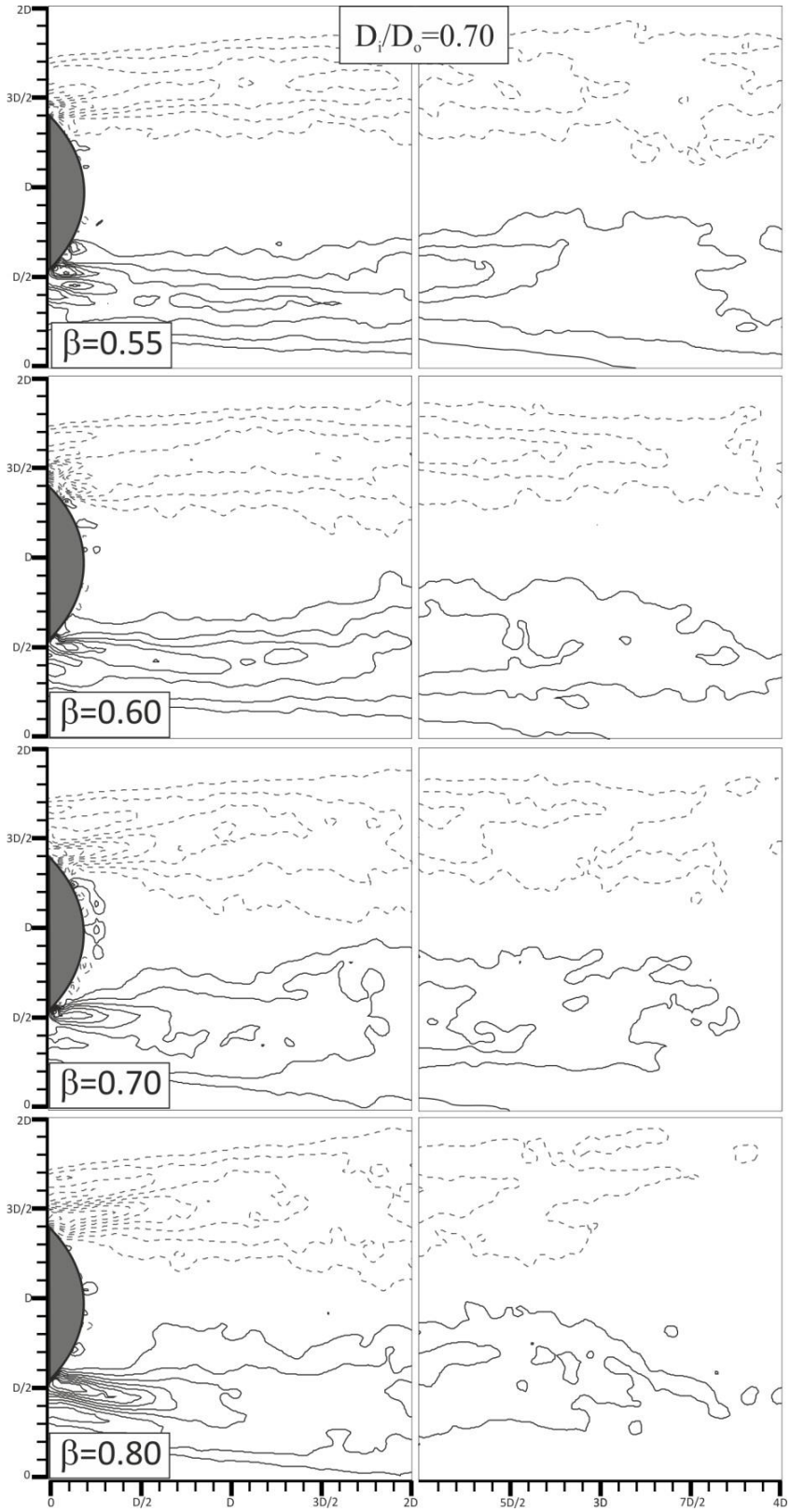

Figure 4.12. Distribution of time averaged vorticity counters at D_i/D_o=0.70 for different porosity

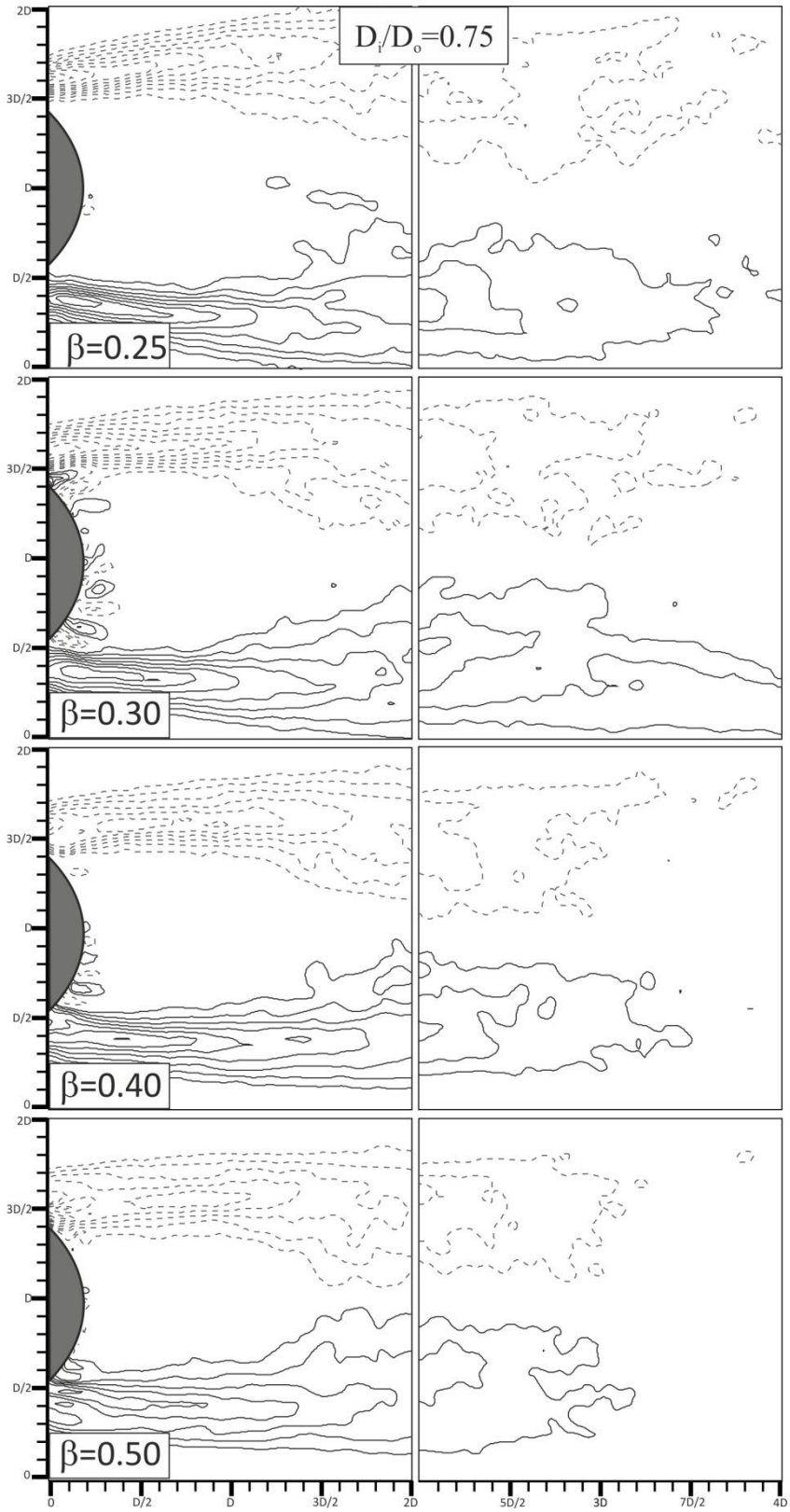
D_i/D_o=0.75
β=0.25
β=0.30
β=0.40
β=0.50
2D
3D/2
D
D/2
0
0
D/2
D
3D/2
2D
5D/2
3D
7D/2
4D

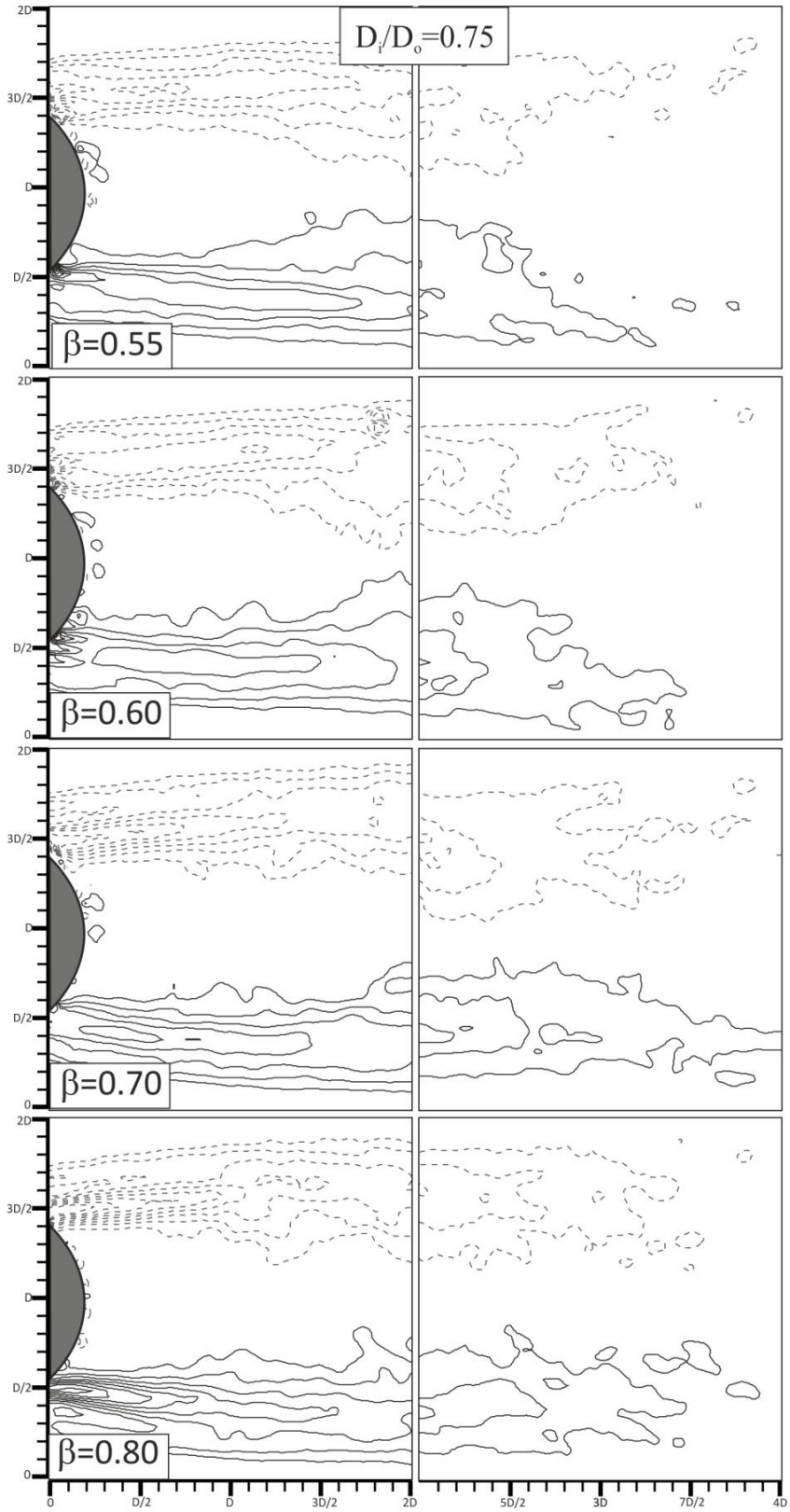

Figure 4.13. Distribution of time averaged vorticity counters at D_i/D_o=0.75 for different porosity

Figures 4.11, 4.12 and 4.13 show the time averaged vorticity contours at D_i/D_o=0.60, 0.70 and 0.75, respectively. Shear layers of these coupled cylinders elongate to second field of view for all porosities, β. If these vorticity contours compared with the results of Figure 4.1, a successfully control of flow downstream of the cylinder is seen. Increasing diameter ratios, D_i/D_o, are more effective on the flow characteristics compared to the variation of porosity, β. Two different vorticity pairs are occurred for porosities of β=0.70 and 0.80 (‘A’ and ‘B’ vorticity pair) at low diameter ratios, D_i/D_o, and, these vorticity pairs are merged with each other after diameter ratio of D_i/D_o=0.60 and symmetrical structure of shear layers with respect to the centerline of the cylinder takes place for higher porosity, β, values. Also, effect of the inner cylinder completely annihilated after D_i/D_o=0.75 for higher porosities, β,.

Figures 4.14 and 4.15 represent the time averaged vorticity contours for D_i/D_o=0.80 and D_i/D_o=0.90 diameter ratios, respectively. It seen from both figures that differences in diameter ratio do not affect the time averaged vorticity structure for all porosity, β, values. In other words, all porosities, β, affect vorticity structure at approximately the same levels for D_i/D_o=0.80 and D_i/D_o=0.90 cases. Despite the fact that the effect of flow control still exists compared to bare cylinders D_i=80 and D_i=90 mm from Figure 4.1, shear layer shortens and gets close to the first field of view. Due to the decrease in the distance between the inner and outer cylinder with the increasing diameter ratios, flow entry into the wake region through the perforated cylinder is reduced. Thus, the effect of the perforated circular cylinder decreases with increasing diameter ratios.

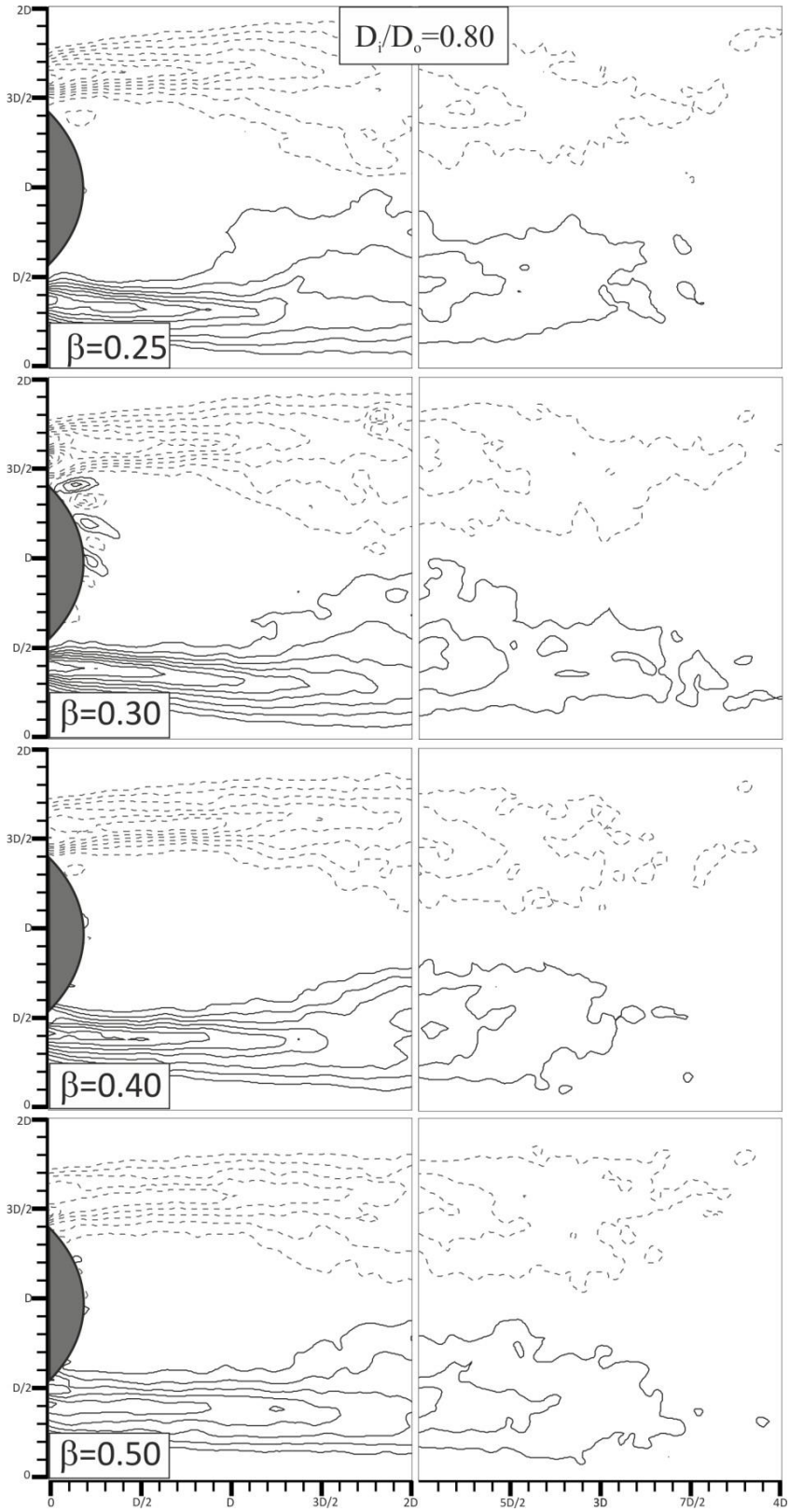
D_i/D_o=0.80
β=0.25
β=0.30
β=0.40
β=0.50
2D
3D/2
D
D/2
0
D/2
D
3D/2
2D
5D/2
3D
7D/2
4D

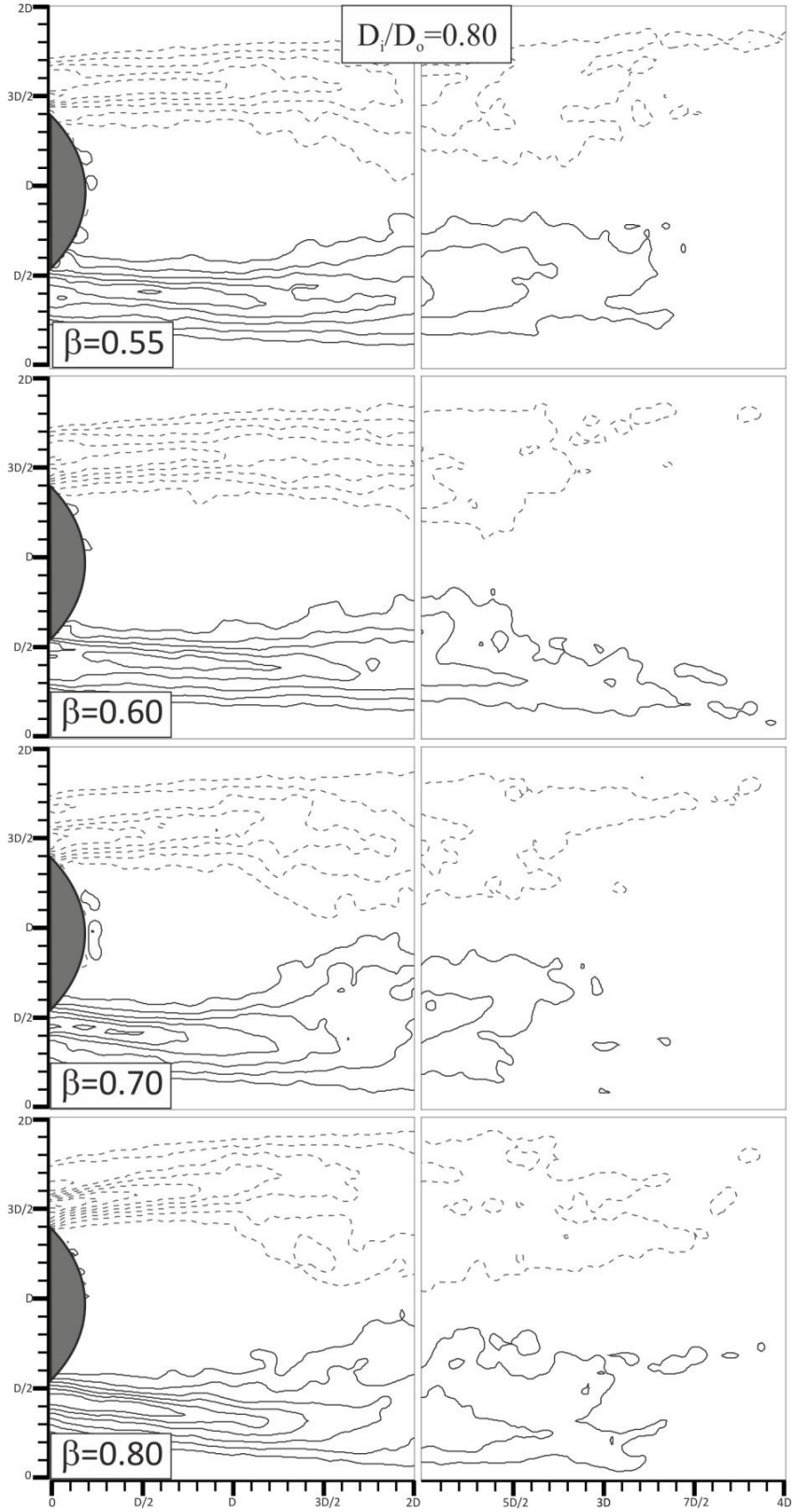

Figure 4.14. Distribution of time averaged vorticity counters at D_i/D_o=0.80 for different porosity

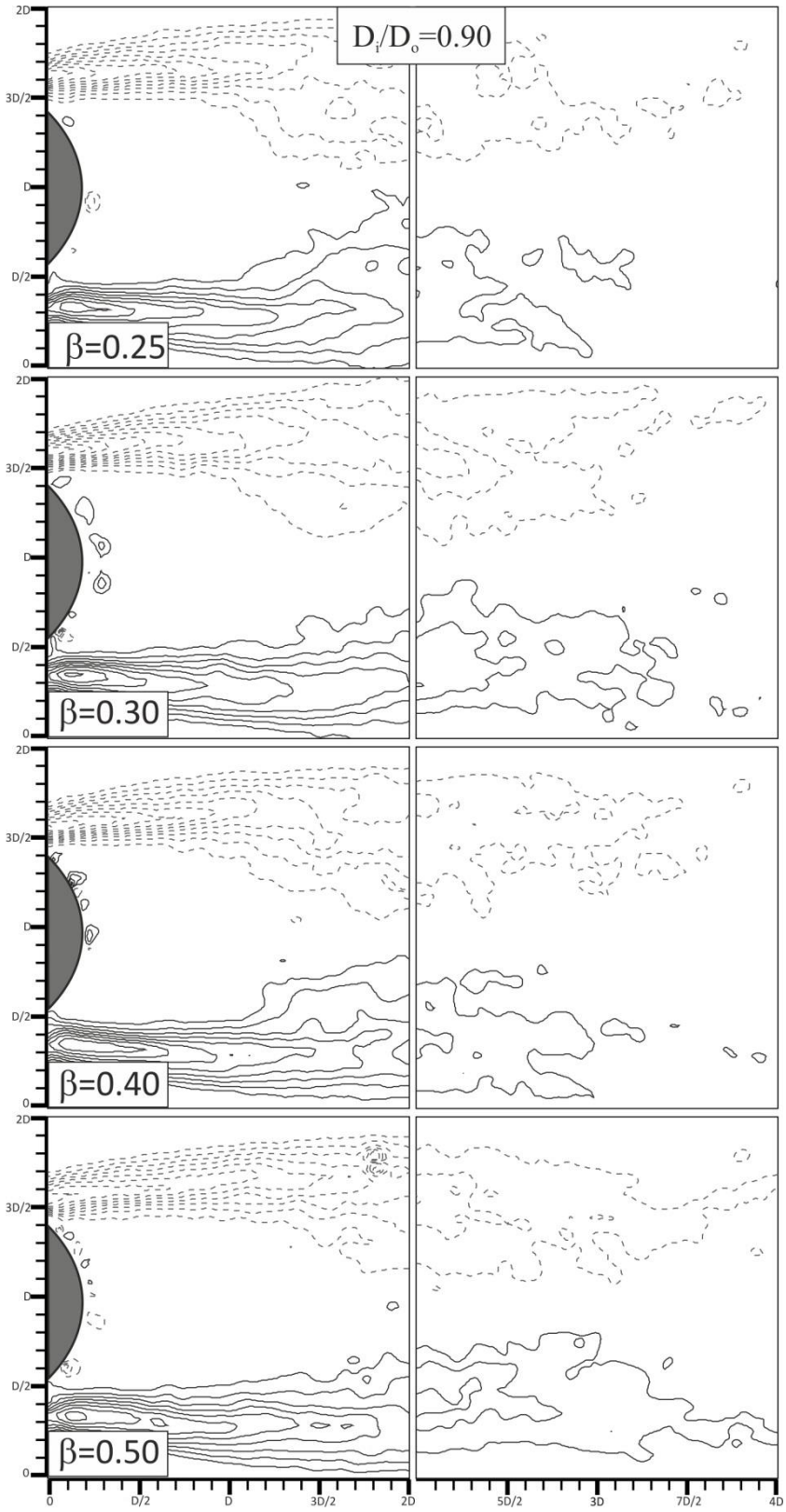
D_i/D_o=0.90
β=0.25
β=0.30
β=0.40
β=0.50
2D
3D/2
D
D/2
0
0
D/2
D
3D/2
2D
5D/2
3D
7D/2
4D

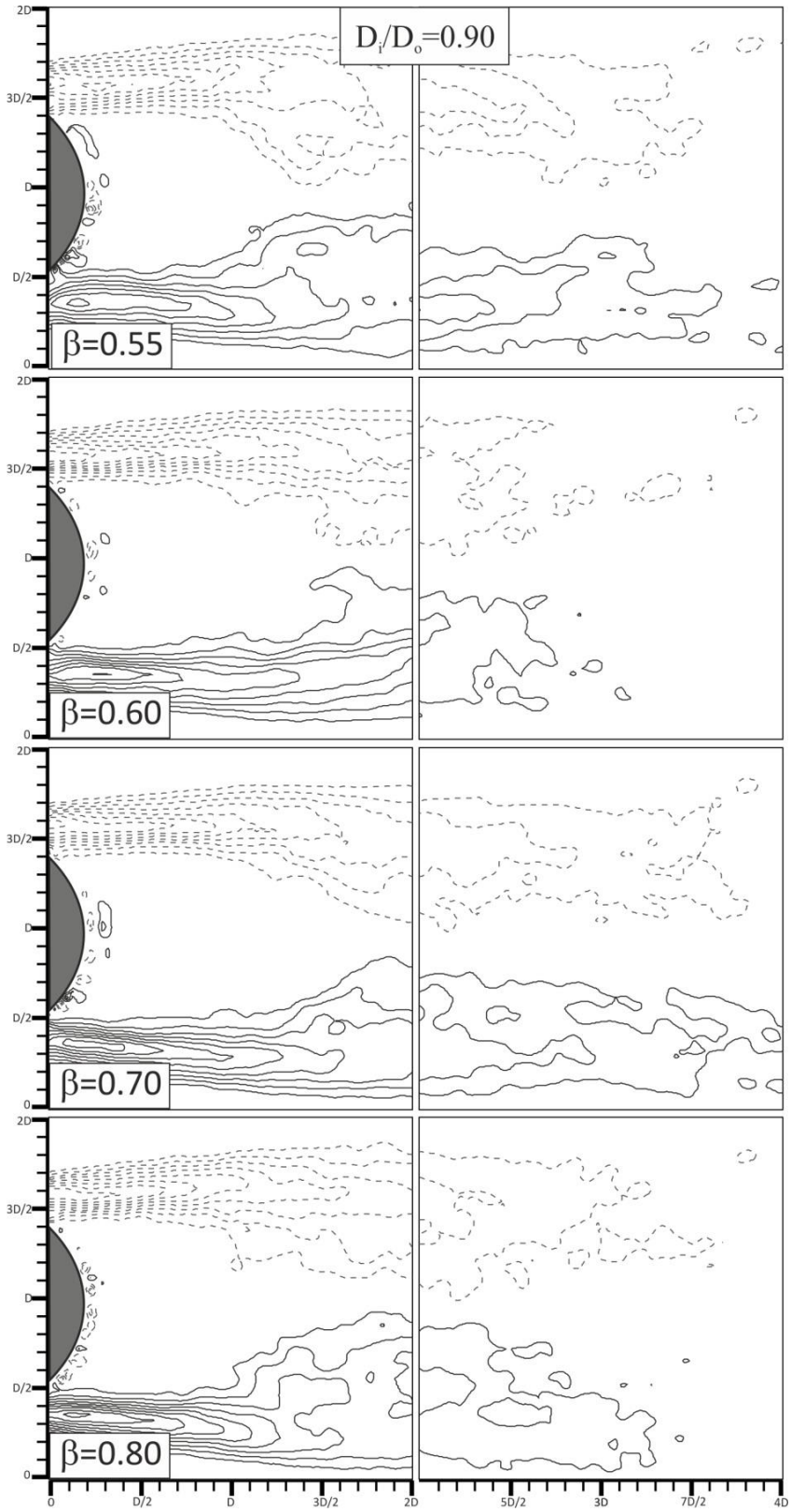

Figure 4.15. Distribution of time averaged vorticity counters at D_i/D_o=0.90 for different porosity

Normalized Reynolds shear stress, $<u'v'>$ contours and dimensionless turbulent kinetic energy, TKE contours are shown in Figures from 4.16 to 4.33 for coupled (shrouded) cylinders. Minimum and incremental values ($\Delta<u'v'>$) of Reynolds shear stress are ±0.002 and 0.002, respectively. Minimum and incremental values (ΔTKE) of turbulent kinetic energy are 0.01. Figure 4.16 shows $<u'v'>$ contours at D_i/D_o=0.25 for various porosity, β. Increasing porosity, β, shifts the peak location of $<u'v'>$ to farther streamwise directions and maximum points are located at the second field of view except for β=0.80. Also, intensity of $<u'v'>$ contours has a decremental trend with increasing porosity, β. Outer cylinder is more effective on the characteristics of the flow structure compared to the inner cylinder for the low porosity, β, within the range of 0.25≤β≤0.40, because of distance between the inner and outer perforated shroud cylinder is very high for D_i/D_o=0.25. Furthermore, it can be delineated from maximum $<u'v'>$ values for D_i/D_o=0.25. While maximum $<u'v'>$ value for the bare (β=0, D_i=25 mm) cylinder is 0.0532, this value reduces to 0.0623, 0.0609, and 0.0546 for β=0.25, β=0.30, and β=0.40, respectively. After porosity β=0.40, of the maximum $<u'v'>$ values of coupled cylinders decreases to a value which is lower than that's evaluated for the bare cylinder. As a result, shedding of vortices from the inner cylinder is suppressed by the jet flows of outer perforated cylinders and these results reveal that the flow control is successfully achieved. For the higher porosity, i.e. β=0.70 and β=0.80, although maximum $<u'v'>$ values are lower than the inner (D_i=25 mm) cylinder case, these porosity ratios cannot be used as a control element since the positive and negative clusters of $<u'v'>$ are located just downstream base of the outer cylinder and it can cause unsteady fluctuations at a rear stagnation point of the cylinder. Figure 4.17 shows TKE contours at D_i/D_o=0.25 for various porosities, β. Characteristics of turbulent kinetic energy have a similar effects such as Reynolds shear stress contours. Maximum TKE value of D_i=25 mm bare cylinder is 0.1900 and it is higher for all other coupled cylinder cases, however the value get closer to 0.1900 for porosities within the range of 0.25≤β≤0.40. Main reason of these results is related with number of the holes on the outer cylinder in which characteristics of outer cylinder exhibit like bare cylinder. Attenuation rate of the maximum value of TKE for the coupled cylinders at D_i/D_o=0.25 were 1.5% at

least and even as approximately 80% at most compared to the bare cylinder for β=0.25 and β=0.70, respectively. However, intensity of TKE increases and peak magnitude occurs close to cylinder base for β=0.70 porosity ratio. Above results reveal that from both $<u'v'>$ and TKE contours most effective control can be achieved for β=0.60 case at this diameter ratio. Attenuation rate of the maximum value of $<u'v'>$ and TKE for β=0.60 is approximately 60% for both of them.

Figures 4.18 and 4.19 present the Reynolds shear stress and TKE contours at D_i/D_o=0.30, respectively. Figures 4.20 and 4.21 present $<u'v'>$ and TKE contours D_i/D_o=0.40, respectively. Outcome of these diameter ratios have similar effects with previous diameter results. At these diameter ratios, the maximum value of the least $<u'v'>$ and TKE occurs at β=0.70. However, Reynolds shear stress contours obtained for D_i/D_o=0.30 and 0.40 diameter ratio at β=0.70 porosity shows that the lowest value of the maximum Reynolds shear stress does not occur due to an effective control. The intensity of contours were concentrated in the near wake region for β=0.70 and β=0.80, on the other hand it shifts to shear layers and elongates to second field of view (i.e. it can be called far wake region). It is easily observed that 'S' shaped unsteady oscillations similar to Karman vortex street are prevented for porosity ratios lower than β=0.70 at the diameter ratios of D_i/D_o=0.30 and D_i/D_o=0.40. Also, peak magnitudes of $<u'v'>$ and TKE are located in the first field of view for β=0.80 at diameter ratios lower than D_i/D_o=0.40. Effect of porosity ratio from 0.70 to 0.80 is seen acutely due to both $<u'v'>$ and TKE contours get closer to each other along the centerline of the coupled cylinder as a result of the effectiveness of the inner cylinder. As a consequence, effect of porosity ratios with respect to variation of diameter ratio is higher in deep water flow compared to shallow water applications (Pinar, 2013).

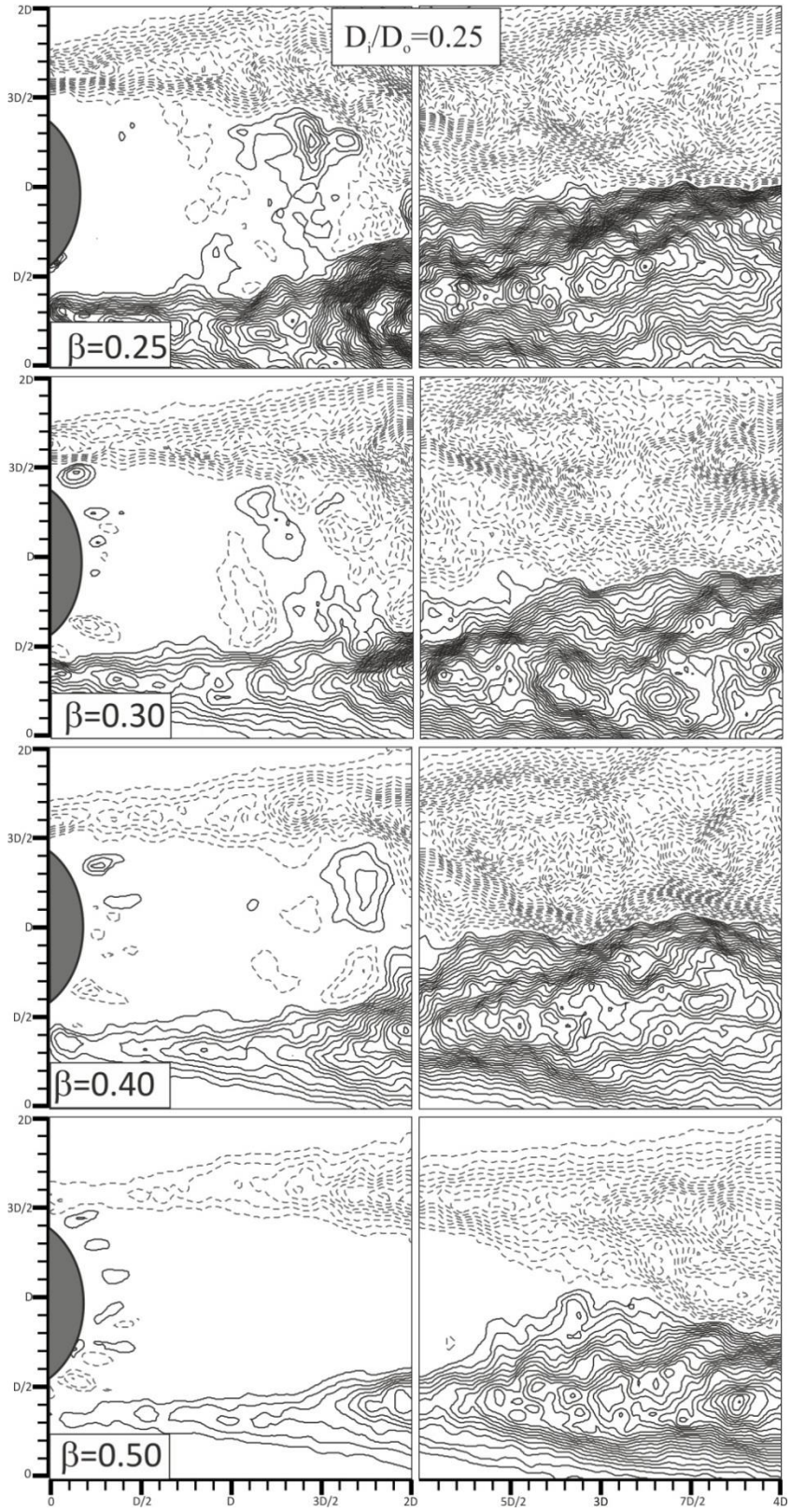
D_i/D_o=0.25
β=0.25
β=0.30
β=0.40
β=0.50
2D
3D/2
D
D/2
0
0
D/2
D
3D/2
2D
5D/2
3D
7D/2
4D

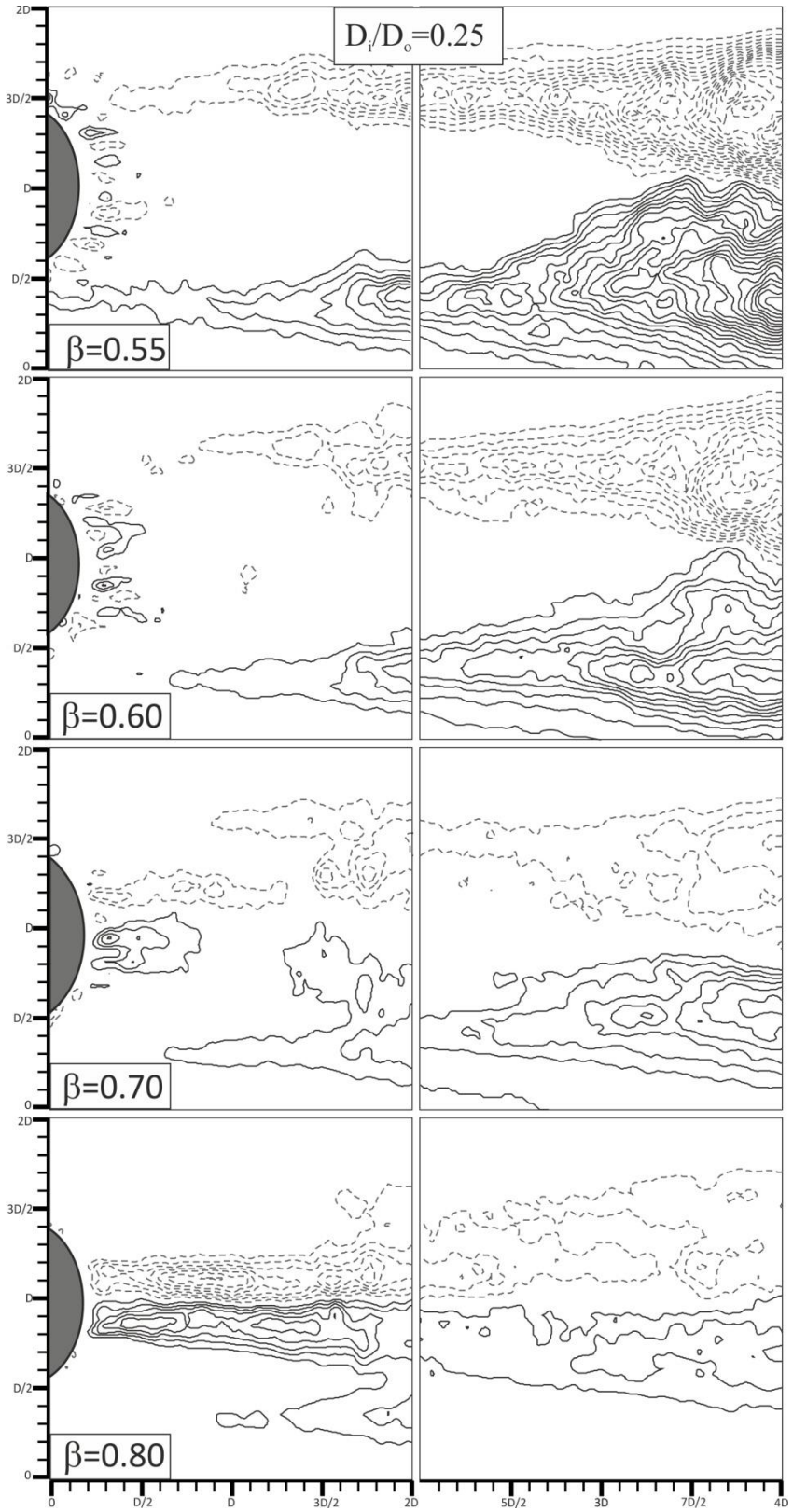

Figure 4.16. Reynolds shear stress distribution downstream of the coupled cylinders at D_i/D_o=0.25 for different β cases

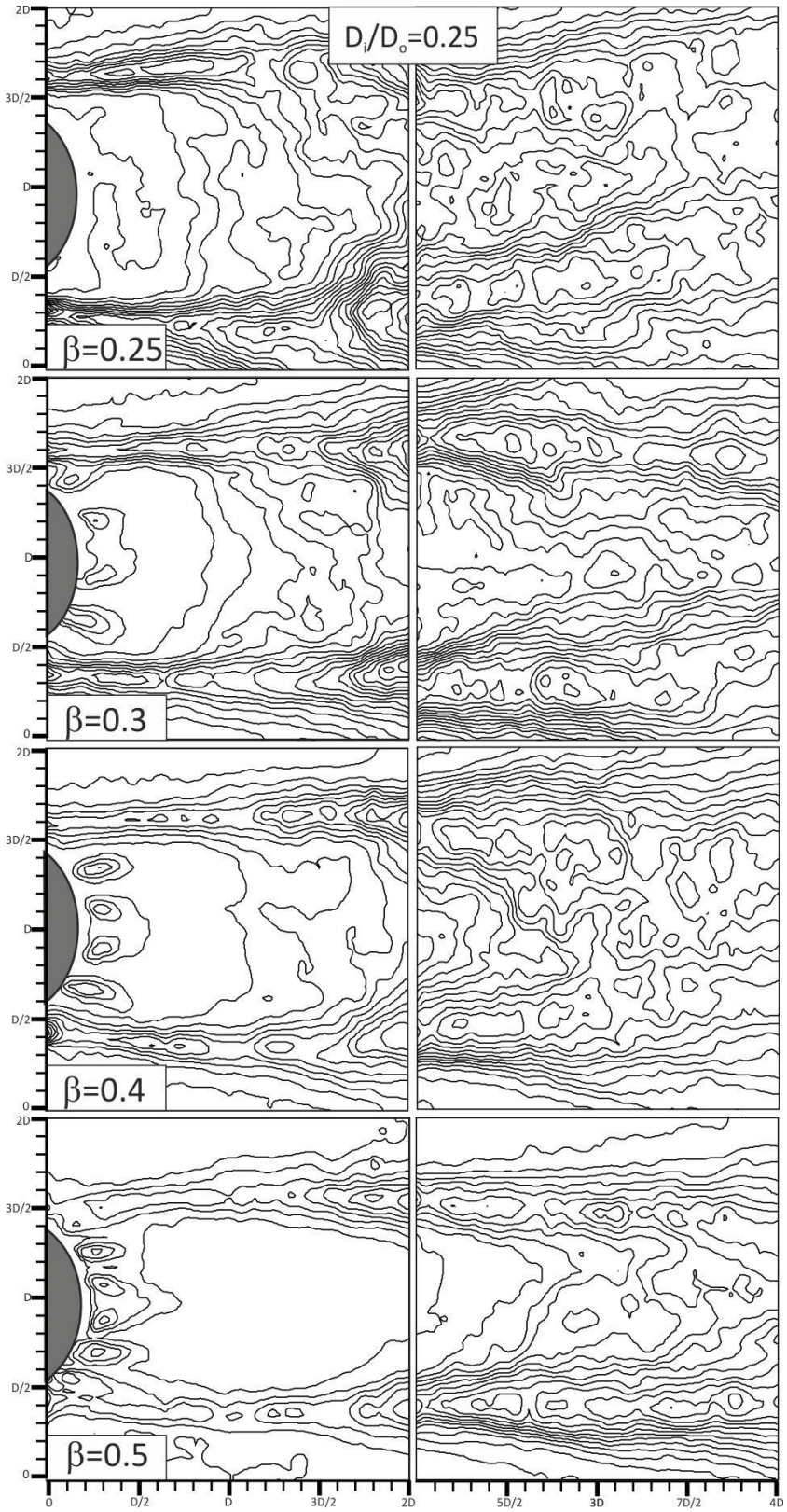
D_i/D_o=0.25
β=0.25
β=0.3
β=0.4
β=0.5
2D
3D/2
D
D/2
0
D/2
D
3D/2
2D
5D/2
3D
7D/2
4D

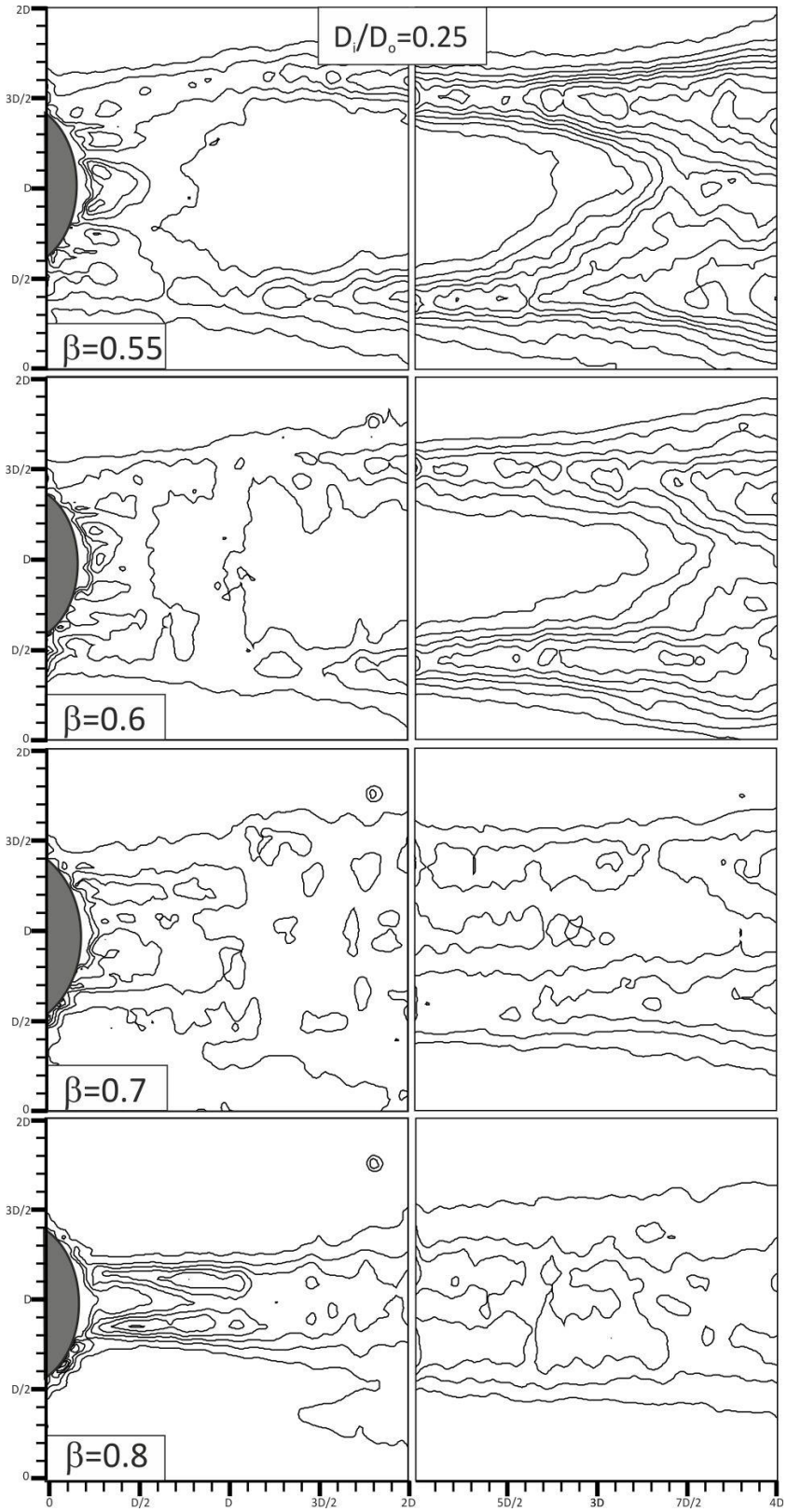

Figure 4.17. Turbulence kinetic energy distribution downstream of the coupled cylinders at D_i/D_o=0.25 for different β cases

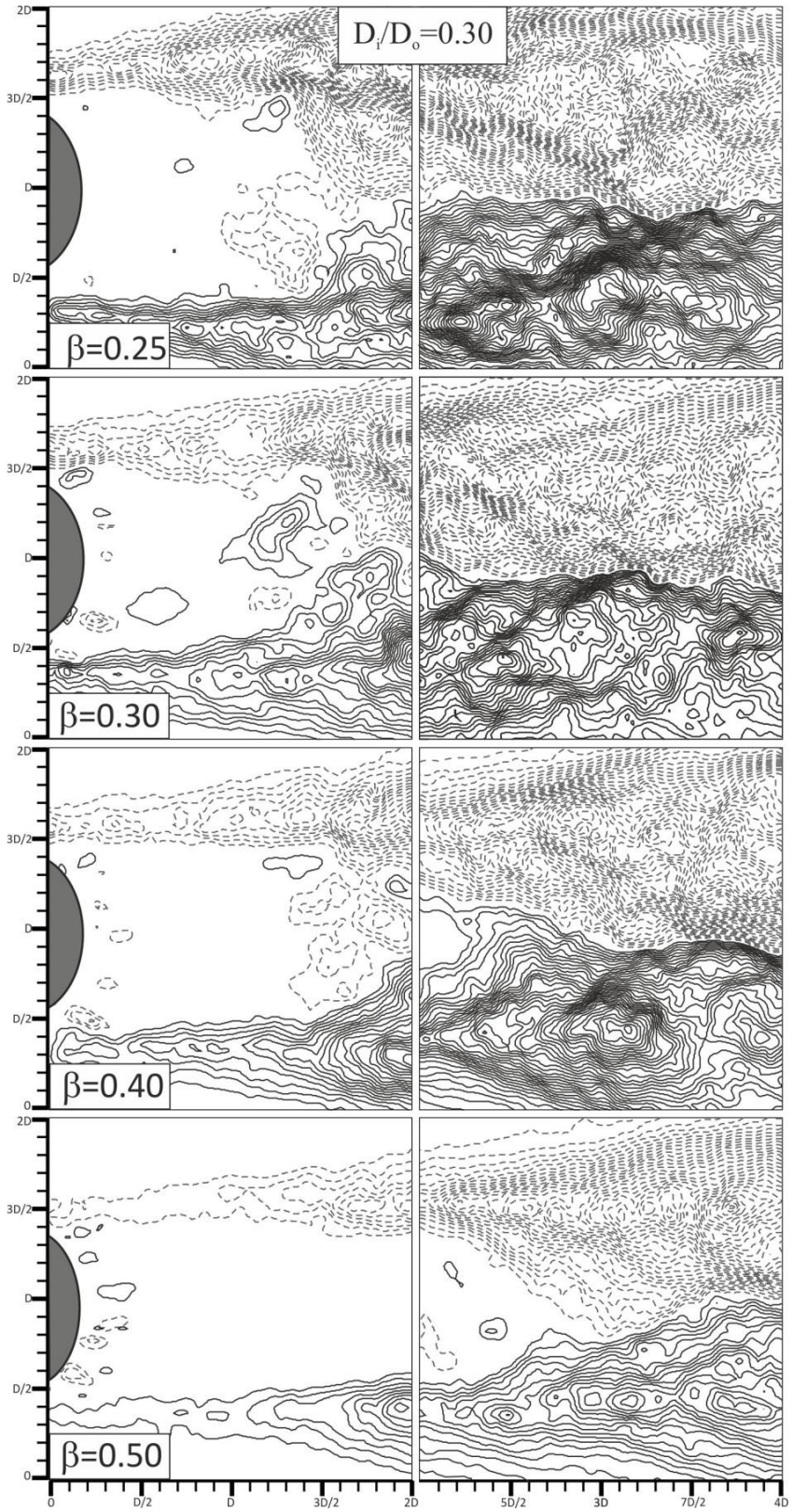
D_i/D_o=0.30
β=0.25
β=0.30
β=0.40
β=0.50
2D
3D/2
D
D/2
0
0
D/2
D
3D/2
2D
5D/2
3D
7D/2
4D

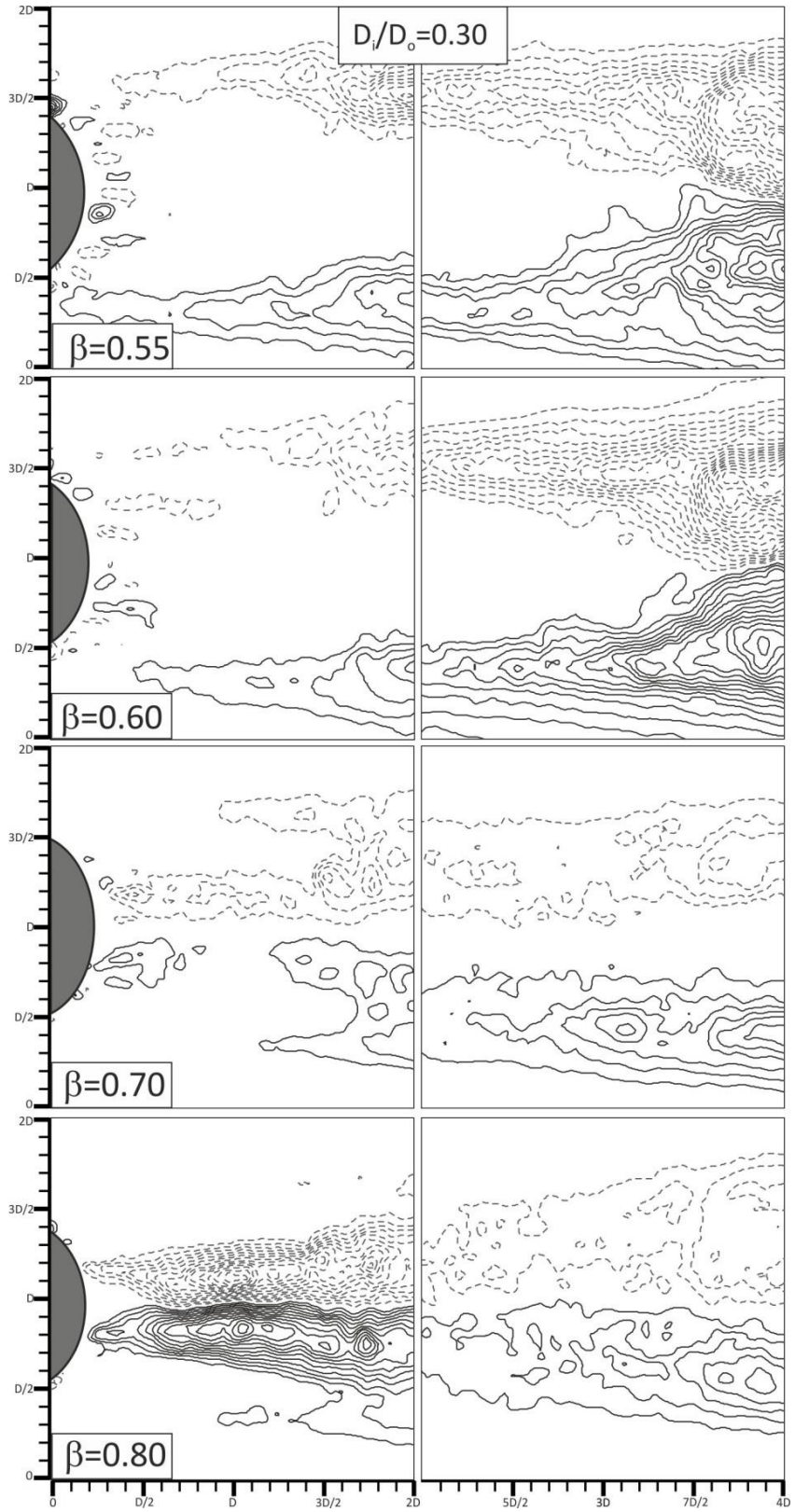

Figure 4.18. Reynolds shear stress distribution downstream of the coupled cylinders at D_i/D_o=0.30 for different β cases

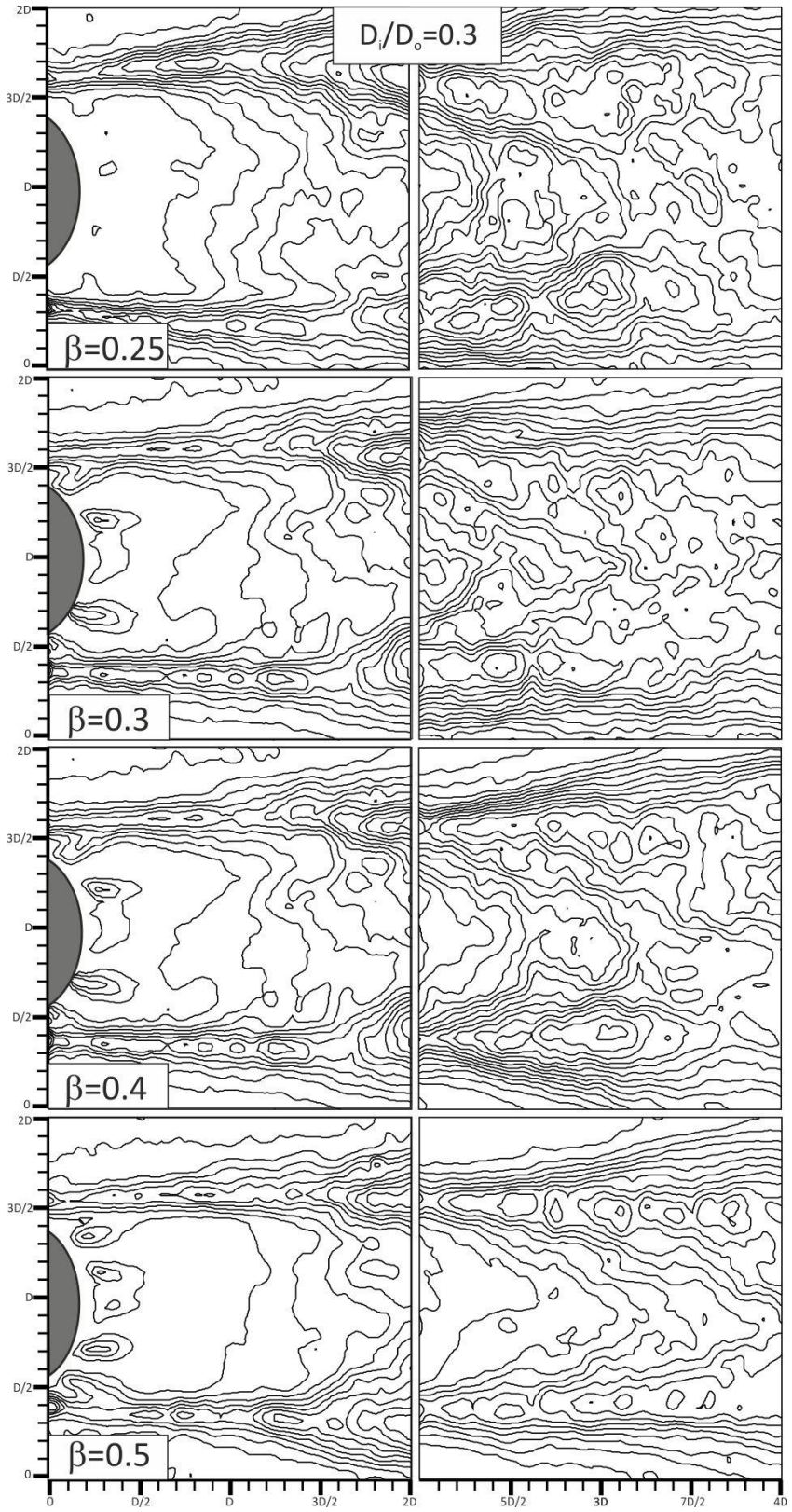
D_i/D_o=0.3
β=0.25
β=0.3
β=0.4
β=0.5
2D
3D/2
D
D/2
0
0
D/2
D
3D/2
2D
5D/2
3D
7D/2
4D

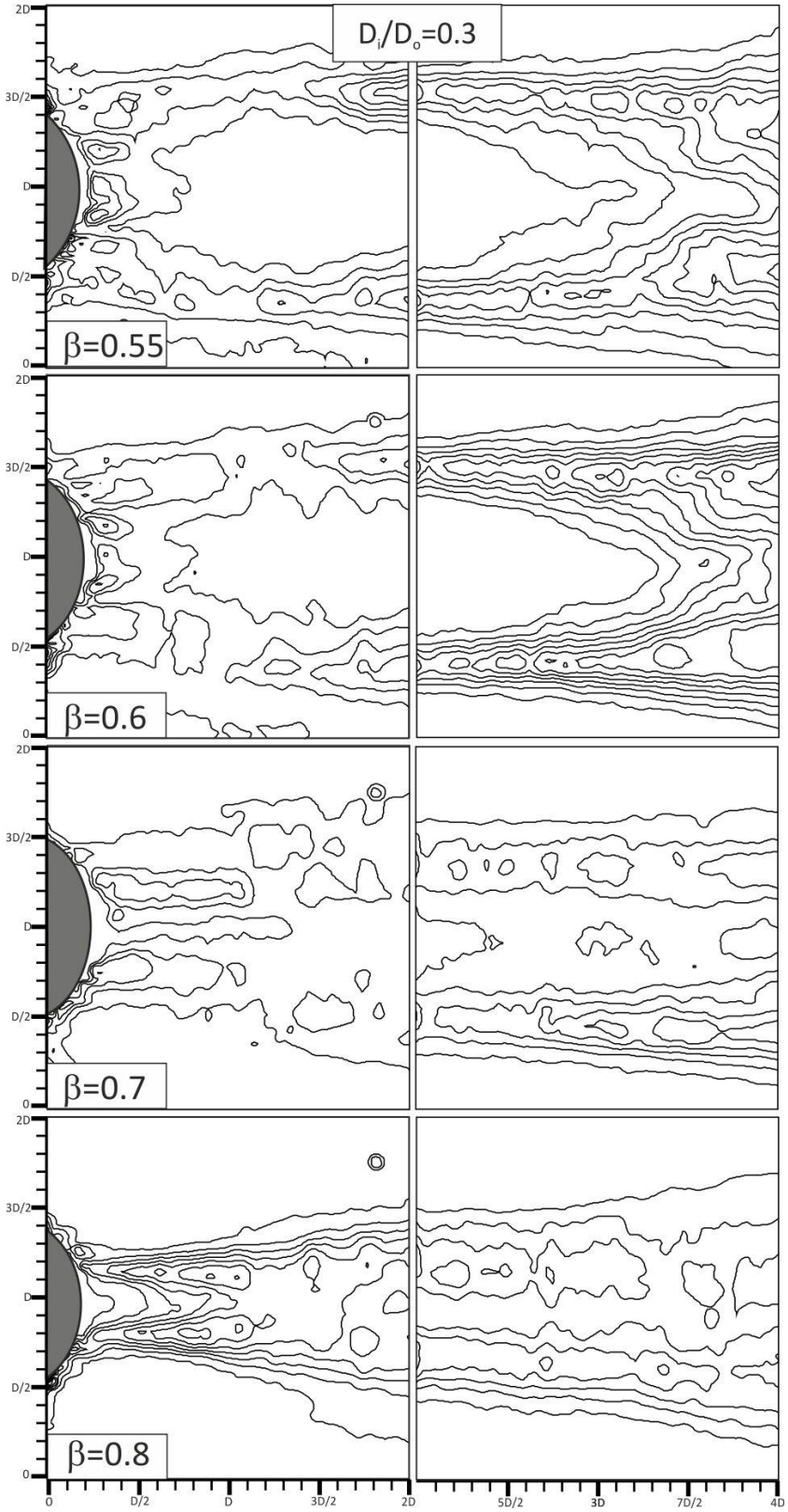

Figure 4.19. Turbulence kinetic energy distribution downstream of the coupled cylinders at D_i/D_o=0.30 for different β cases

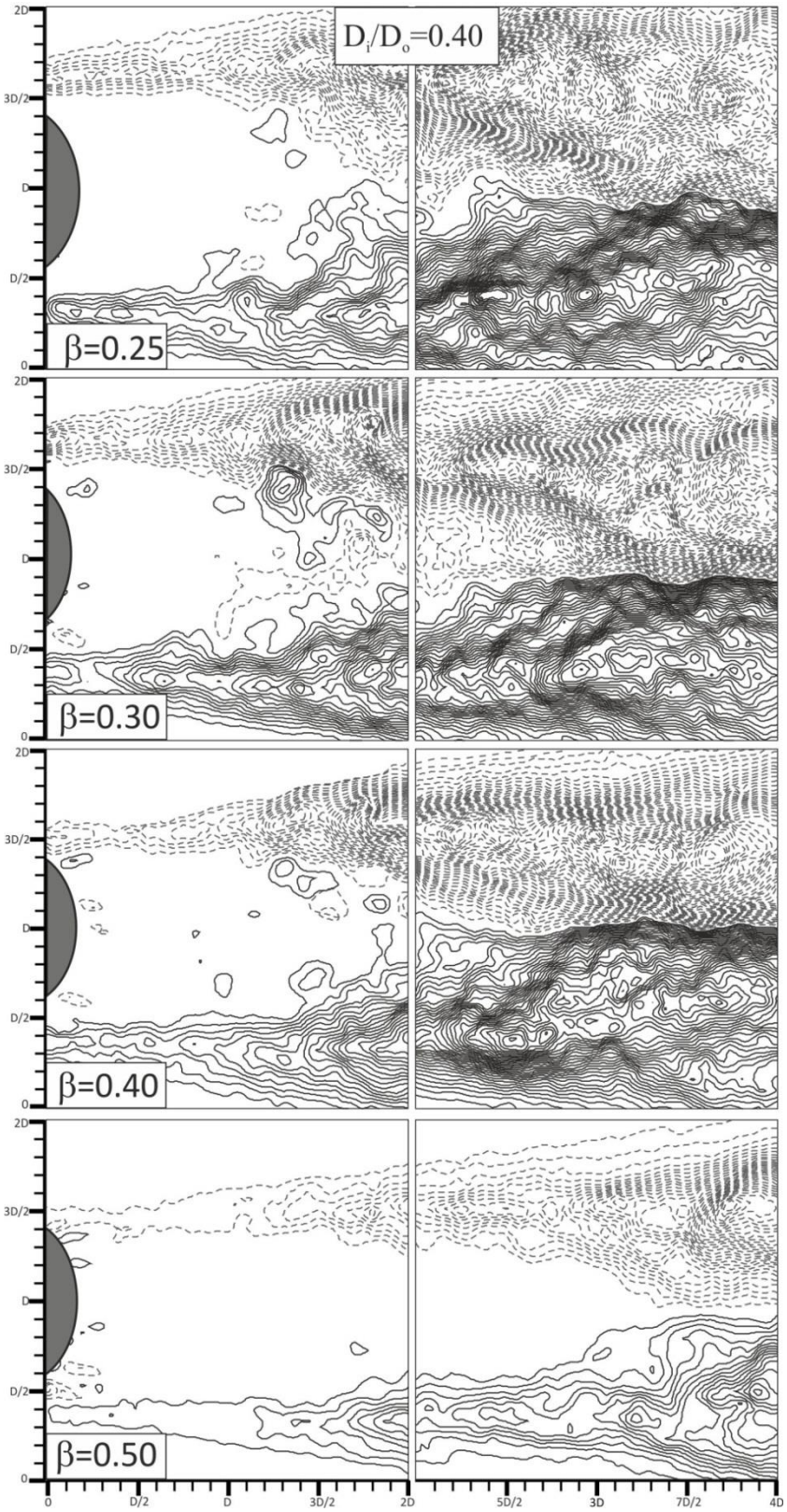
D_i/D_o=0.40
β=0.25
β=0.30
β=0.40
β=0.50
2D
3D/2
D
D/2
0
D/2
D
3D/2
2D
5D/2
3D
7D/2
4D

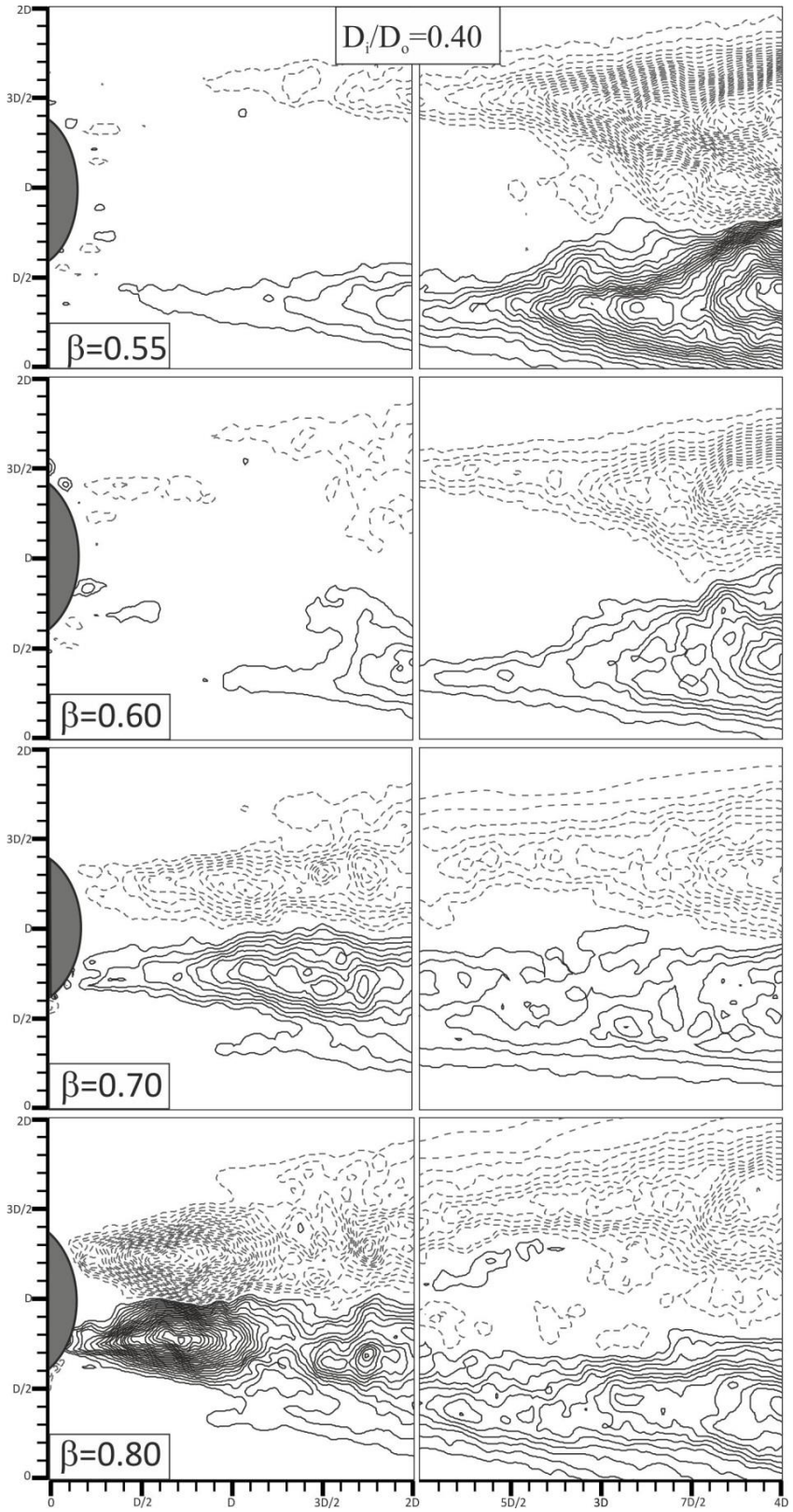

Figure 4.20. Reynolds shear stress distribution downstream of the coupled cylinders at D_i/D_o=0.40 for different β cases

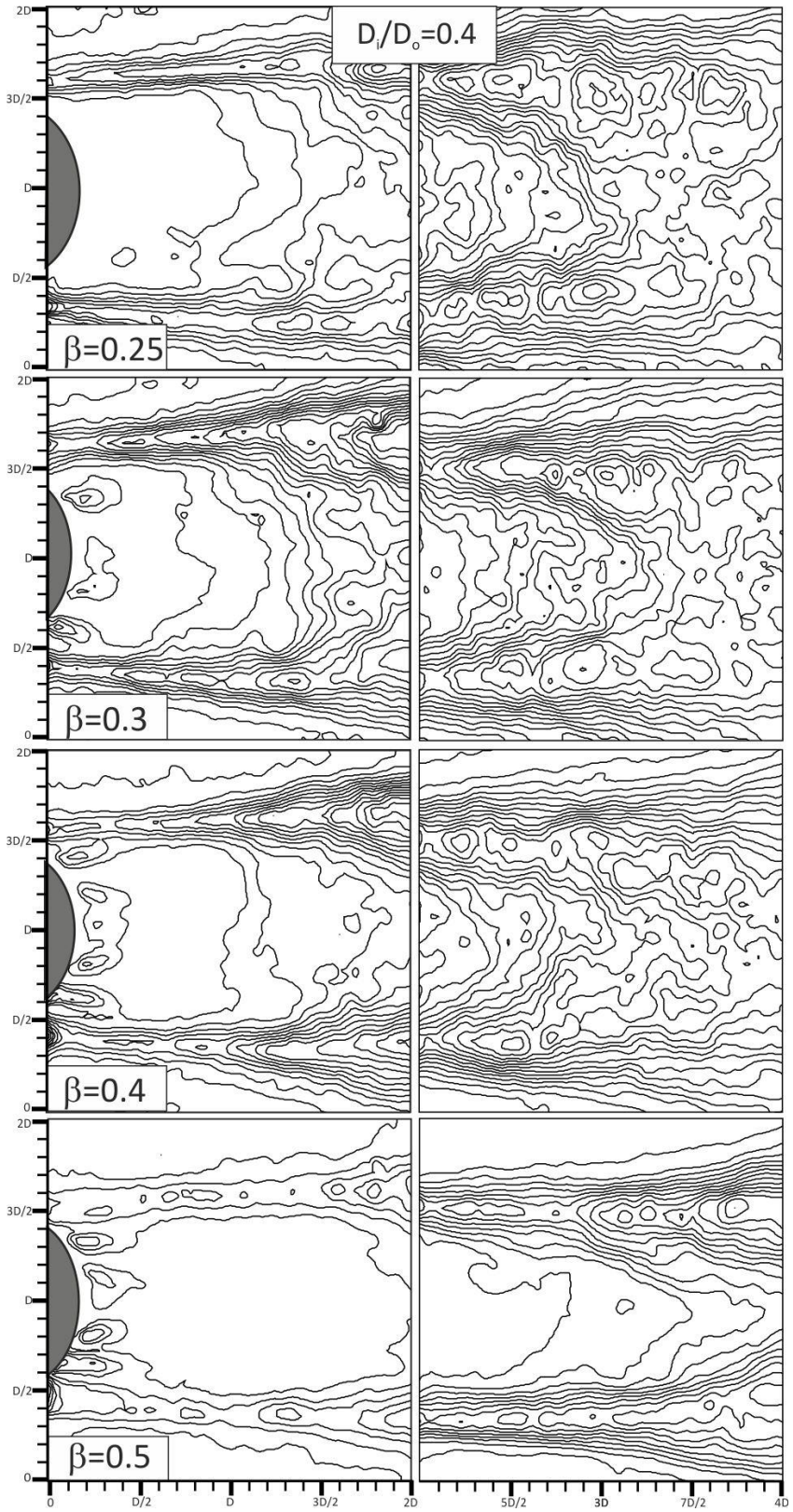
D_i/D_o=0.4
β=0.25
β=0.3
β=0.4
β=0.5
2D
3D/2
D
D/2
0
0
D/2
D
3D/2
2D
5D/2
3D
7D/2
4D

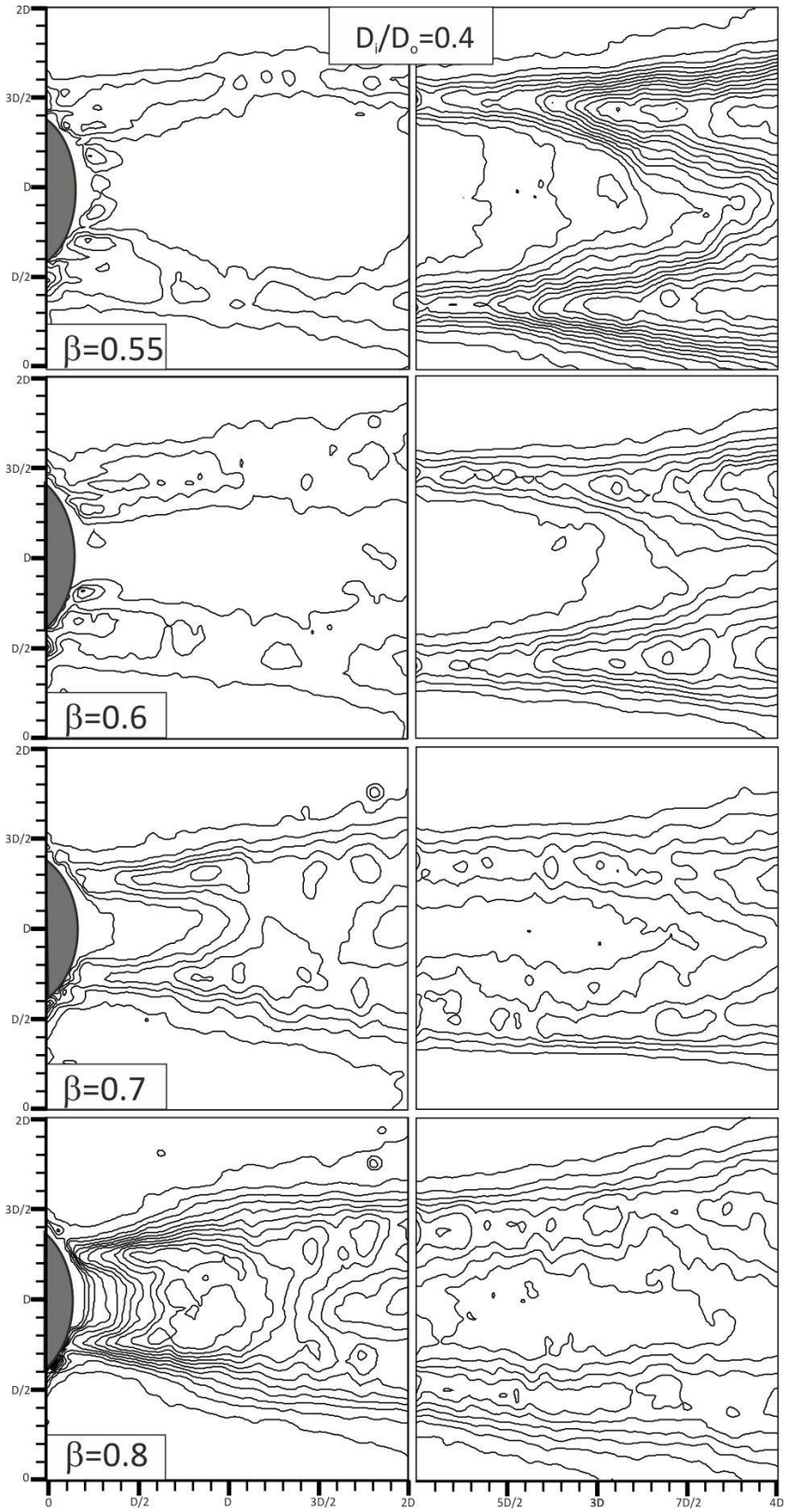

Figure 4.21. Turbulence kinetic energy distribution downstream of the coupled cylinders at D_i/D_o=0.40 for different β cases

Figures 4.22 and 4.23 present the Reynolds shear stress and TKE contours at D_i/D_o=0.50, respectively. Porosity, β, has a significant effect on the flow structure for D_i/D_o=0.50 case compared to the diameter ratios lower than D_i/D_o=0.50. Within the range of 0.3≤β≤0.6, Reynolds shear stress and TKE intensity along the shear layers decrease with the increasing porosity, β, and interact with each other in the downstream region at the end of second field of view (peak magnitudes approximately located 3.5D of the cylinder away from the cylinder base). The flow emanating through the holes on the outer cylinder causing a jet flow prevents the vorticity on each side of the coupled cylinder by intercepting the interaction of vortices and thus momentum transfer increases into the wake region. As a result, $<u'v'>$ and TKE values in the wake region decrease in comparison to the bare cylinder case. The reason of this kinetic energy intensification in shear layers is the result of prevention of Karman vortices; however, the Kelvin-Helmholtz vorticity becomes more dominant on the shear layers between the free-stream region and the wake region. More effective flow control can be achieved at D_i/D_o=0.50 as a result of lower distance between inner and outer perforated cylinder. Peak magnitude of $<u'v'>$ and TKE value of D_i=50 mm bare cylinder is found to be 0.0969 and 0.2886, respectively and attenuation rate of the maximum value of $<u'v'>$ and TKE is approximately 70% and 65% at most, respectively compared to bare cylinder.

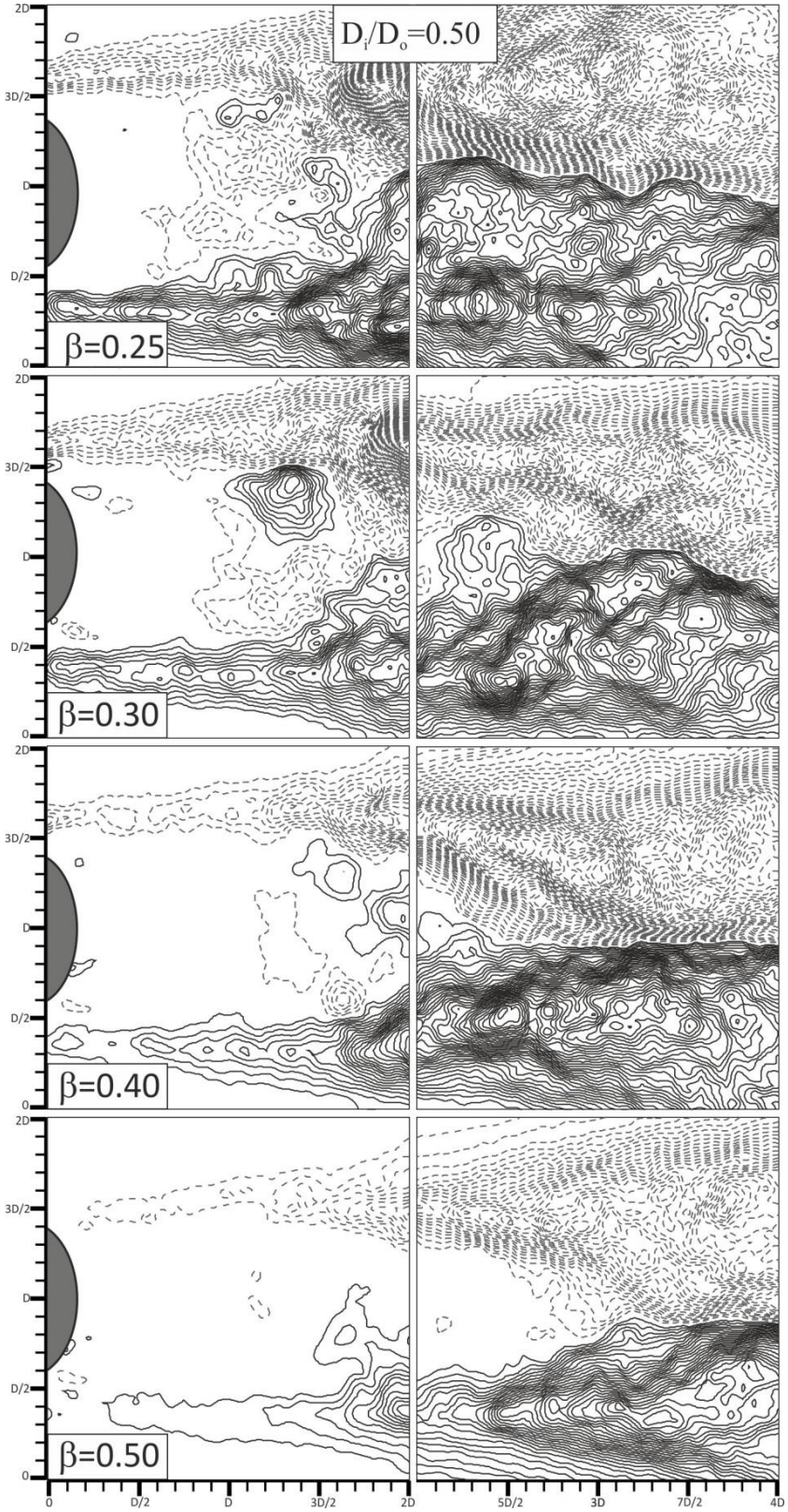
D_i/D_o=0.50
β=0.25
β=0.30
β=0.40
β=0.50
2D
3D/2
D
D/2
0
0
D/2
D
3D/2
2D
5D/2
3D
7D/2
4D

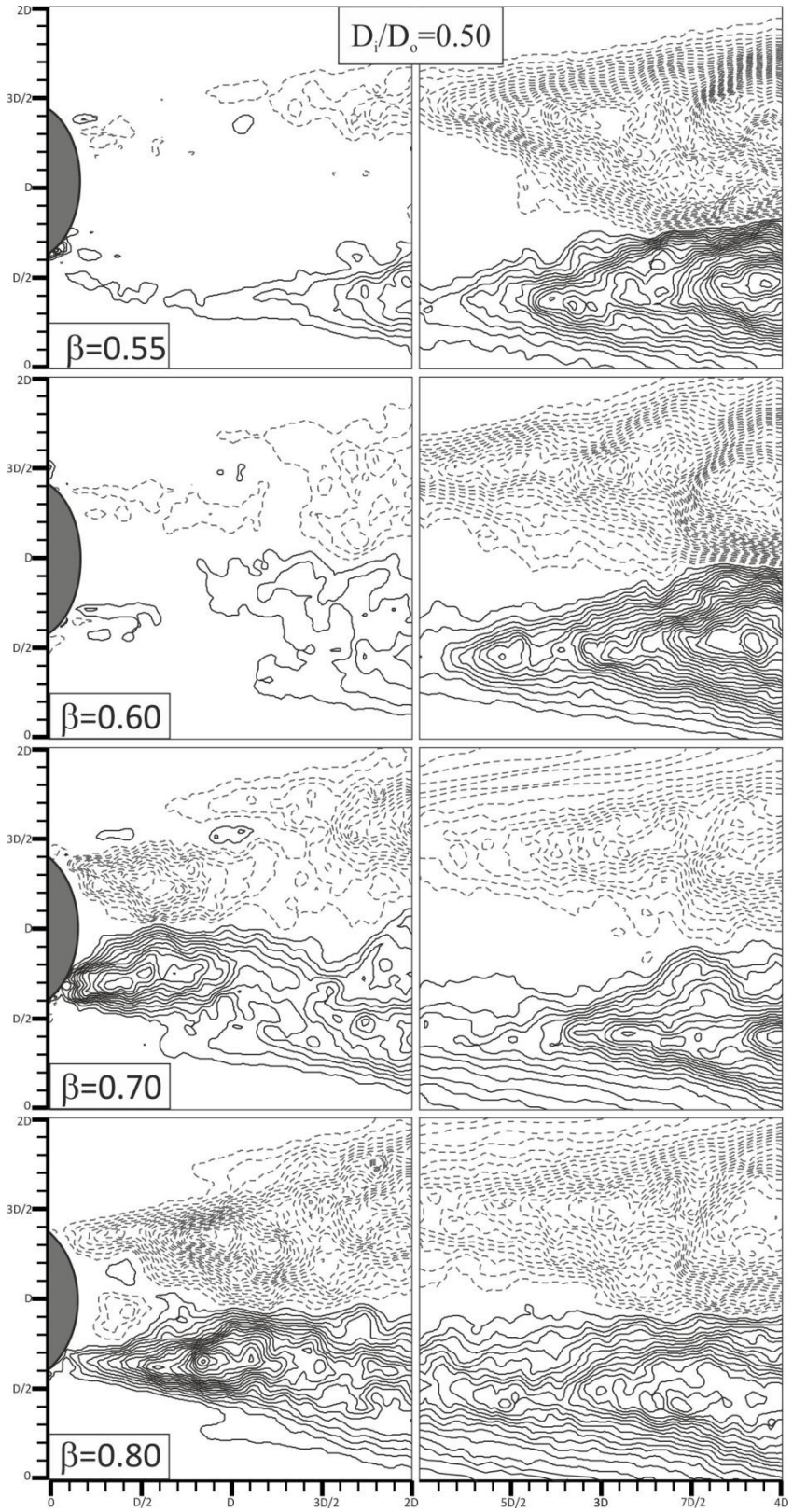

Figure 4.22. Reynolds shear stress distribution downstream of the coupled cylinders at D_i/D_o=0.50 for different β cases

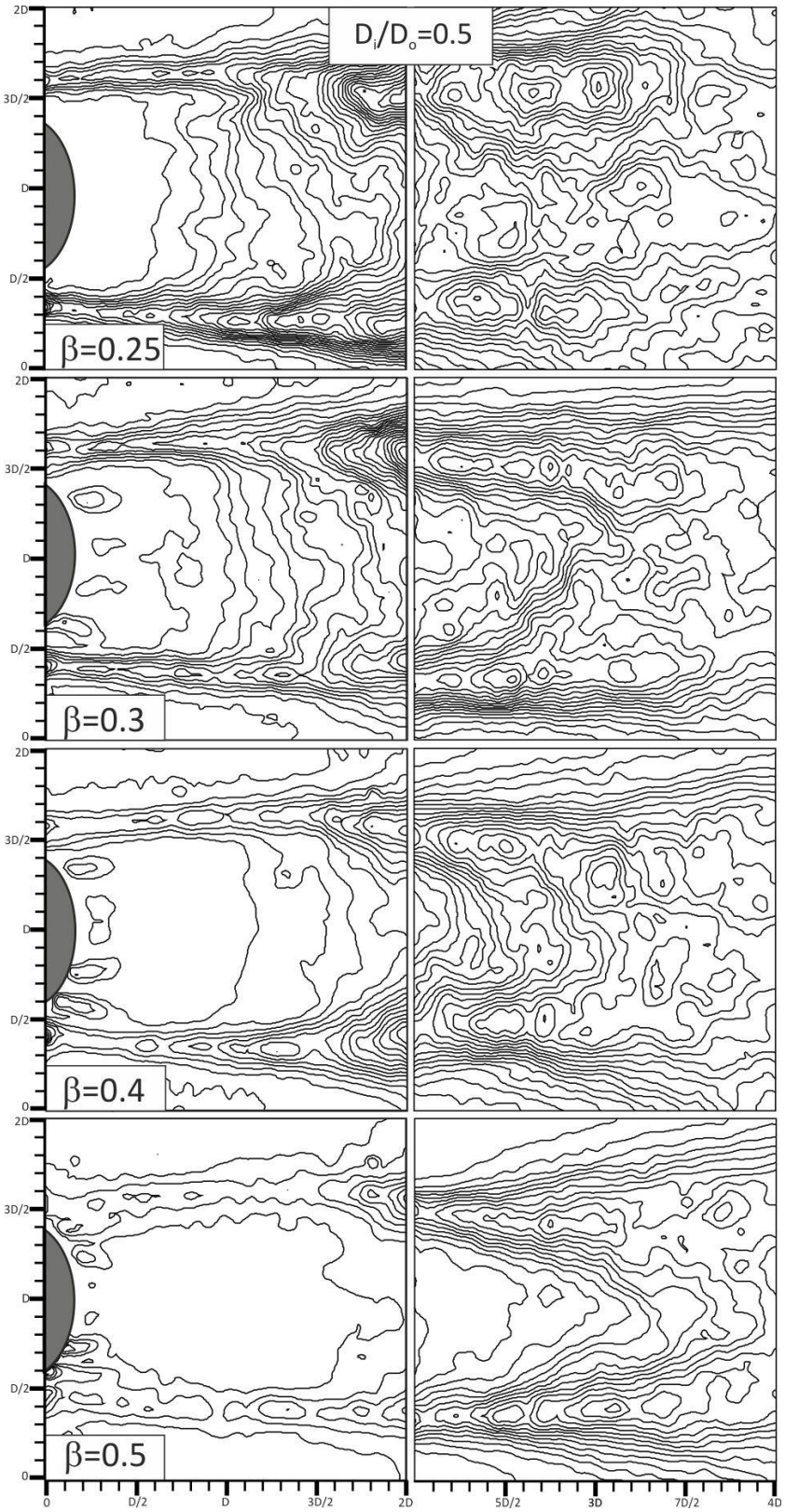
D_i/D_o=0.5
β=0.25
β=0.3
β=0.4
β=0.5
2D
3D/2
D
D/2
0
0
D/2
D
3D/2
2D
5D/2
3D
7D/2
4D

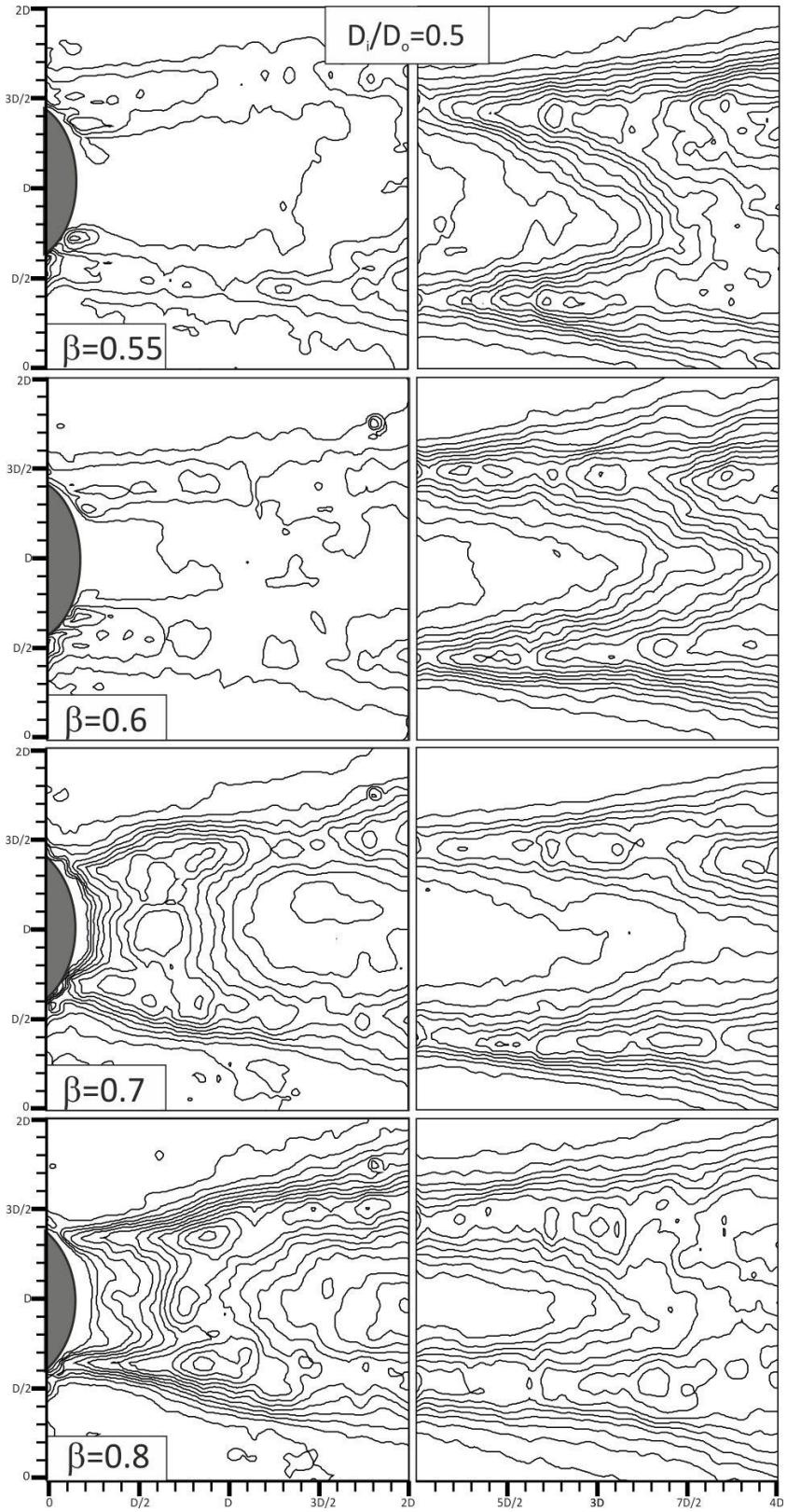

Figure 4.23. Turbulence kinetic energy distribution downstream of the coupled cylinders at D_i/D_o=0.50 for different β cases

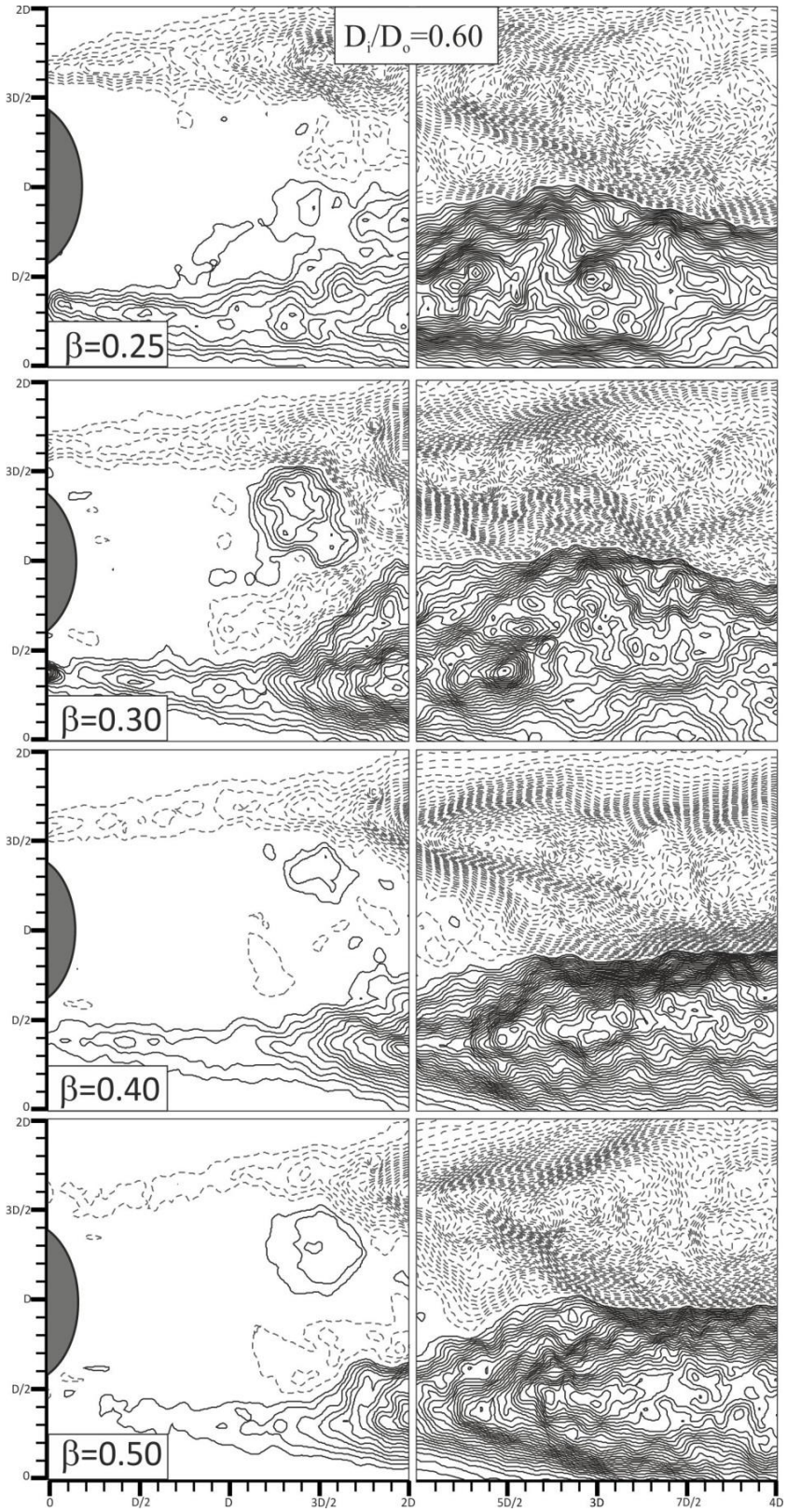
D_i/D_o=0.60
β=0.25
β=0.30
β=0.40
β=0.50
2D
3D/2
D
D/2
0
D/2
D
3D/2
2D
5D/2
3D
7D/2
4D

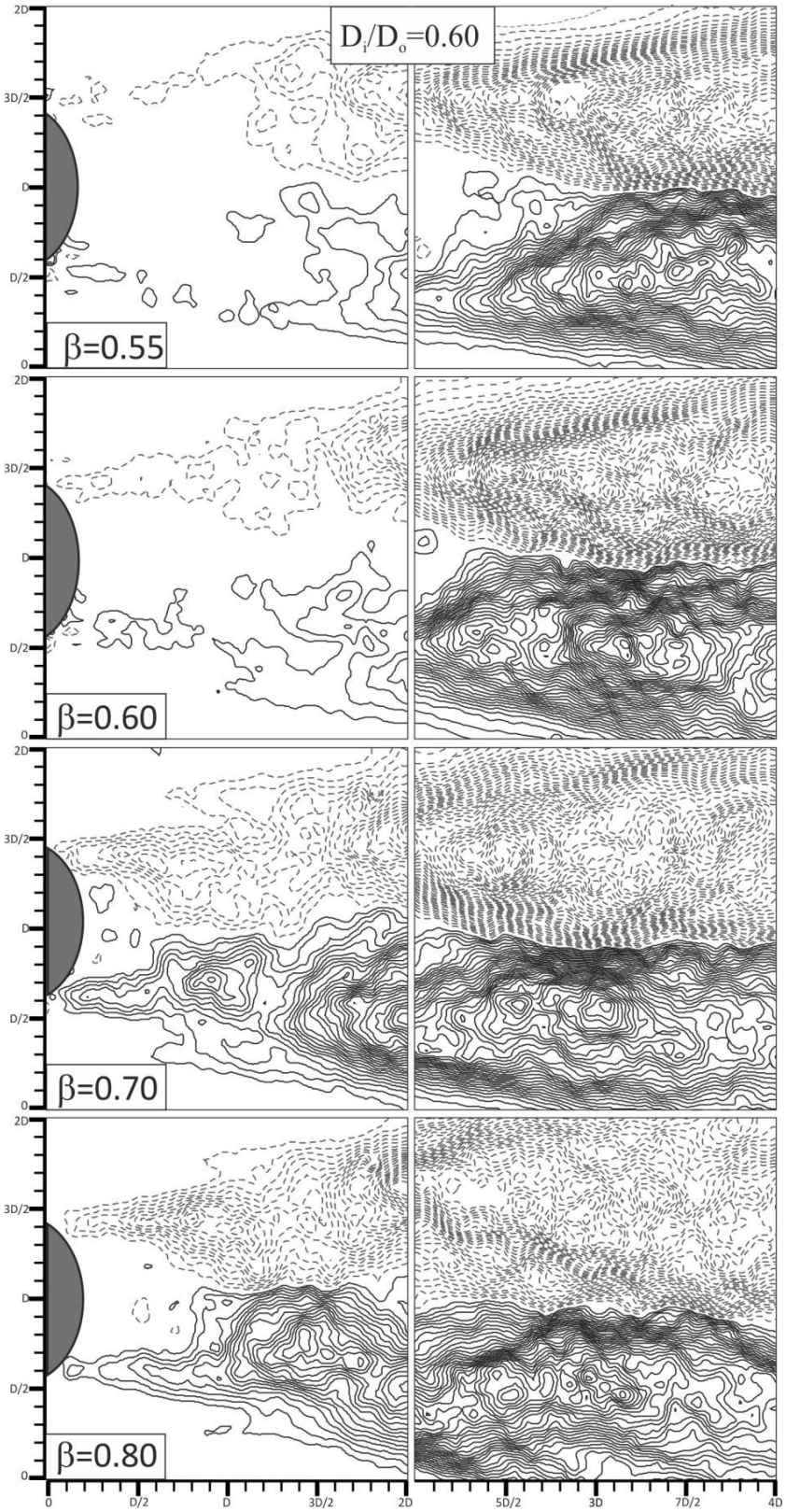

Figure 4.24. Reynolds shear stress distribution downstream of the coupled cylinders at D_i/D_o=0.60 for different β cases

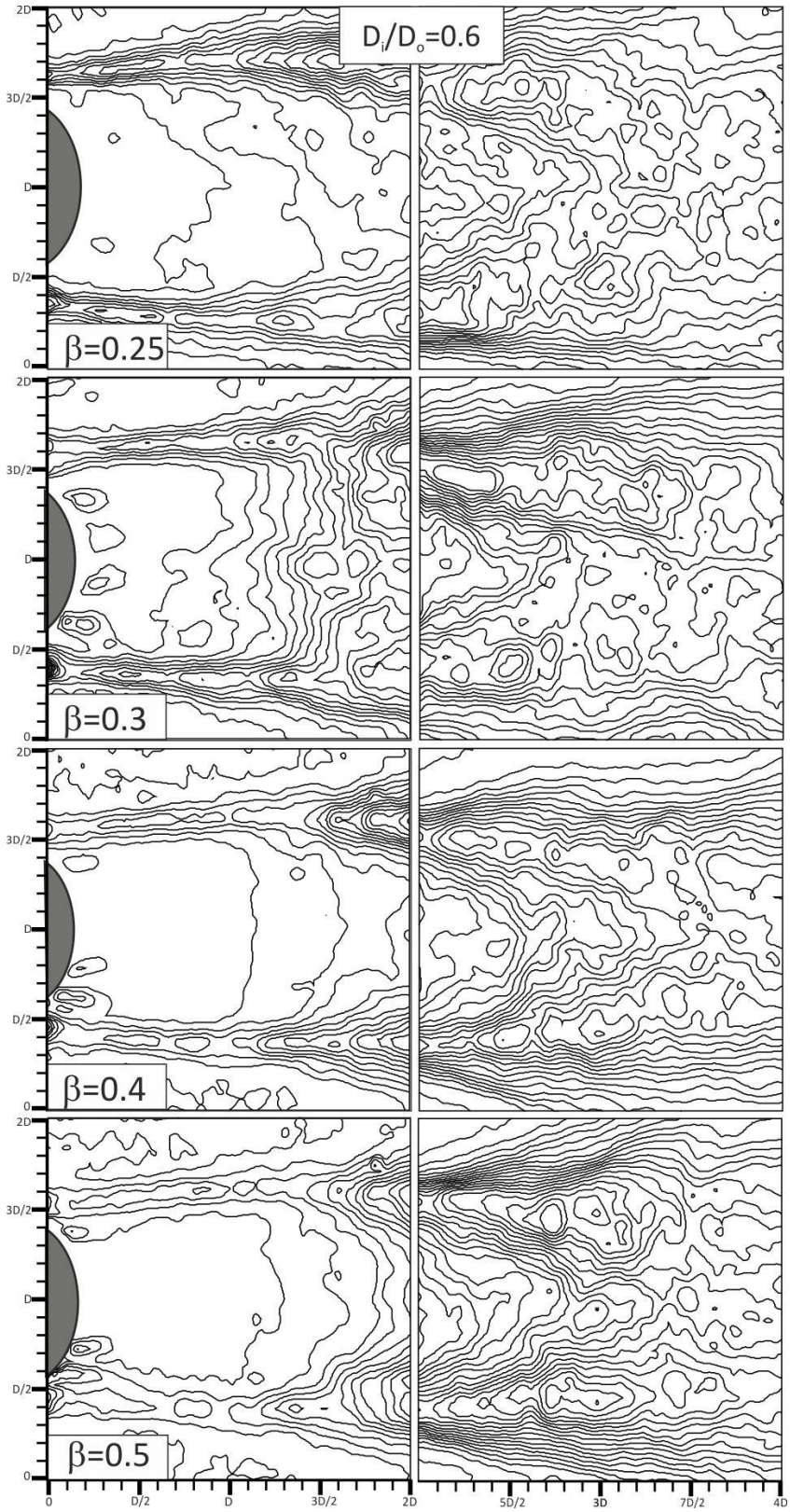
D_i/D_o=0.6
β=0.25
β=0.3
β=0.4
β=0.5
2D
3D/2
D
D/2
0
0
D/2
D
3D/2
2D
5D/2
3D
7D/2
4D

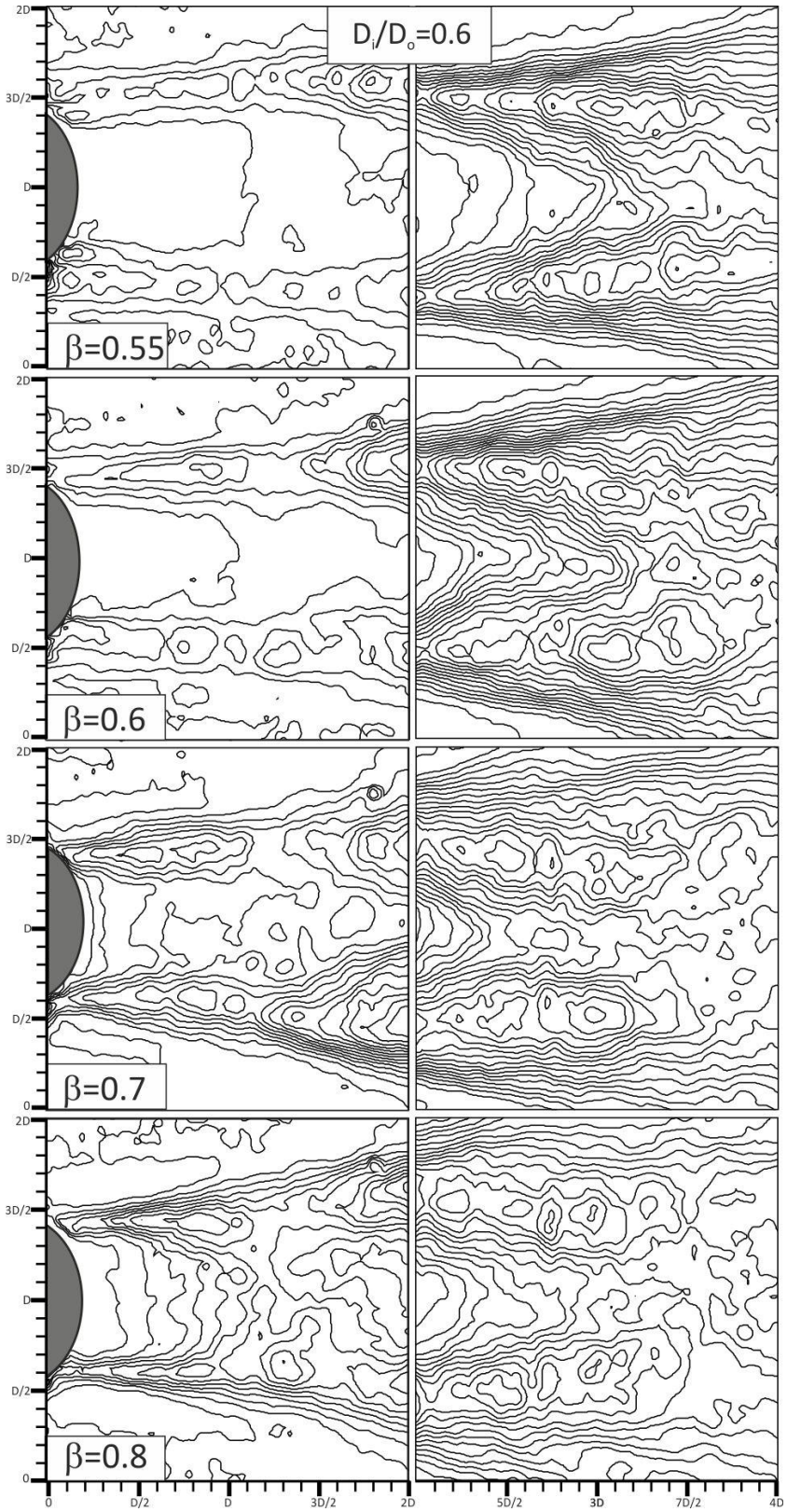

Figure 4.25. Turbulence kinetic energy distribution downstream of the coupled cylinders at D_i/D_o=0.60 for different β cases

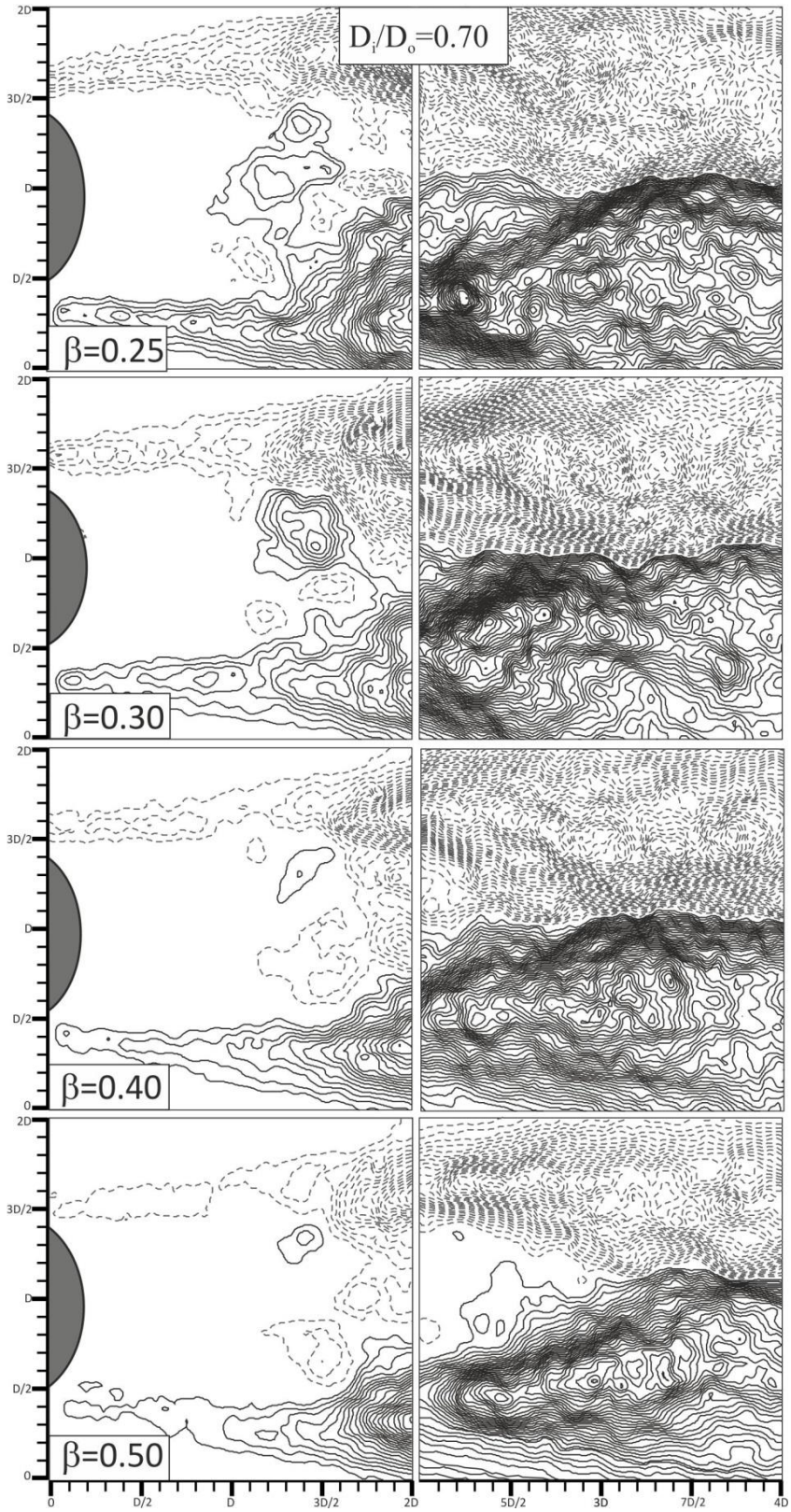
D_i/D_o=0.70
β=0.25
β=0.30
β=0.40
β=0.50
2D
3D/2
D
D/2
0
0
D/2
D
3D/2
2D
5D/2
3D
7D/2
4D

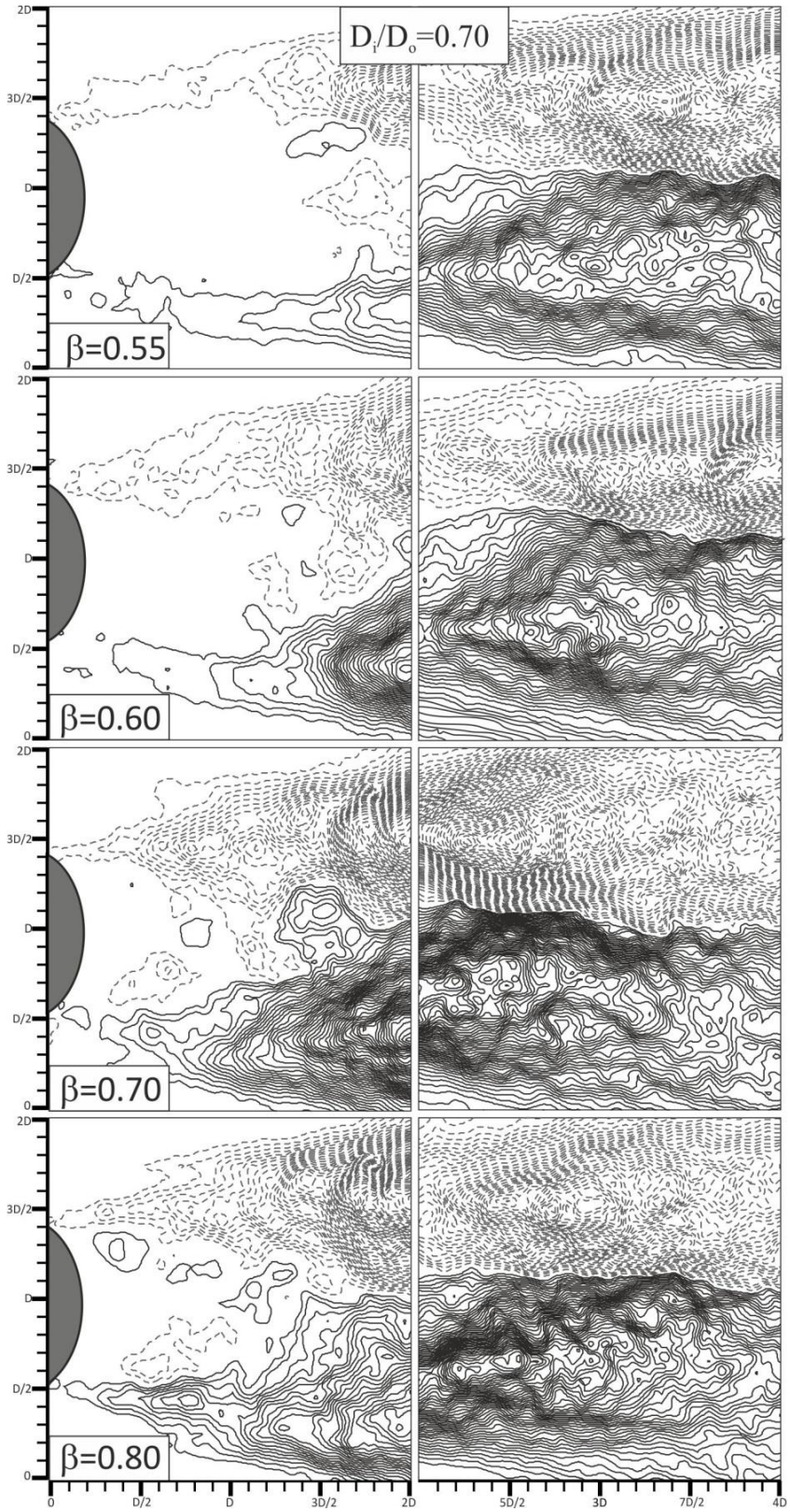

Figure 4.26. Reynolds shear stress distribution downstream of the coupled cylinders at D_i/D_o=0.70 for different β cases

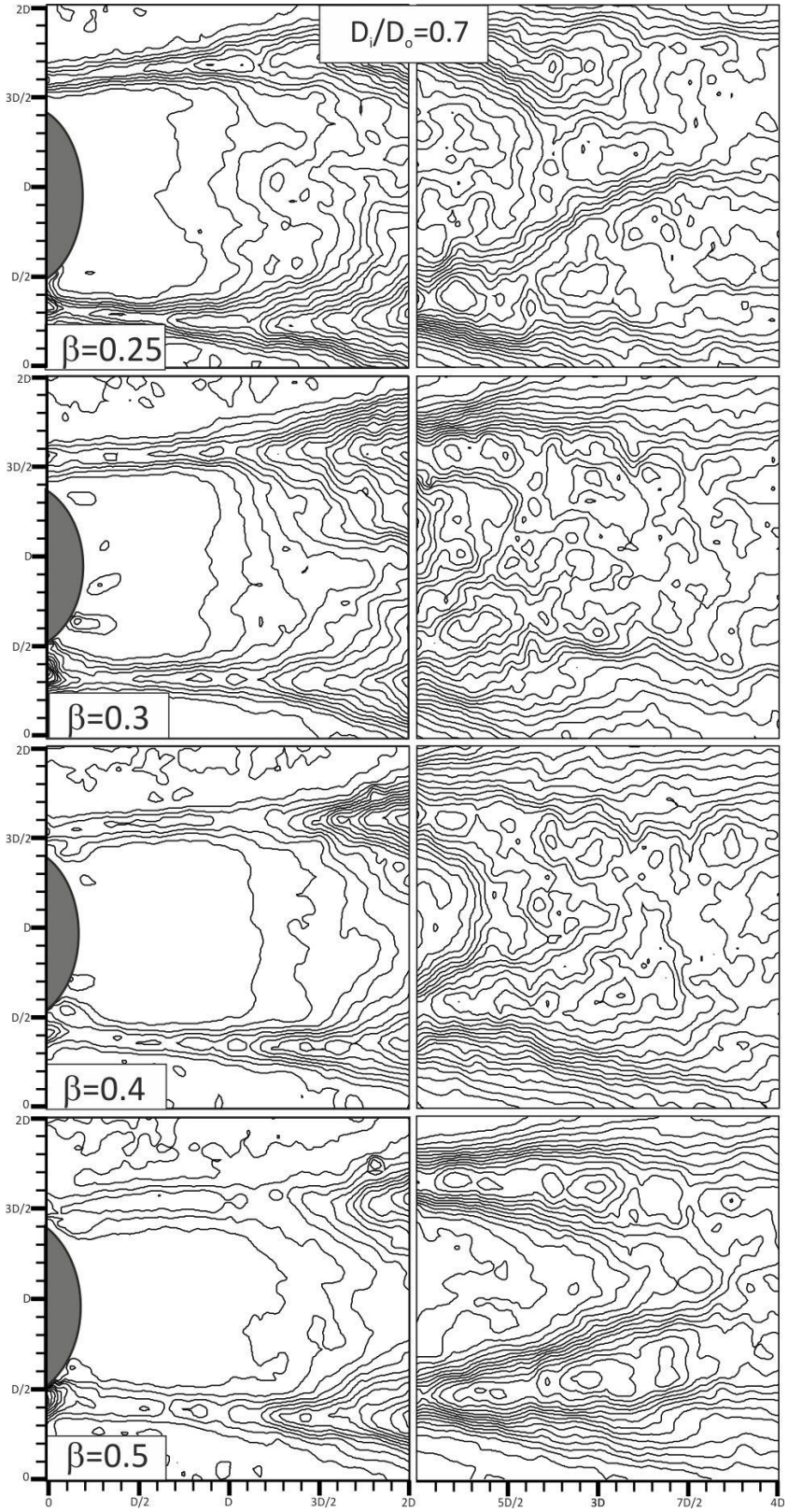
D_i/D_o=0.7
β=0.25
β=0.3
β=0.4
β=0.5
2D
3D/2
D
D/2
0
0
D/2
D
3D/2
2D
5D/2
3D
7D/2
4D

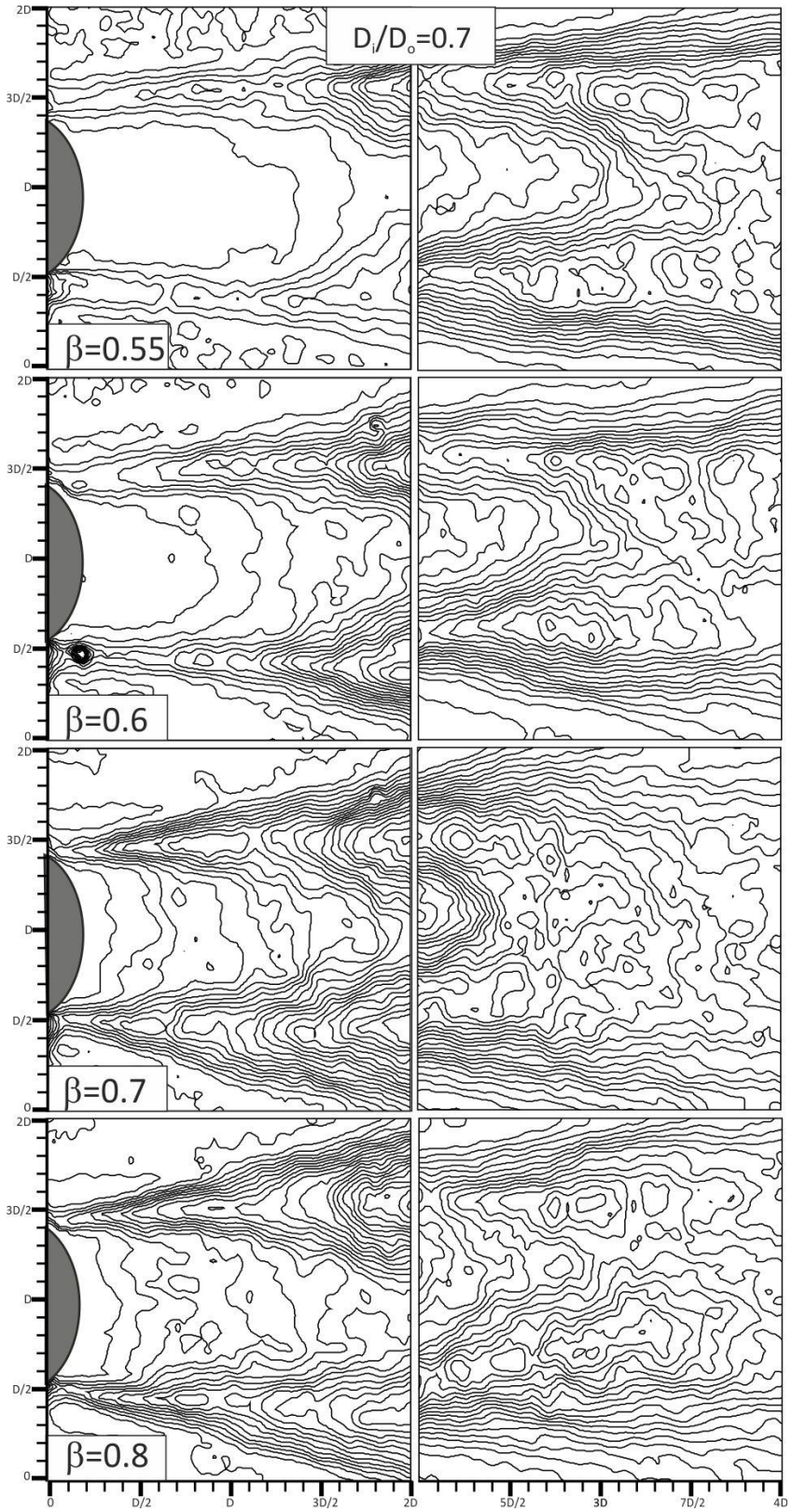

Figure 4.27. Turbulence kinetic energy distribution downstream of the coupled cylinders at D_i/D_o=0.70 for different β cases

Figures 4.24 and 4.26 present patterns of Reynolds shear stress at D_i/D_o=0.60 and D_i/D_o=0.70, respectively. Figures 4.25 and 4.27 show turbulent kinetic energy contours at D_i/D_o=0.60 and D_i/D_o=0.70, respectively. Comparing maximum values of both $<u'v'>$ and TKE values of different diameter ratios, another result comes up that increasing diameter ratio causes an increase in the maximum value of $<u'v'>$ as well as TKE intensity. For instance to show this tendency, while the peak magnitude of Reynolds shear stress was 0.0315 for D_i/D_o=0.3 and β=0.60 case, it was found that the value of Reynolds shear stress becomes 0.0684 for D_i/D_o=0.60 and β=0.60 case. As the diameter ratio increases, the effect of the outer cylinder on the flow structure decreases because of decreasing the distance between the inner and outer cylinders. Lower magnitude positive and negative $<u'v'>$ clusters are seen between $0.25 \leq \beta \leq 0.50$ for both D_i/D_o=0.60 and D_i/D_o=0.70 cases. Also, for these diameter ratios, $<u'v'>$ and TKE contours are concentrated along shear layers in the downstream direction for porosity ratios of β<0.70. However, peak magnitudes of turbulent kinetic energy values of these diameter ratios remain almost constant for all porosity, β. Most effective control to annihilate unsteady vibrations can be, again, denoted as β=0.60 for both D_i/D_o=0.60 and D_i/D_o=0.70 diameter ratios.

Figures 4.28 and 4.29 present Reynolds shear stress and TKE contours for D_i/D_o=0.75, respectively. This diameter ratio was chosen to show the effects of higher values of diameter ratio. Peak magnitudes of coupled cylinders approach to the beginning of second field of view (approximately 2.5D away from the cylinder base for all porosity, β). A lower magnitude of $<u'v'>$ cluster is formed at the rear stagnation point for all concentric cylinders. This is the proof of reduction in the control effect. TKE contours are concentrated along shear layers with increasing porosity, β. Peak magnitude of TKE value for D_i=75 mm bare cylinder is found to be 0.4322 and then this value reduces to 0.1941 (55% reduction) at β=0.25. After β=0.25 porosity value, maximum TKE value remains almost constant.

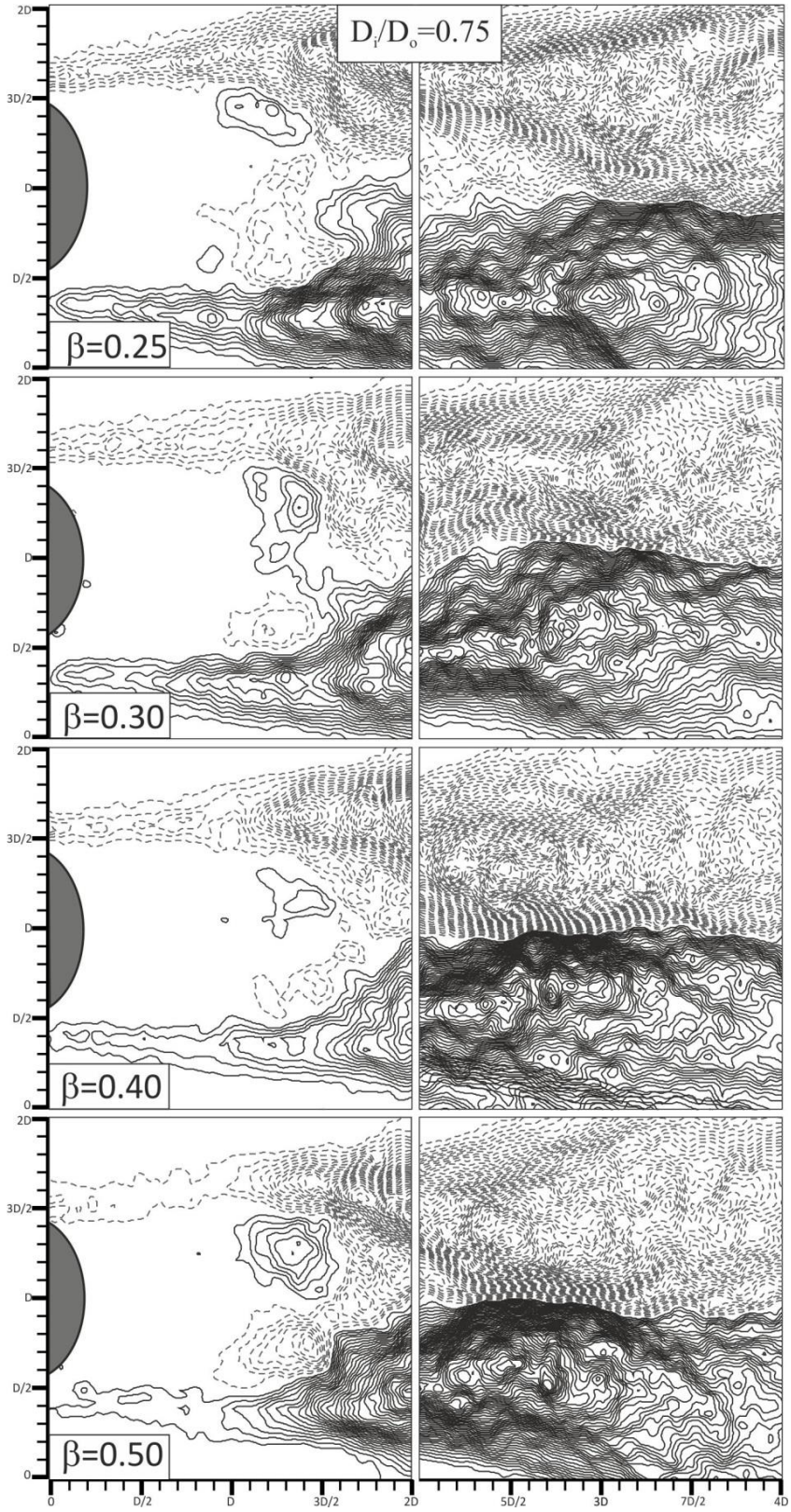
D_i/D_o=0.75
β=0.25
β=0.30
β=0.40
β=0.50
2D
3D/2
D
D/2
0
D/2
D
3D/2
2D
5D/2
3D
7D/2
4D

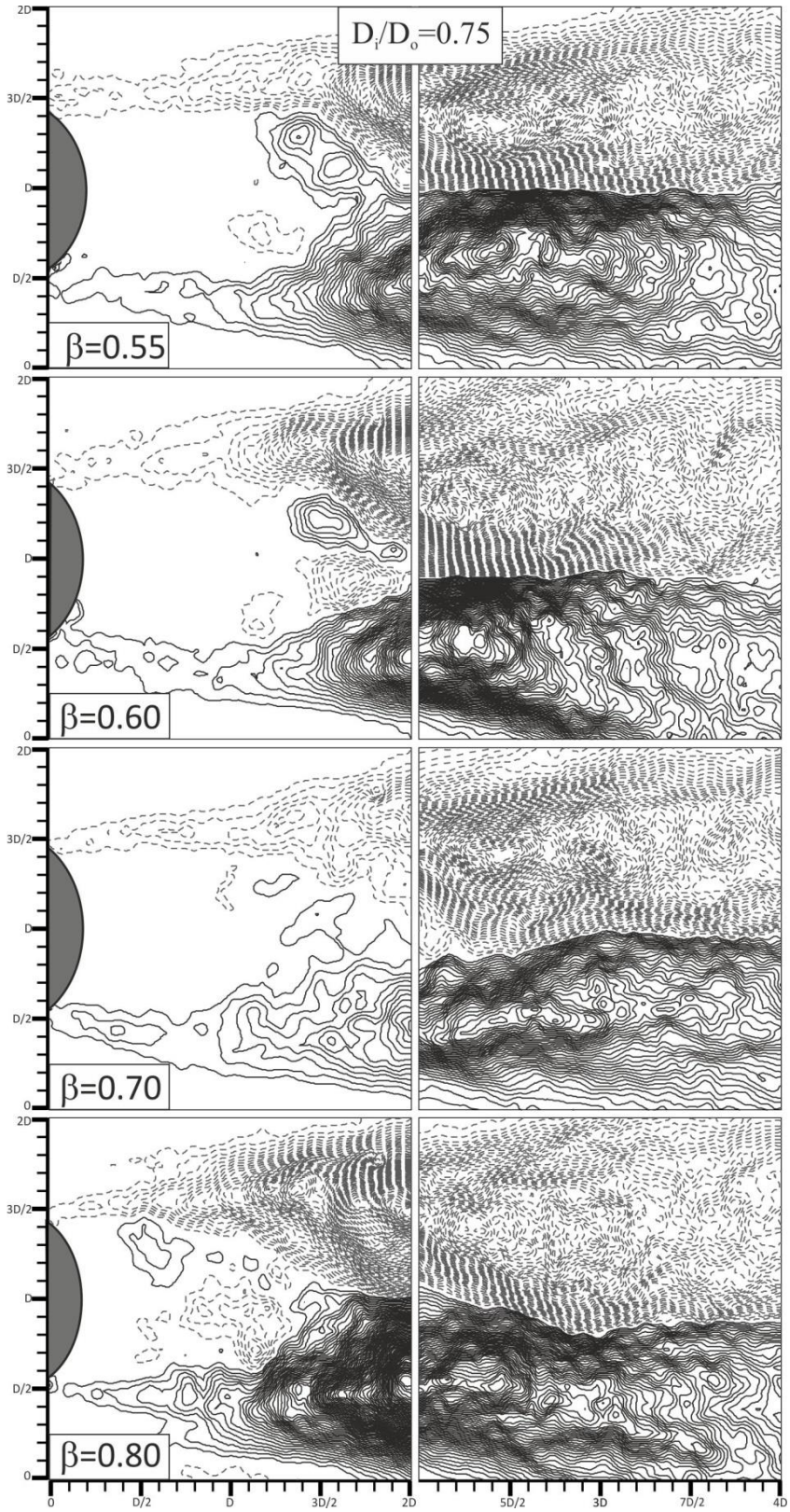

Figure 4.28. Reynolds shear stress distribution downstream of the coupled cylinders at D_i/D_o=0.75 for different β cases

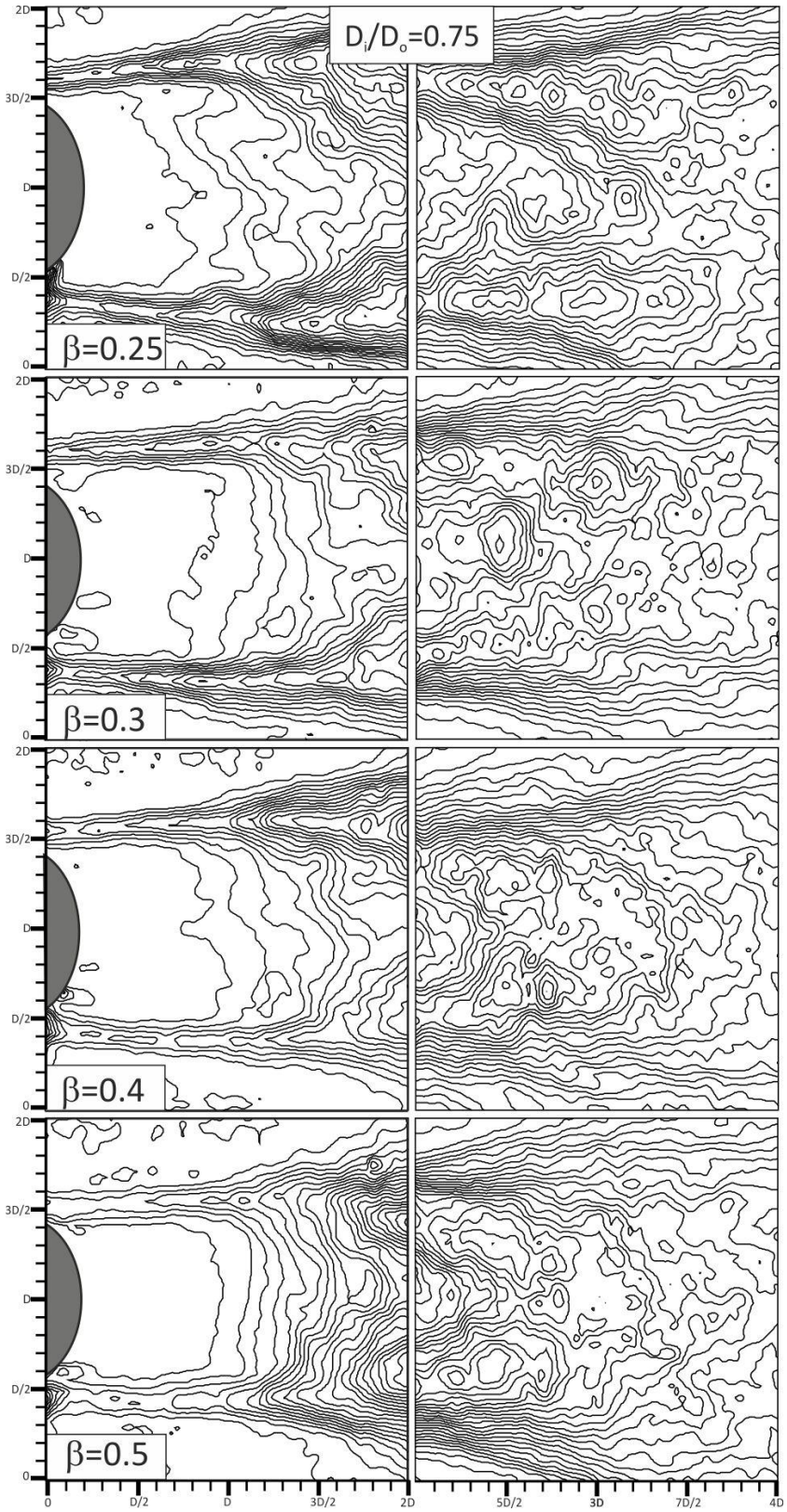
D_i/D_o=0.75
β=0.25
β=0.3
β=0.4
β=0.5
2D
3D/2
D
D/2
0
0
D/2
D
3D/2
2D
5D/2
3D
7D/2
4D

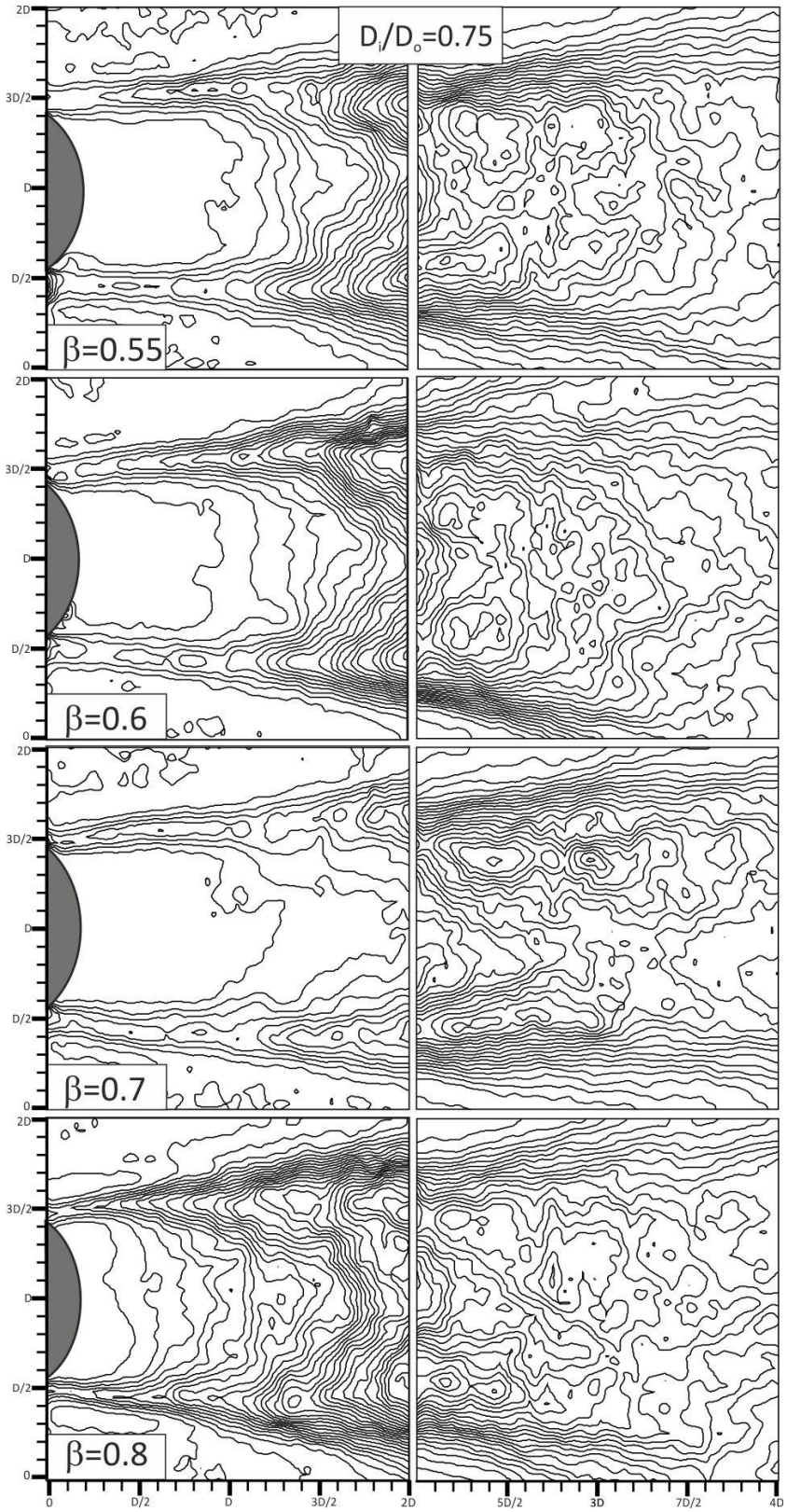

Figure 4.29. Turbulence kinetic energy distribution downstream of the coupled cylinders at D_i/D_o=0.75 for different β cases

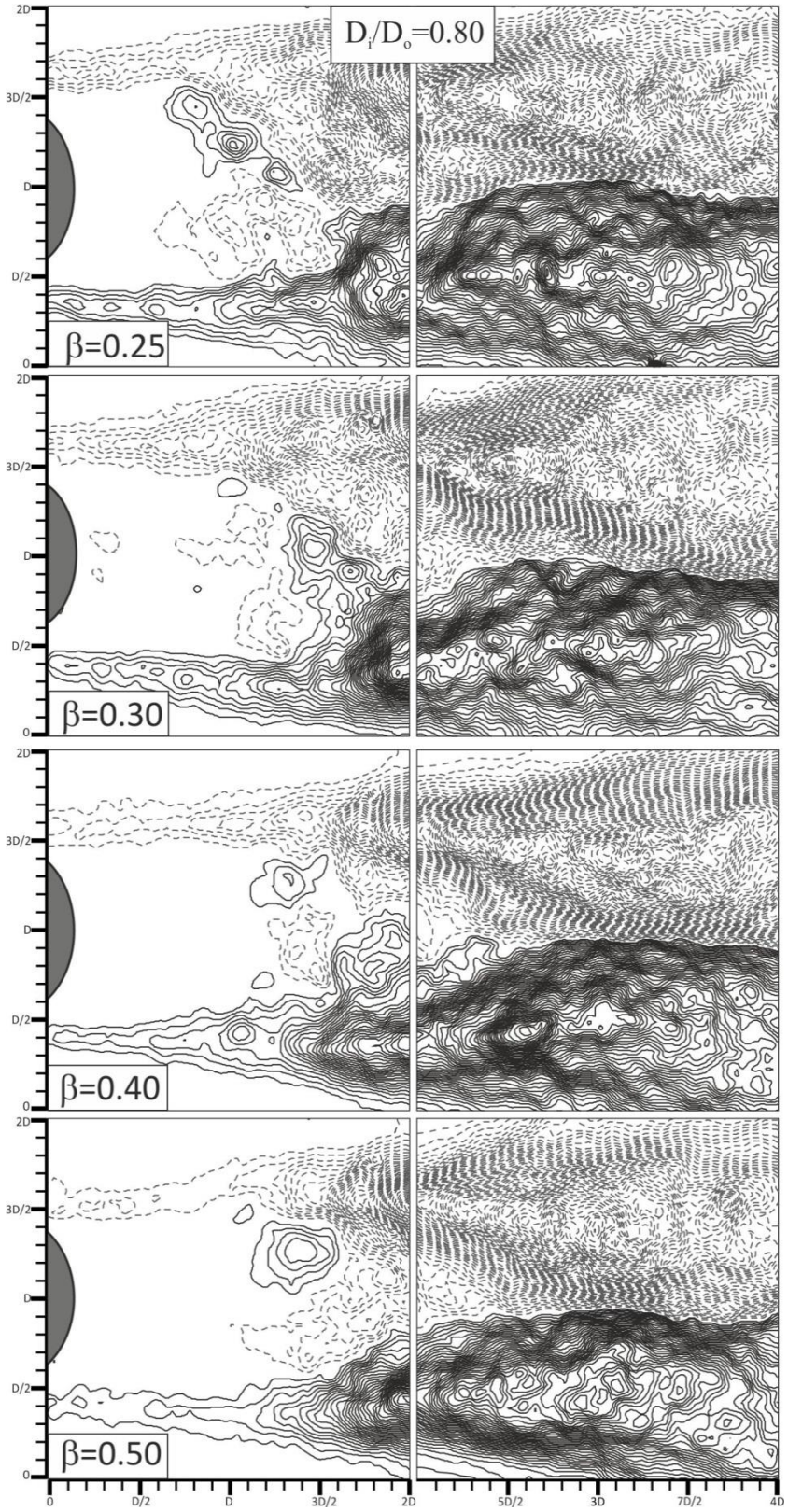
D_i/D_o=0.80
β=0.25
β=0.30
β=0.40
β=0.50
2D
3D/2
D
D/2
0
0
D/2
D
3D/2
2D
5D/2
3D
7D/2
4D

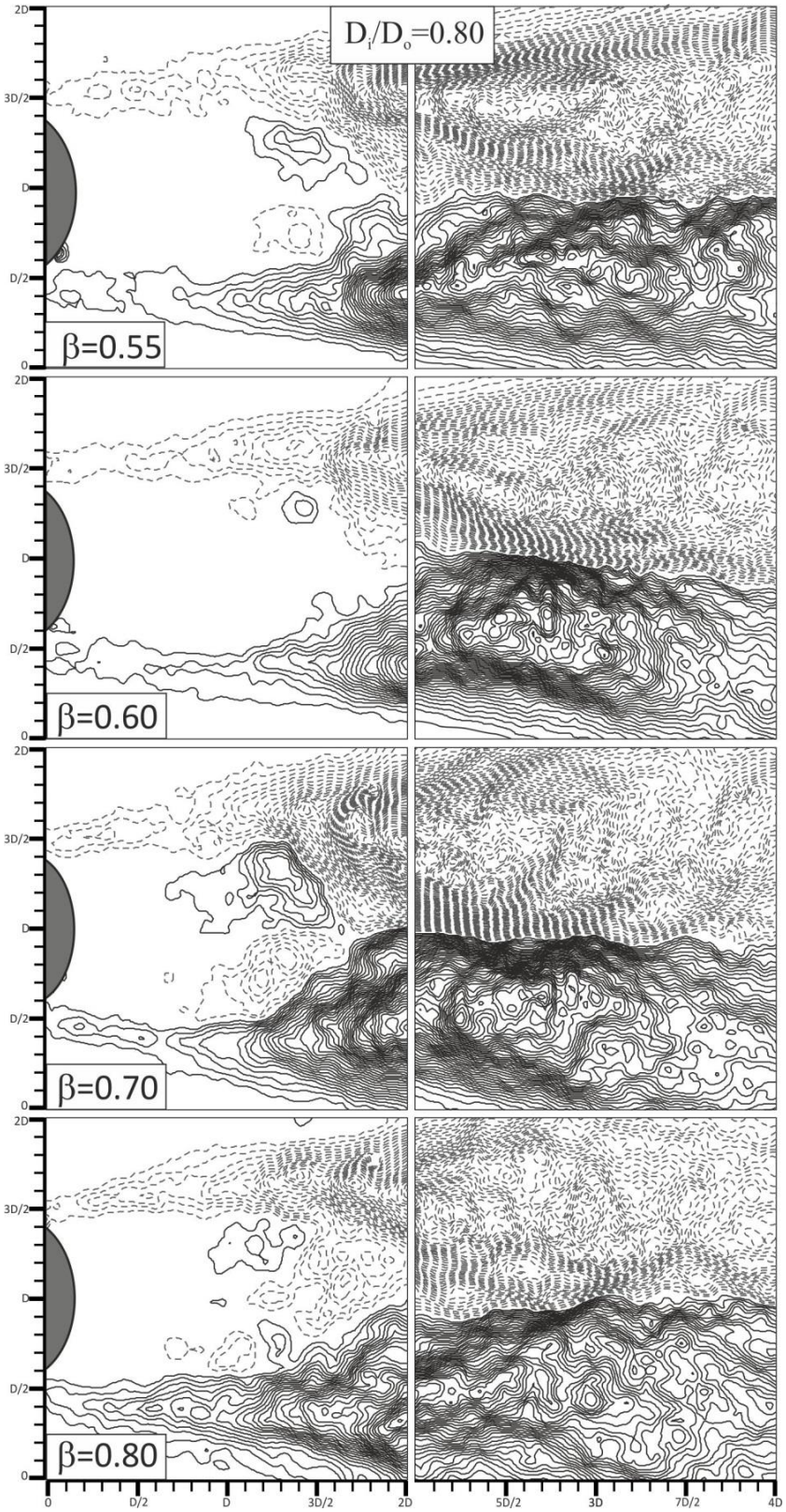

Figure 4.30. Reynolds shear stress distribution downstream of the coupled cylinders at D_i/D_o=0.80 for different β cases

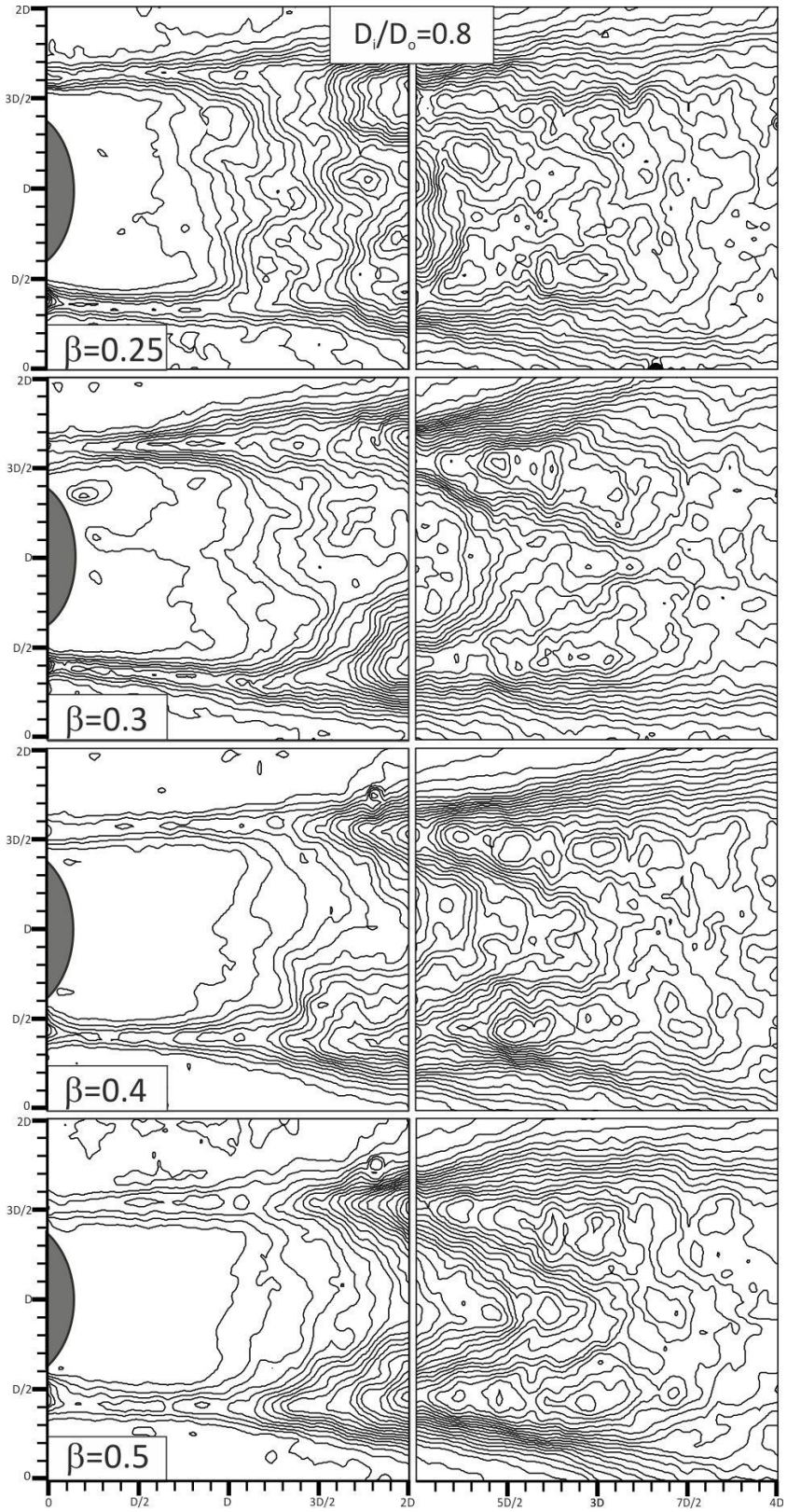
D_i/D_o=0.8
β=0.25
β=0.3
β=0.4
β=0.5
2D
3D/2
D
D/2
0
0
D/2
D
3D/2
2D
5D/2
3D
7D/2
4D

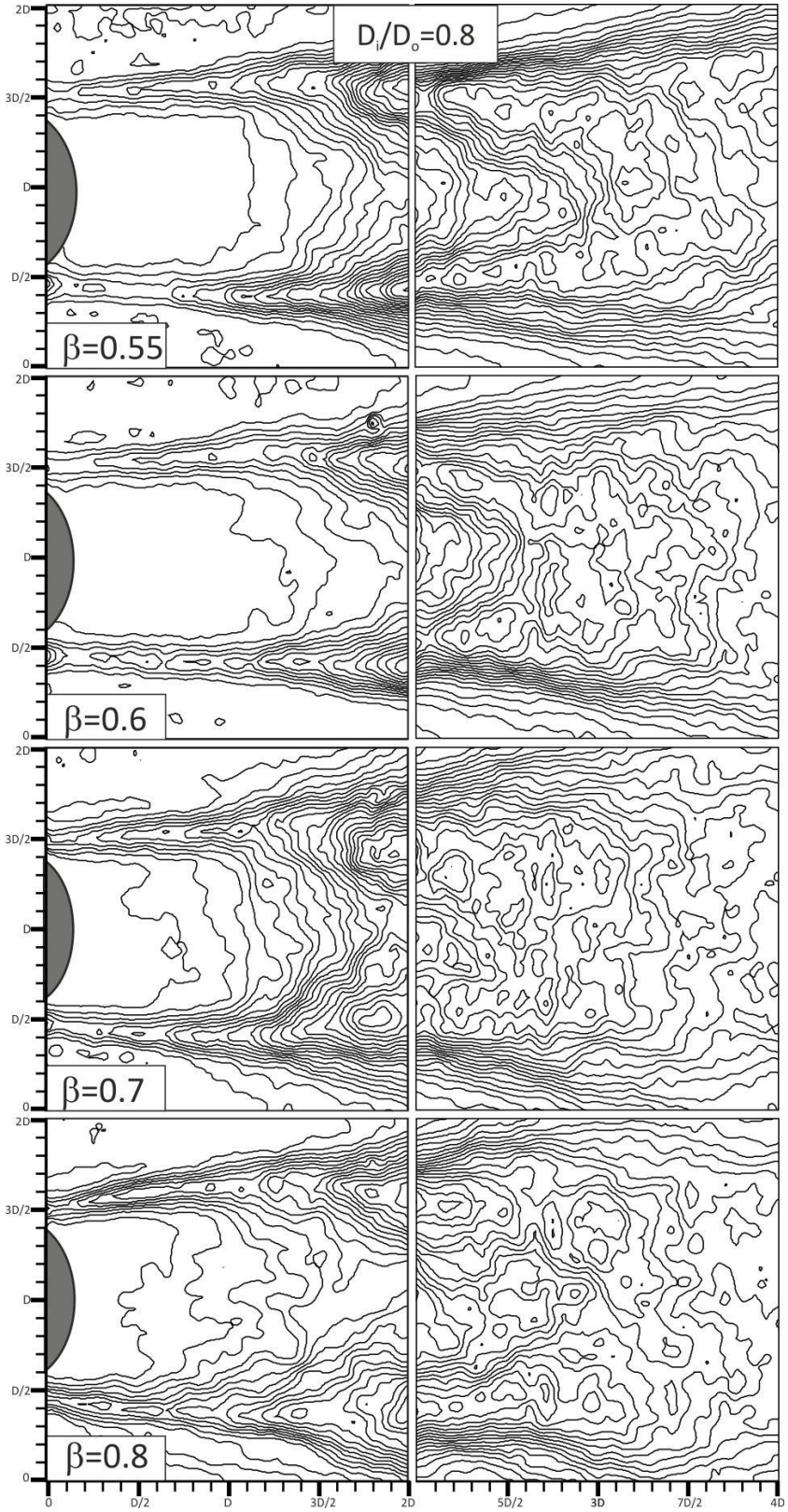

Figure 4.31. Turbulence kinetic energy distribution downstream of the coupled cylinders at D_i/D_o=0.80 for different β cases

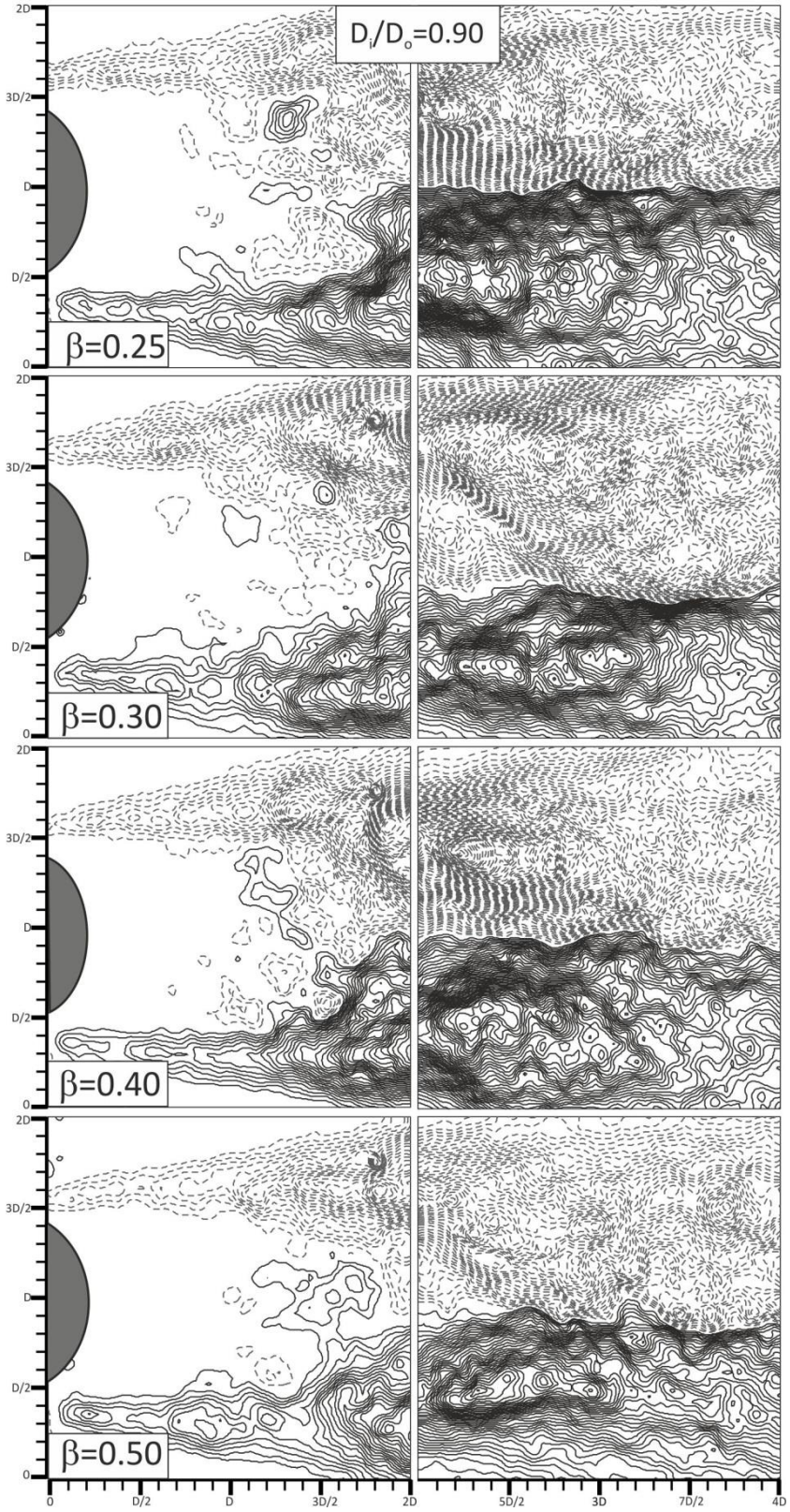
D_i/D_o=0.90
β=0.25
β=0.30
β=0.40
β=0.50
2D
3D/2
D
D/2
0
D/2
D
3D/2
2D
5D/2
3D
7D/2
4D

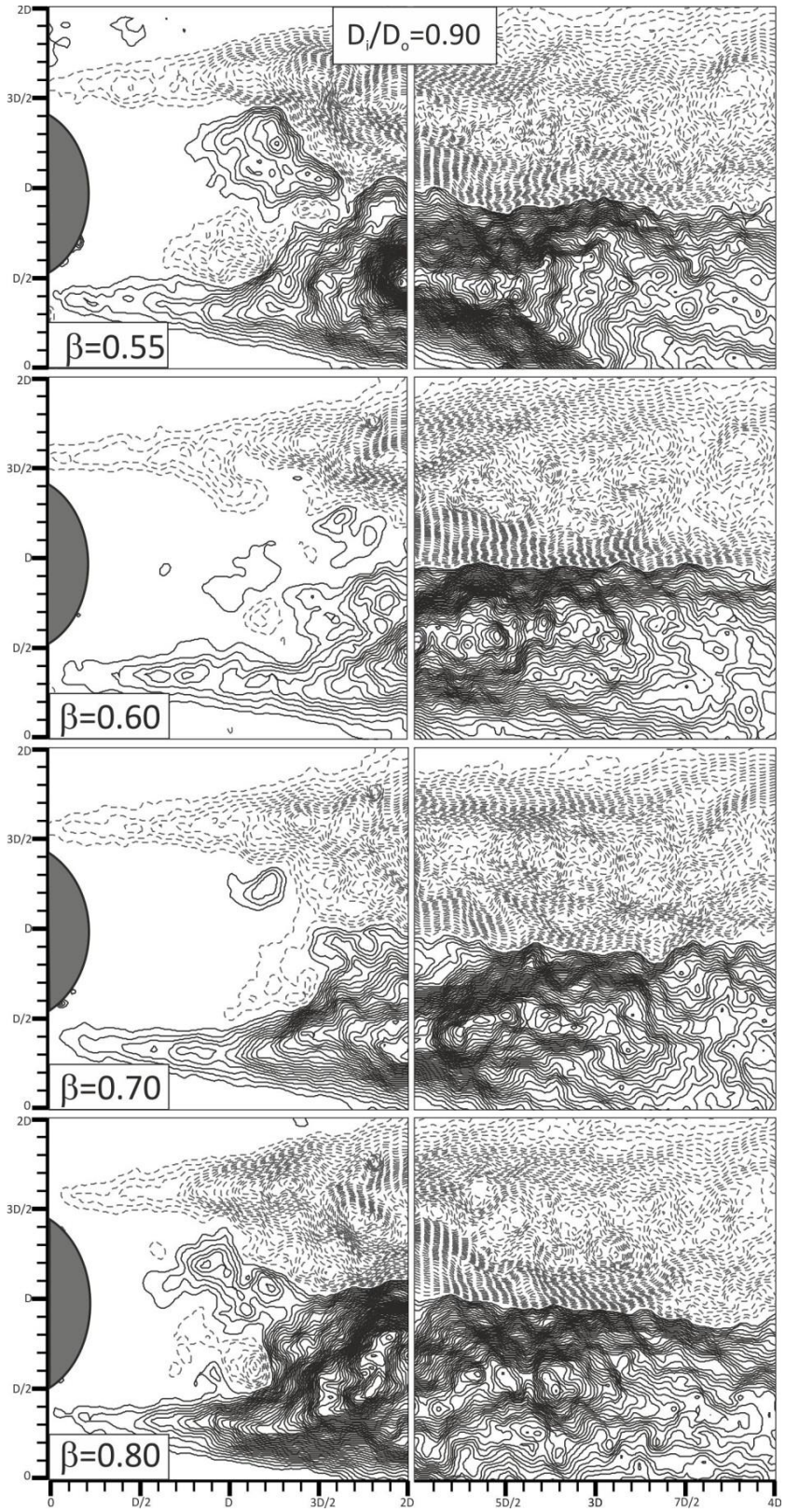

Figure 4.32. Reynolds shear stress distribution downstream of the coupled cylinders at D_i/D_o=0.90 for different β cases

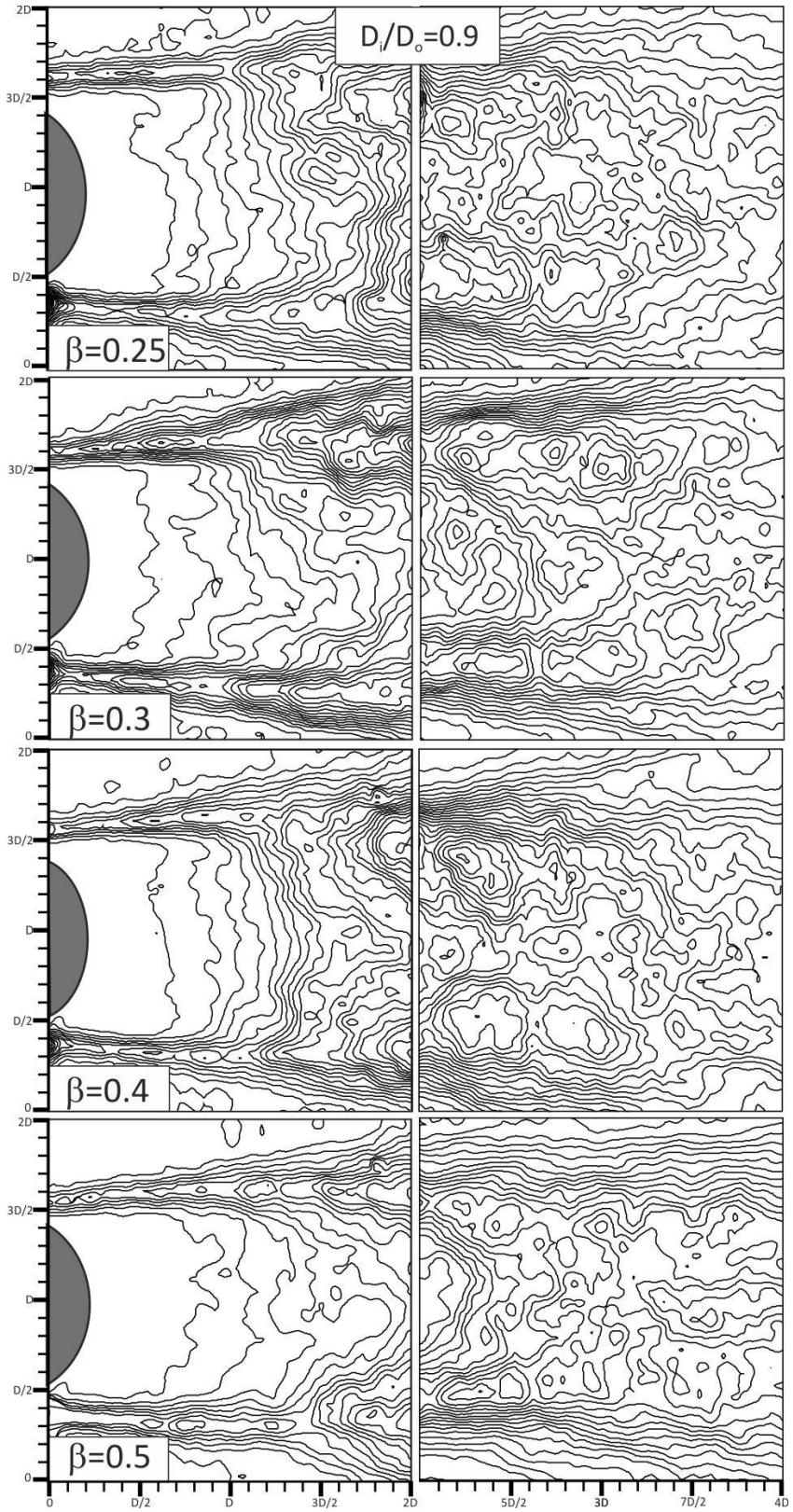
D_i/D_o=0.9
β=0.25
β=0.3
β=0.4
β=0.5
2D
3D/2
D
D/2
0
0
D/2
D
3D/2
2D
5D/2
3D
7D/2
4D

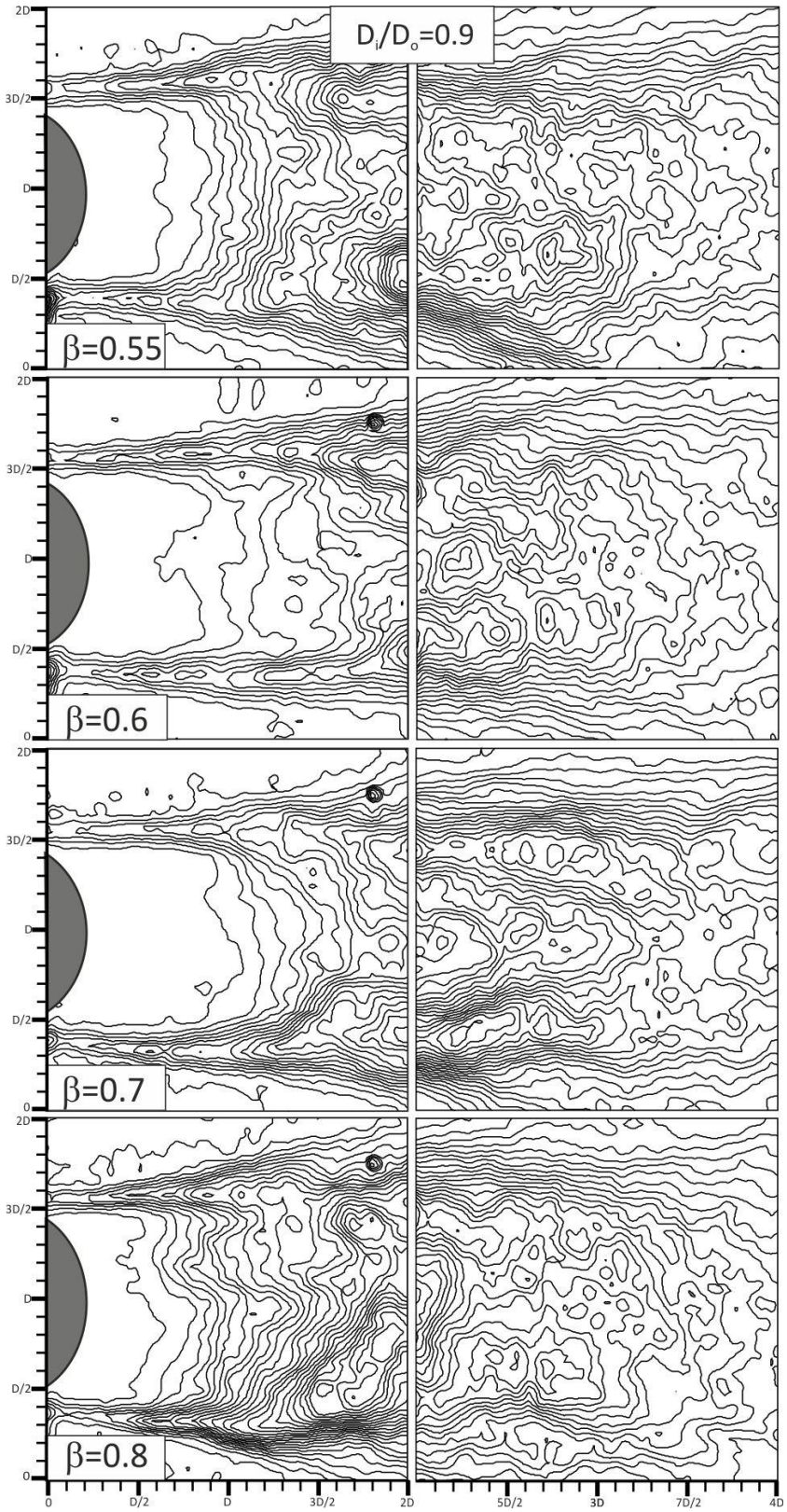

Figure 4.33. Turbulence kinetic energy distribution downstream of the coupled cylinders at D_i/D_o=0.90 for different β cases

Figures 4.30 and 4.32 show Reynolds shear stress contours at D_i/D_o=0.80 and D_i/D_o=0.90, respectively. Figures 4.31 and 4.33 show turbulent kinetic energy contours at D_i/D_o=0.80 and D_i/D_o=0.90, respectively. For these diameter ratios, very low distance between inner and outer cylinder makes inner cylinder more dominant on the formation of flow structure compared to outer perforated cylinder. For this reason, $<u'v'>$ and TKE contour figures clearly indicate that variations in porosity do not have any significant effect on the flow structure. However, flow control is carried out at these diameter ratios with respect to the bare cylinder cases, D_i=80 mm and D_i=90 mm, although their control effect is not well enough compared to other diameter ratios. Most effective control was achieved at porosity β=0.50 for both D_i/D_o=0.80 and D_i/D_o=0.90 cases. Maximum values of $<u'v'>$ are found to be 0.1268 and 0.1498 for D_i=80 mm and D_i=90 mm, respectively. The peak values of $<u'v'>$ are attenuated to 0.0744 (approximately 40% reduction) and 0.0755 (approximately 50% reduction) for D_i/D_o=0.80 and D_i/D_o=0.90, respectively.

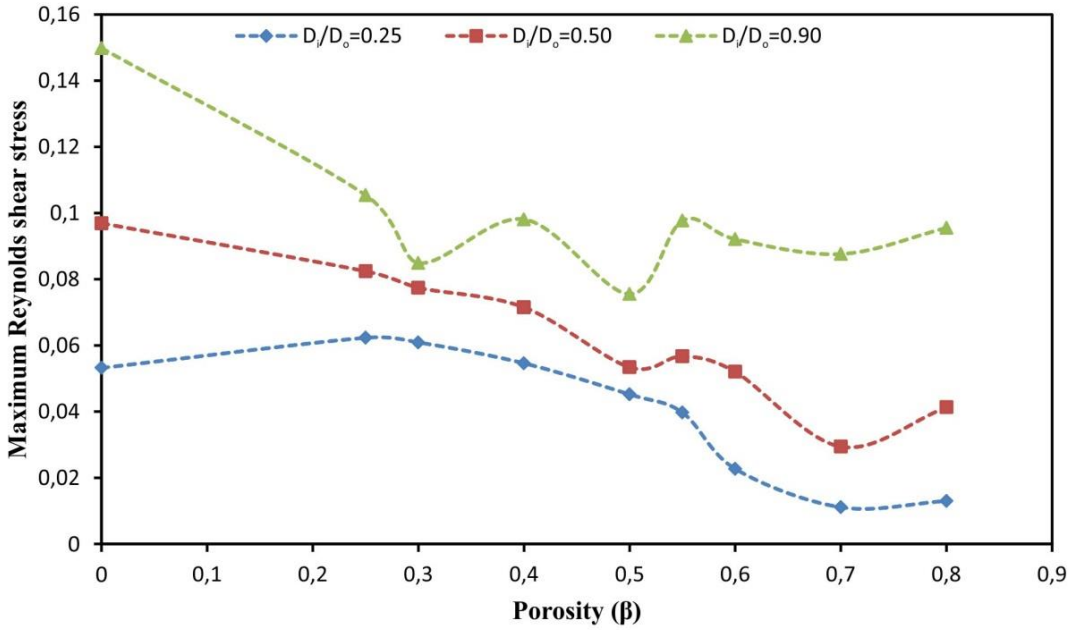

Figure 4.34. Variation of maximum Reynolds shear stress with respect to porosity for different coupled cylinders

Effect of porosity, β, with respect to diameter ratios, D_i/D_o, on the maximum $<u'v'>$ and TKE values are presented in Figures 4.34 and 4.35, respectively. Effect of nine diameter ratios are analyzed with the trend of three diameter ratios for both figures. Figure 4.34 indicates that control of low porosity, β, is not very effective for low diameter ratios (D_i/D_o<0.50) since the effect of jet flow occurred through holes on the outer cylinder is not sufficient to enhance momentum transfer into the wake region. Maximum $<u'v'>$ value has a reduction trend with increasing porosity, β. Figure 4.35 denotes similar influence for maximum TKE results. Also, for high diameter ratios (D_i/D_o>0.50), attenuation rate of maximum TKE remains almost constant with increasing porosity, β.

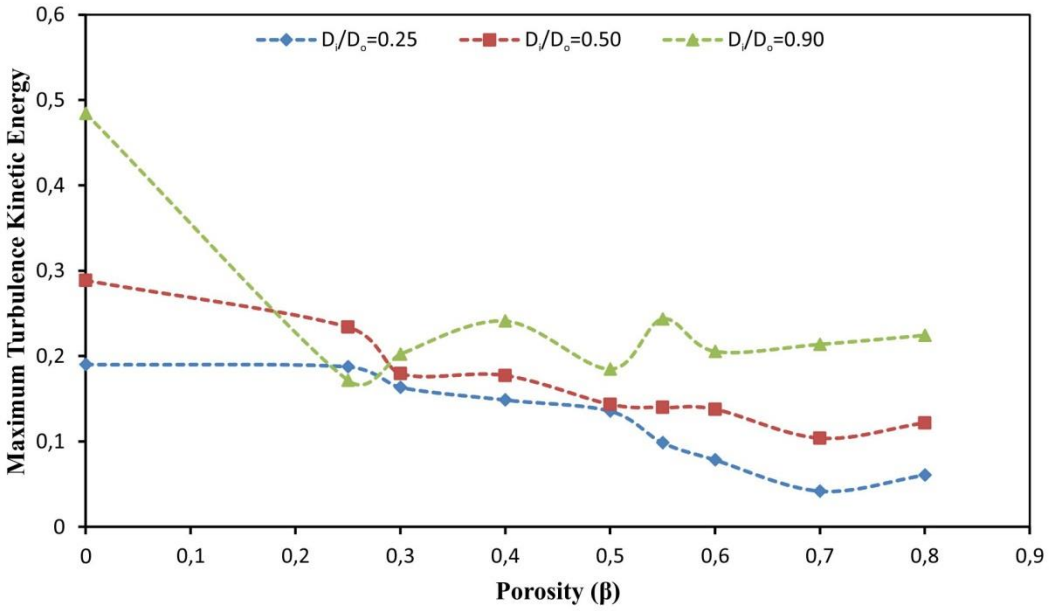

Figure 4.35. Variation of maximum turbulence kinetic energy with respect to porosity for different coupled cylinders

5. CONCLUSIONS

The aim of present study was to show the effect of perforated outer cylinders (D_o) which can be used as a control element in order to control the flow structure in the near wake of circular bare cylinders. The flow characteristics downstream of concentrically placed coupled (shrouded) cylinders were investigated quantitatively by the Particle Image Velocimetry (PIV) technique. The main parameters affecting the flow control were defined as a diameter ratio of inner and outer cylinder (D_i/D_o) and porosity ratio of outer cylinder (β). Effect of the parameters on unsteady flow structure were scrutinized for seven porosity ratios (β=0.25, 0.30, 0.40, 0.50, 0.60, 0.70 and 0.80) and nine diameter ratios (D_i/D_o=0.25, 0.30, 0.40, 0.50, 0.60, 0.70, 0.80 and 0.90). Diameter of the outer cylinder was kept constant as D_o=100 mm while diameter of the inner cylinder was varied within the range of $25 \leq D_i \leq 90$ mm.

Flow control can be achieved by means of the jet flow emanating from the holes on the surface of the perforated cylinders which effectively prevents the formation of well–organized Karman vortex street. It was understood from the experiments that suppression of vortex shedding depends on variation of diameter ratio, D_i/D_o and porosity, β. Shear layers elongates in the downstream direction by losing their magnitudes with increasing porosity, β, compared to the bare cylinder cases. Effect of the outer perforated cylinder was more dominant on turbulence statistics compared to inner cylinder for both $0.25 \leq \beta \leq 0.30$ and $0.25 \leq D_i/D_o \leq 0.40$ cases. It was observed that the diameter ratio is effective on the flow control for low porosity ratios ($0.25 \leq \beta \leq 0.40$); while, the porosity ratio is effective for high diameter ratios ($0.50 \leq D_i/D_o \leq 0.90$) on the flow control. For D_i/D_o=0.80, the flow control had minimum effect since the inner and outer cylinders act as a single cylinder and finally, the turbulence intensity increased. The turbulent statistics (Reynolds shear stress and Turbulence Kinetic Energy) show that the fluctuations are reduced dramatically in the wake region by use of a perforated cylinder as a control element. Most effective control was revealed for $0.50 \leq \beta \leq 0.60$ for all diameter ratios. However, it was also found that the maximum turbulence statistics get close to the first field of view with increasing diameter ratios. The results showed that

concentrically placed perforated cylinders will be an alternative passive control method in order to prevent vortex shedding for deep water applications such as bridge piers, high-rise buildings, chimneys etc.

REFERENCES

ADRIAN, R.J, 1991. Particle-imaging techniques for experimental fluid mechanics. Annual Review of Fluid Mechanics, 23:261–304.

AKILLI, H. , SAHIN, B. , TUMEN, N.F. , 2005. Suppression of vortex shedding of circular cylinder in shallow water by a splitter plate. Flow Measurement and Instrumentation, Turkey, 16:211–219.

AKILLI, H., KARAKUS, C. , AKAR, A. , SAHIN, B. , TUMEN, N.F. , 2008. Control of vortex shedding of circular cylinder in shallow water flow using an attached splitter plate. Journal of Fluids Engineering-T ASME, Turkey, 130:041401.

AMITAY, M., HONOHAN, A., TRAUTMAN, M., GLEZER, A., 2004. Modification of the aerodynamic characteristics of bluff bodies using fluidic actuators. AIAA 97-2004.

APELT, B., WEST, G.S., SZEWCZYK, A.A., 1973. The effects of wake splitter plates on the flow past a circular cylinder in the range $10^4 < Re < 10^5$, Journal of Fluid Mechanics, 61 (1) 187–198.

ASSI, G.R.S., BEARMAN, P.W., KITNEY, N., 2009. Low drag solutions for suppressing vortex-induced vibration of circular cylinders. Journal of Fluids and Structures, UK, 25 (2009) 666–675.

ASSI, G.R.S., BEARMAN, P.W., KITNEY, N., TOGNARELLI, M.A., 2010. Suppression of wake-induced vibration of tandem cylinders with free-to-rotate control plates. Journal of Fluids and Structures, Brazil, 26 (2010) 1045–1057.

BAEK, H., KARNIAKIDIS, G.E., 2009. Suppressing vortex-induced vibrations via passive means. Journal of Fluids and Structures, USA, 25 (2009) 848–866.

BAEK, H., KARNIAKIDIS, G.E., 2009. Suppressing vortex-induced vibrations via passive means. Journal of Fluids and Structures, USA, 25 (2009) 848–866.

BADR, H., COUTANCEAU, M., DENNIS, S., MENARD C., 1990. Unsteady flow past a rotating circular cylinder at Reynolds numbers 1000 and 10000. Journal of Fluid Mechanics, 220:459– 484.

BALACHANDAR, R., CHU, V.H., and ZHANG, J., 1997. Experimental study of turbulent concentration flow field in the wake of a bluff body. Journal of Fluid Engineering, 199: 263-270.

BAO, Y. and TAO, J., 2013. The passive control of wake flow behind a circular cylinder by parallel dual plates. Journal of Fluids and Structures, 37:201-209.

BAZ, A. and RO, J. 1991 Active control of flow-induced vibrations of a flexible cylinder using direct velocity feedback. Journal of Sound and vibration, 146, 33-45.

BEARMAN, P.W., 1965. Investigation of flow behind a two-dimensional model with blunt trailing edge and fitted with splitter plates, Journal of Fluid Mechanics, 21, 241–255.

_____, 1984. Vortex shedding from oscillating bluff bodies. Annual Review of Fluid Mechanics, 16: 195-222.

_____, 2011. Circular cylinder wakes and vortex-induced vibrations, Journal of Fluids and Structures, 27: 648–658.

BEARMAN, P.W., OWEN, J.C., 1997. Reduction of bluff-body drag and suppression of vortex shedding by the introduction of wavy separation lines. Journal of Fluids and Structures, UK, 12, 123-130.

BEARMAN, P., BRANKOVIC, M., 2003. Experimental studies of passive control of vortex-induced vibration. European Journal of Mechanics B/Fluids, UK, 23: 9-15.

BISHOP, R. E. D. and HASSAN, A. Y., 1964. The lift and drag forces on a circular cylinder oscillating in a flowing fluid, Proc. R. Soc., London, Ser. A 277, 51.

BLEVINS R, D., 1985. The effect of sound on vortex shedding. Journal of Fluid Mechanics, 161:217-237.

BLEVINS R, D., 1990. Flow-Induced Vibration. Van Nostrand Reinhold Company, New York.

BLOOR, M.S., 1964. The transition to turbulence in the wake of a circular cylinder. Journal of Fluid Mechanics, 19: 290-304.

CAGNEY, N. and BALABANI, S., 2013. Wake modes of a cylinder undergoing free streamwise vortex-induced vibrations. Journal of Fluids and Structures, 38:127-145.

CHEN, D., JIRKA, H., 1995. Experimental study of plane turbulent wakes in a shallow water layer. Fluid Dynamics Research, 16: 11-41.

_____, 1997. Absolute and convective instabilities of plane turbulent wakes in a shallow water layer. Journal of Fluid Mechanics, 338: 157-172.

CHEN, Z., NADINE, A., 2003. Active control of cylinder wake. Communications in Nonlinear Science and Numerical Simulation, China, 10 (2005) 205–216.

CHOI, H., JEON, W-P., KIM, J., 2008. Control of flow over a bluff body. Annual Review of Fluid Mechanics, 40:113-39.

CIMBALA, M., GARG, S., 1991. Flow in the wake of a freely rotatable cylinder with splitter plate. AIAA Journal, 29:1001-1003.

FENG, L.H., WANG, J.J., 2010. Circular cylinder vortex-synchronization control with a synthetic jet positioned at the rear stagnation point. Journal of Fluid Mechanics, 662:232-259.

FENG, L.H., WANG, J.J., PAN, C., 2010. Effect of novel synthetic jet on wake vortex shedding modes of a circular cylinder. Journal of Fluids and Structures, China, 26 (2010) 900–917.

FFOWCS-WILLIAMS, J.E., and ZHAO, B.C., 1989. The active control of vortex shedding. Journal of Fluids and Structures, 3, 115-122.

FILLER, J.R., MARSTON, P.L. and MIH, W.C., 1991. Response of the shear layers separating from the circular cylinder to small amplitude rotational oscillations. Journal of Fluid Mechanics, 231, 481-499.

FUJISAWA, N., TAKEDA, G., IKE, N., 2003. Flow control around a circular cylinder by internal acoustic excitation. Journal Fluid Structures, 17:903–913.

FUJISAWA, N., TAKEDA, G., IKE, N., 2004. Phase-averaged characteristics of flow around circular cylinder under acoustic excitation control. Journal of Fluids and Structures, Japan, 19 (2004) 159–170.

GERARD, J.H., 1964. The mechanics of the formation region of vortices behind bluff bodies. Journal of Fluid Mechanics, 25: 401-413.

_____, 1966. The mechanics of formation region of vortices behind bluff bodies, Journal of Fluid Mechanics, 25 401–413.

GLEZER, A., AMITAY, M., 2002. Synthetic jets. Annual Review of Fluid Mechanics, 34: 503-529.

GOVARDHAN, R., WILLIAMSON, C.H.K., 2000. Modes of vortex formation and frequency response of a freely vibrating cylinder. Journal of Fluid Mechanics 420, 85–130.

GOZMEN, B., AKILLI, H., SAHIN, B., 2013. Passive control of circular cylinder wake in shallow flow. Measurement, 46:1125-1136.

GIORIA, R.S., JABARDO, P.J.S., CARMO, B.S., MENEGHINI, J.R., 2009. Floquet stability analysis of the flow around an oscillating cylinder. Journal of Fluids and Structures, UK, 25 (2009) 676–686.

GRIFFIN, O. M. and VOTAW, C. W., 1972. The vortex street in the wake of a vibrating cylinder, Journal of Fluid Mechanics, 55, 31.

GRIFFIN, M.O., 1978. A universal Strouhal number for the 'locking-on' of vortex shedding to the vibration of bluff cylinders, J. Fluid Mech., 85 591–606.

GRIFFIN, M., and HALL, M.S., 1991. Vortex shedding lock-in and flow control in bluff body wakes. ASME Journal of Fluids Engineering, 113, 526-537.

HO, C.M., AND HUERRE, P., 1984. Perturbed free shear layers. Annual Review of Fluid Mechanics, 16: 365-424.

INOUE, O., 1985. A new approach to flow problems past a porous plate. AIAA Journal, 23, 1916–1921.

JUKES, T. N., CHOI, K.S., 2009. Flow control around a circular cylinder using pulsed dielectric barrier discharge surface plasma. Physics of Fluids, 21:127-139

KNELL, B.J., 1969.The drag of a circular cylinder fitted with shrouds, Natl. Phys. Lab., UK, Aero. Rep. no. 1297.

KONSTANTINIDIS, E., BALABANI, S., 2007. Symmetric vortex shedding in the near wake of a circular cylinder due to streamwise perturbations. Journal of Fluids and Structures, Greece, 23 (2007) 1047–1063.

KUMAR, R.A., SOHN, C-H., and BANGALORE, H.L., 2008. Passive Control of Vortex-Induced Vibrations: An Overview. Recent Patents on Mechanical Engineering, Korea, 1, 1-11.

KUO, C.-H., CHIOU, L.-C., CHEN, C.-C., 2007. Wake flow pattern modified by small control cylinders at low Reynolds numer. Journal of Fluids and Structures, Taiwan, 23 (2007) 938–956.

KUO, C.-H., CHEN, C.-C., 2009. Passive control of wake flow by two small control cylinders at Reynolds number 80. Journal of Fluids and Structures, Taiwan, 25 (2009) 1021–1028. Journal of Fluids and Structures, Republic of Korea, 24 (2008) 2–17.

KWON K., CHOI, H., 1996. Control of laminar vortex shedding behind a circular cylinder using splitter plates. Physics of Fluids, 10:479– 485.

LEE, S.-J., LEE, J.-Y., 2008. PIV measurements of the wake behind a rotationally oscillating circular cylinder. Journal of Fluids and Structures, Republic of Korea, 24 (2008) 2–17.

MANSINGH, V., OOSTHUIZEN, P.H., 1990. Effects of splitter plates on the wake flow behind a bluff body, AIAA J. 28:778-783.

MIAU, J.J., YANG, J.H., LEE, K.R., 1993. Suppression of low frequency variations in vortex shedding by a splitter plate behind a bluff body, Journal of Fluids and Structure, 7:897-912.

MUDDADA, S., PATNAIK, B.S.V., 2009. An active flow control strategy for the suppression of vortex structures behind a circular cylinder. Europian Journal of Mechanics B/Fluids, India, 29 (2010) 93–104.

NAKAMURA, H., IGARASHI, T., 2008. Omnidirectional reductions in drag and fluctuating forces for a circular cylinder by attaching rings. Journal of Wind Engineering, Japan, 96 (2008) 887–899.

NOSENCHUCK, D.M., BROWN, G.L., CULVER, H.C., ENG. T.I., and HUANG, I.S., 1995. Spatial and temporal characteristics of boundary layers controlled with the Lorentz force. Twelfth Australasian Fluid Mechanics Conference, Australia.

OKAJIMA, A., TAKATA, H., and ASANUMA, T., 1975. Viscous flow around a rotationally oscillating circular cylinder. Reports of Institute of Space and Aeronautical Science, Tokyo, (532), 311-338.

ONGOREN, A., and ROCKWELL, D., 1988. Flow structure from an oscillating cylinder Part 2. Model competition in the near wake. Journal of Fluid Mechanics, 191:225-245

OWEN, J.C., BEARMAN, P.W., and SZEWCZYK, A.A., 2001. Passive control of VIV with drag reduction. Journal of Fluids and Structures, UK, (2001) 15, 597-605.

OZONO, S., 1999. Flow control of vortex shedding by a short splitter plate asymmetrically arranged downstream of a cylinder. Physics of Fluids, 11, (10):2928 –2934.

PATNAIK, B.S.V., WEI, G.W., 2002. Controlling wake turbulence. Physical Review Letters, 88: 54-66.

PINAR, E., 2013. Flow control of a cylinder in shallow water using perforated cylinder. Cukurova University Institute of Natural and Applied Sciences, Turkey, Ph.D Thesis.

ROSHKO A. 1954. On the development of turbulent wakes from vortex streets. NACA Rep. 1191.

_____, 1955. On the drag and shedding frequency of two-dimensional bluff bodies, NACA Tech. Note no.3169.

ROUSSOPOULOS, K., 1993. Feedback control of vortex shedding at low Reynolds numbers. Journal of Fluid Mechanics, 24, 267-296.

SARPKAYA, T., 2004. A critical review of the intrinsic nature of vortex-induced vibrations. Journal of Fluids and Structures, 19:389–447.

SCHAFER, F., BREUER, M., DURST, F., 2009. The dynamics of the transitional flow over a backward facing step. Journal of Fluid Mechanics, 623:85-119.

SHENG, J., MENG, H., FOX, R.O., 2000. A large eddy PIV method for turbulence dissipation rate estimation. Chemical Engineering Science, 55:4423-4434.

SHUKLA, S., GOVARDHAN R.N., ARAKERI J.H., 2009. Flow over a cylinder with a hinged-splitter plate. Journal of Fluids and Structures, India, 25: 713-720.

TANEDA, S., 1978. Visual observations of the flow past a circular cylinder performing a rotary oscillation. Journal of Physical Society of Japan, 45, 1038-1043.

TAO J.S., HUANG X.Y., CHAN, W.K., 1996. A flow visualization study of feedback control of vortex shedding from a circular cylinder. Journal of Fluids and Structures, 10:965 –970.

TOKUMARU, P.T., and DIMOTAKIS, P.E., 1991. Rotary oscillation control of a cylinder wake. Journal of Fluid Mechanics, 224, 77-90.

TURHAL, A.O., CUHADAROGLU, B., 2010. The effects of surface injection through a perforated square cylinder on some aerodynamic parameters. Experimental Thermal and Fluid Science, Turkey, 34 (2010) 725–735.

TURKI, S., 2008. Numerical simulation of passive control on vortex shedding behind square cylinder using splitter plate. Engineering Applications of Computational Fluid Mechanics, 2:514–524.

UNAL, M.F., and ROCKWELL, D., 1987. On vortex formation from a cylinder, Part 1: The initial instability. Journal of Fluid Mechanics, 190: 491-512.

_____, 1988. On vortex formation from a cylinder, Part 2: Control by Splitter-Plate Interference. Journal of Fluid Mechanics, 190: 513-529.

WANG, J., SHAN, R., ZHANG, C., FENG, L., 2010. Experimental investigation of a novel two-dimensional synthetic jet. European Journal of Mechanics B/Fluids, China, 29 (2010) 342_350.

WEIER, T., GERBETH, G., MUTSCHKE, G., PLATACIS, E., and LIEALAUSIS, O., 1998. Experiments on Cylinder Wake Stabilization in an Electrolyte

Solution by Means of Electromagnetic Forces Localized on the Cylinder Surface, Experimental Thermal and Fluid Science, 16:84-91.

WESTERWEEL, J., 1993. Digital particle image Velocimetry - theory and application, Delft University Press.

WILLIAMSON, C.H.K. and ROSHKO, A., 1988. Vortex formation in the wake of an oscillating cylinder. Journal of Fluids and Structures, 2:355-381.

WILLIAMSON, C.H.K. and GOVARDHAN, R., 2004. Vortex – induced vibrations. Annual Review of Fluid Mechanics, 36:413–55.

WONG, H. Y., 1985. Wake stabilization by the action of base bleed. Trans. ASME: J. Fluids Engineering, 107, 378–384.

WOOD, C. J., 1964. The effect of base bleed on a periodic wake. J. R. Aero. Soc. 68, 477–482.

_____, 1967. Visualization of incompressible wake with base bleed, Journal of Fluid Mechanics, 29, (2) 259–272.

WU, W., YUAN, J., CHENG, L., 2007. Multi-high-frequency perturbation effects on flow-induced vibration control. Journal of Sound and Vibration, Hong Kong, 305 (2007) 226–242.

XU, J.C., SEN, M., GAD-EL-HAK, M., 1993. Dynamics of rotable cylinder with splitter plate in uniform flow. Journal of Fluids and Structures, 7(4):401-416.

YU, M-H. and MONKEWITZ, P. A. 1990. The effect of nonuniform density on the absolute instability of two-dimensional inertial jets and wakes Physics of Fluids A 2(7):1175-1181.

ZDRAVKOVICH, M. M. 1981 Review and classification of various aerodynamic and hydrodynamic means for suppressing vortex-shedding. Journal of Wind Engineers and Industrial Aerodynamics, 7:145–189.

ZHANG, H., FAN, B.-C.., CHEN, Z.-H., 2009. Optimal control of cylinder wake flow by electro-magnetic force based on adjoint flow field. European Journal of Mechanics B/Fluids, China, 29, 53–60.

ZHANG, H., FAN, B.-C.., CHEN, Z.-H., 2010. Computations of optimal cylinder flow control in weakly conductive fluids. Computers and Fluids, China, 39 1261–1266.

ZHOU, L., CHENG, M.,HUNG, K.C., 2005. Suppression of fluid force on a square cylinder by flow control. Journal of Fluids and Structures, China, 21 151–167.

ZOU, L., LIN, Y., 2009. Force reduction of flow around a sinusoidal wavy cylinder. Journal of Hydrodynamics, China, 21(3):308-315.

CIRRICULUM VITAE

Muhammed Murat AKSOY was born in 1988 in Adana. He graduated from Danisment Gazi Anatolian High School, and enrolled in Mechanical Engineering Department of Cukurova University in 2007. He was also enrolled in Industrial Engineering Department at the same university as a double major student in 2008. He graduated as a Mechanical Engineer in May 2011 and as an Industrial Engineer in May 2012 from the university.